MSc. Thesis
Geology
Economic Geology

MINERALIZATION AND FORMATION CONDITIONS OF METAMORPHIC REMOBILIZATION VEINS, STORLIDEN VHMS DEPOST, SKELLEFTE DISTRICT, NORTH SWEDEN

Petri Kristian Uuttu

2014

Supervisor: prof. Thomas Wagner

HELSINGIN YLIOPISTO
GEOTIETEIDEN JA MAANTIETEEN LAITOS
GEOLOGIAN OSASTO

PL 64 (Gustaf Hällströmin katu 2)
00014 Helsingin yliopisto

HELSINGIN YLIOPISTO – HELSINGFORS UNIVERSITET – UNIVERSITY OF HELSINKI

Tiedekunta/Osasto – Fakultet/Sektion – Faculty/Section	Laitos – Institution – Department
Matemaattis-luonnontieteellinen	Geotieteiden ja maantieteen laitos

Tekijä – Författare – Author
Petri Kristian Uuttu

Työn nimi – Arbetets titel – Title
Mineralization and formation conditions of metamorphic remobilization veins, Storliden VHMS deposit, Skellefte district, north Sweden

Oppiaine – Läroämne – Subject
geologia

Työn laji – Arbetets art – Level	Aika – Datum – Month and year	Sivumäärä – Sidoantal – Number of pages
Pro Gradu-tutkielma	11.2014	75

Tiivistelmä – Referat – Abstract

Skelleften alueella pohjois-Ruotsissa sijaitsevat paleoproterotsooiset VHMS-esiintymät ovat käyneet läpi alueellisen metamorfismin (ajoitettu 1,84 – 1,82 Ga) oloissa jotka vaihtelivat vihreäliuskefasieksesta amfibolifasiekseen. Metamorfismi johti malmimineraalien remobilisaatioon ja malmia sisältävien kvartsi- ja sulfidijuonten muodostumiseen. Tämän tutkielman tarkoituksena on tutkia Skelleftessä sijaitseva Storlidenin VHMS-esiintymän mineralogiaa ja mineraalikemiaa, ja määrittää missä oloissa remobilisaatio tapahtui.

Esiintymän sulfidirikkaat remobilisaatiojuonet koostuvat kahdesta tyypistä:
juonista jotka koostuvat pääosin magneettikiisusta ja kuparikiisusta, ja juonista jotka koostuvat pääosin lyijyhohteesta ja bournoniitistä, usein symplektiittisinä yhteenkasveumina, ja lisäksi huomattavista pitoisuuksista gudmundiittiä ja tetraedriittiä. Sinkkivälkettä ja arseenikiisua esiintyy useissa näytteissä kummastakin juonityypistä. Lisäksi esiintymä sisältää sulfidiköyhiä kvartsi- ja kalsiittijuonia. Esiintymä sisältää myös sulfidipitoisia kalsiittijuonia jota ovat muodostuneet metamorfismin jälkeen ja joita ei käsitelty tässä tutkielmassa.

Juonien sisältämä sinkkivälke ja kloriitti omaavat matalamman rauta-pitoisuuden kuin samat mineraalit massiivimalmissa ja sivukivessä. Juonien sinkkivälke omaa myös korkeamman Cd-pitoisuuden. Tetraedriitin koostumus eroaa myös huomattavasti juonien ja massiivisen malmin välillä. Juonien sisältämä tetraedriitti omaa huomattavasti matalammin arseenipitoisuuden ja korkeamman Fe/(Fe+Zn)-suhteen.

Remobilisaatiolämpötilat määriteltiin arseenikiisugeotermometrialla. Lasketut lämpötilat ovat väliltä 325 – 480 °C, keskimäärin 425 °C massiivimalmille ja 412 °C remobilisaatiojuonille. Massiivimalmin sinkkivälkkeen koostumuksen presteella määriteltiin metamorfismin tapahtuneen 6,3 – 8,5:n kbar paineessa (keskimäärin 7,5 kbar). Kvartsijuonten ja malmin sivukiven sisältämästä kloriitista lasketut lämpötilat ovat alhaisempia kuin arseenikiisusta lasketut, keskimäärin n. 200 °C tai vähemmän juonissa ja n. 300 °C sivukivessä (tarkat arvot riippuvat käytetystä geotermometristä). Alemmat lämpötilat viittaavat siihen että kloriitti on joko muodostunut tai muuttunut metamorfismin retrograadivaihessa. Kvartsijuonista lasketut veden δ18O-arvot vaihtelevat välillä 4,7 – 8,8 ‰ (keskimäärin 7,2 ‰), mikä sopii yhteen metamorfisen veden δ18O-pitoisuuden kanssa.

Lasketut arvot paineelle ja lämpötilalle sopivat yhteen muiden Skellfeten alueella sijaitsevista malmiesiintymistä tehtyjen tutkimusten kanssa. Suurin osa niistä mitatuista lämpötiloista ja paineista vaihtelevat välillä 300 – 500 °C ja 5 – 8 kbar massiivimalmilla sekä 200 – 450 °C ja 0,5 – 5 kbar juonille. δ18O-arvot ovat myös yhteensopivia muualta Skelleften alueelta sijaitsevista kvartsijuonista mitattujen arvojen kanssa (3,7 – 11,6 ‰).

Avainsanat – Nyckelord – Keywords
Remobilisaatio, Metamorfismi, Geotermobarometria, Arseenikiisu, Sinkkivälke, Kloriitti

Säilytyspaikka – Förvaringställe – Where deposited
Helsingin Yliopisto, geotieteiden ja maantieteen laitos, Kumpulan tiedekirjasto

Muita tietoja – Övriga uppgifter – Additional information

HELSINGIN YLIOPISTO – HELSINGFORS UNIVERSITET – UNIVERSITY OF HELSINKI

Tiedekunta/Osasto – Fakultet/Sektion – Faculty/Section	Laitos – Institution – Department
Faculty of Science	Geosciences and Geography

Tekijä – Författare – Author
Petri Kristian Uuttu

Työn nimi – Arbetets titel – Title
Mineralization and formation conditions of metamorphic remobilization veins, Storliden VHMS deposit, Skellefte district, north Sweden

Oppiaine – Läroämne – Subject
geology

Työn laji – Arbetets art – Level	Aika – Datum – Month and year	Sivumäärä – Sidoantal – Number of pages
MSc. project	11.2014	75

Tiivistelmä – Referat – Abstract

The Paleoproterozoic volcanically hosted massive sulfide deposits of the Skellefte district, northern Sweden has been subjected to regional metamorphism in greenschist to amphibole facies conditions at 1.84 – 1.82 Ga, resulting in the remobilization of ore minerals and formation of ore-bearing quartz and sulfide veins. The aim of this project is to study the mineralogy and mineral chemistry of the Storliden VHMS deposit in the Skellefte district and determine the conditions the remobilization of ore minerals took place in.

The sulfide-rich remobilization veins in the deposit consist of two types: ones composed mostly of pyrrhotite and chalcopyrite, and ones composed mostly of galena and bournonite, often as symplectitic intergrowths, with gudmundite and tetrahedrite occurring in notable amounts as well. Arsenopyrite and sphalerite were found in multiple veins of both types. Additionally, sulfide-poor quartz- and calcite veins occur in the deposit. There are also sulfide-bearing calcite veins that post-date the metamorphism, and were not included in this study.

Sphalerite and chlorite from the veins both have lower Fe-content than same minerals in the massive ore and the host rock of the ore, respectively. Sphalerite form the veins also has a significantly higher Cd-content compared to the massive ore. The tetrahedrite from the veins also has a clearly different composition than in the massive ore, with considerably lower As-content and higher Fe/(Fe+Zn) ratio.

Arsenopyrite geothermometry was used to determine that the remobilization took place at temperature of 325 – 480 °C, with mean T of 425 °C for the massive ore and 412 °C for the remobilization veins. The composition of sphalerite from the massive ore was used to determine that the pressure during metamorphism was 6.3 – 8.5 kbar, with mean of 7.5 kbar. Thermometric data obtained from chlorite in the quartz veins and the host rock of the ore indicates lower temperatures than the data from arsenopyrite, with mean T of around 200 °C or less for the veins and around 300 °C for the host rock (exact temperature depending on the geothermometer used). The lower range of temperatures likely reflects formation or re-equilibration during the retrograde stage of the metamorphism. The δ18O-data for water calculated from the quartz veins range from 4.7 to 8.8 ‰ with mean δ18O of 7.2 ‰, which is within the δ18O-range of metamorphic water.

The values for pressure and temperature obtained conform to data reported by other authors from various deposits in the Skellefte district, which mostly fall between temperatures of 300 – 500 °C and pressures of 5 – 8 kbar for the massive ore, and 200 – 450 °C and 0.5 – 5 kbar for the veins. The δ18O-data is likewise within the range reported from quartz veins elsewhere in the Skellefte district (ranging from 3.7 to 11.6 ‰).

Avainsanat – Nyckelord – Keywords
Remobilization, Metamorphism, Geothermobarometry, Arsenopyrite, Sphalerite, Chlorite

Säilytyspaikka – Förvaringställe – Where deposited
University of Helsinki, Department of Geosciences and Geography, Kumpula Science Library

Muita tietoja – Övriga uppgifter – Additional information

CONTENTS

1. INTRODUCTION

The Paleoproterozoic Skellefte district is a majort ore district in norther Sweden, containing large amounts of volcanic hosted massive sulfide (VHMS) deposits. The volcanic rocks hosting the ore deposits have an age of roughly 1.9 Ga, and are interpreted to have formed during accretion related to the Svecokarelian orogeny. Since their formation, the rocks and ores have undergone metamorphism under greenschist to higher facies conditions, as well as multiple phases of deformation. Metamorphism and remobilization of sulfide minerals, likely facilitated by metamorphic fluids, is a key factor in the formation of economically viable concentrations of ore minerals in metamorphic terranes, as the remobilization of the VHMS results in upgrading of the ore grade, and therefore in richer deposits. Understanding of the conditions remobilization took place in is important to understanding the geology of ore deposits and finding potential locations of previously unknown deposits. Furthermore, the composition the fluids involved in remobilization and the conditions in which minerals precipitated from them provides information about the metamorphic conditions in the area. While much work has already published about the VHMS deposits in the Skellefte district, for example the papers by Weihed et al. (2002), Wagner et al. (2004), Barret et al. (2005), Årebäck et al. (2005) and Weihed (2010), particularly on the largest deposits such as Kristeneberg and Boliden, many of the smaller deposits have been less studied. The aim of this paper is to study samples from one such deposit, the Storliden deposit located in the northwestern part of the district, and provide characterization of mineralogy and mineral chemistry, as well as establish the formation conditions of the deposit using mineral geothermobarometry.

2. GEOLOGICAL SETTING

2.1. Geology of the Skellefte district

The Skellefte district is a Paleoproterozoic ore-bearing volcanic-sedimentary domain in northern Sweden (Fig. 1), which covers an area of 150 by 50

kilometers, from Boliden in the east to Kristineberg in the west. The area contains over 85 massive sulfide deposits, mainly in the uppermost parts of the Skellefte group, the lowest stratigraphic unit in the district (Fig. 2), which is a volcanic sequence of felsic to intermediate volcanoclastic rocks, subvolcanic porphyritic intrusions, and lavas (Årebäck et al. 2005; Weihed et al. 1992; Weihed et al. 2002; Weihed 2010). The Skellefte group can be subdivided into two lower volcanic formations and an upper sedimentary formation (Weihed et al. 1992). The lower volcanic formation consists of rather homogeneous felsic pyroclastic deposits and lavas with minor intercalations of mafic lavas and pyroclastic rocks. The deposition of this formation terminated with a stage of hydrothermal activity and deposition of thin beds of fine-grained, volcanogenic sediments. The upper volcanic formation is geochemically bimodal and is comprised of mafic and felsic volcanites, reworked volcanic sediments, porphyry domes, lavas, and tuffs. The upper sedimentary formation is composed mostly of greywackes, with general coarsening upwards from fine grained greywackes to conglomerates (Weihed et al. 1992). Tholeitic lavas and tuffs are intercalated with the sediments in the western part of the district (Weihed et al. 1992). The Skellefte group has the total thickness of over 3 km. The volcanites of the group have been dated at around 1.89 – 1.88 Ga using U-Pb zircon geochronology (Årebäck et al. 2005; Weihed et al. 1992; Weihed et al. 2002; Weihed 2010). The Skellefte group is overlain by the sedimentary rocks of the Vargfors group, composed mostly of shales and turbiditic clastic rocks with some limestones and locally intercalated volcanic rocks. The Vargfors group has been dated at 1.875 Ga (Årebäck et al. 2005; Weihed et al. 1992; Weihed et al. 2002; Weihed 2010). There are at least three generations of granitoids, as well as one dioritic-gabbroic intrusion, intruding the rocks of the Skellefte district. The oldest intrusive rocks are the Jörn granitoids, the first generation of which (Jörn GI) are coeval with the Skellefte and Vargforst group rocks (~1.89 Ga) (Weihed et al. 1992; Wilson et al. 1987). The GI granitoids were succeeded by emplacement of GII – GIV of Jörn granitoids (Weihed et al. 1992). The Gallejaur monzodiorite-gabbro is slightly younger than the Jörn granitoids, having been dated at 1.873 ± 10 Ga (Skiöld 1988; Weihed 1992). These intrusive rocks are genetically related to the mafic volcanic rocks of the Vargfors group

(Weihed et al. 1992; Weihed et al. 2002). The Härno-Skellefte granitoids have been dated at 1.822 ± 5 Ga (Claesson and Lundqvist 1990; Weihed et al. 1992) and are considered late orogenic. The youngest intrusive rocks are the Revsund and Sorsele type granitoids, which are post-orogentic and have been dated at 1.80 – 1.77 Ga (Weihed et al. 1992).

The VHMS ores occur in the upper parts of the Skellefte group and in some cases in the lower part of the Vargfors group, and are considered to be of exhalative and replacement origin and largely syngenic with their volcanic host rocks (1.89 – 1.88 Ga). Some ore deposits (e.g. Boliden) have been proposed to be of epithermal origin and may be considerably younger than most VHMS ores (~1.85 Ga) (Weihed et al. 1992; Weihed et al. 2002).

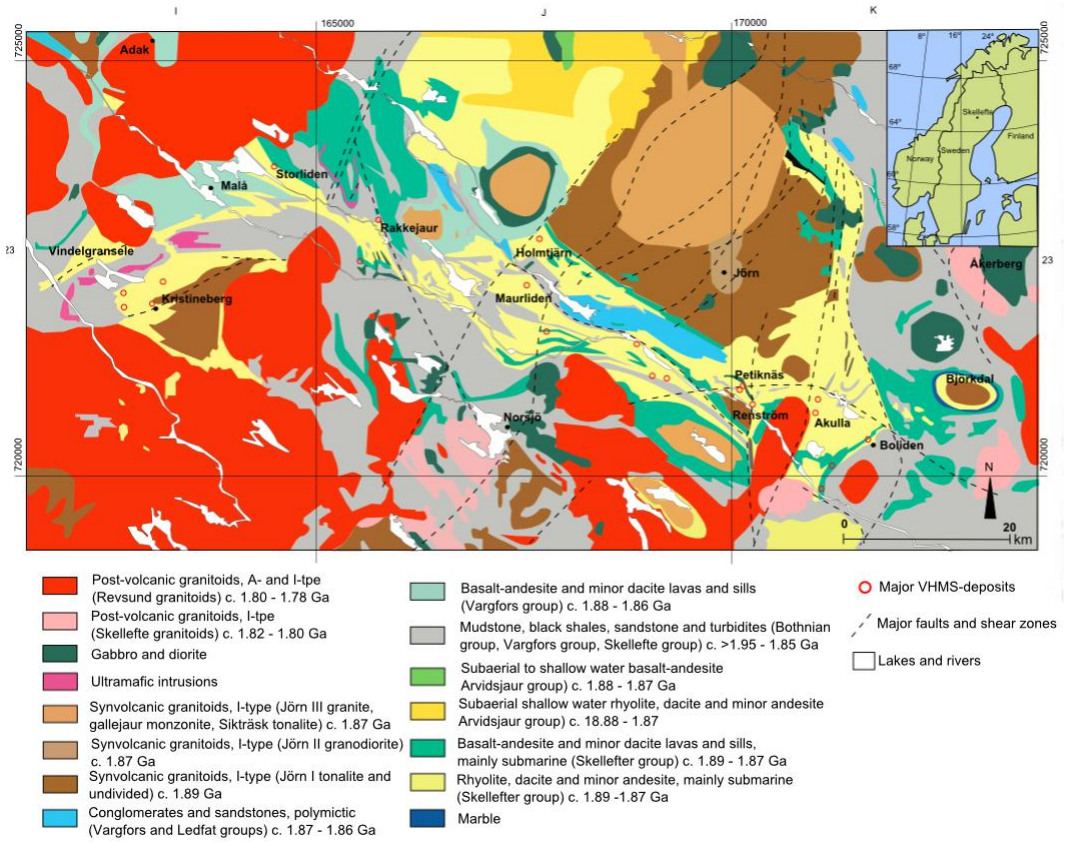

Figure 1: Geological map of the Skellefte district. Based on Årebäck et al. (2005).

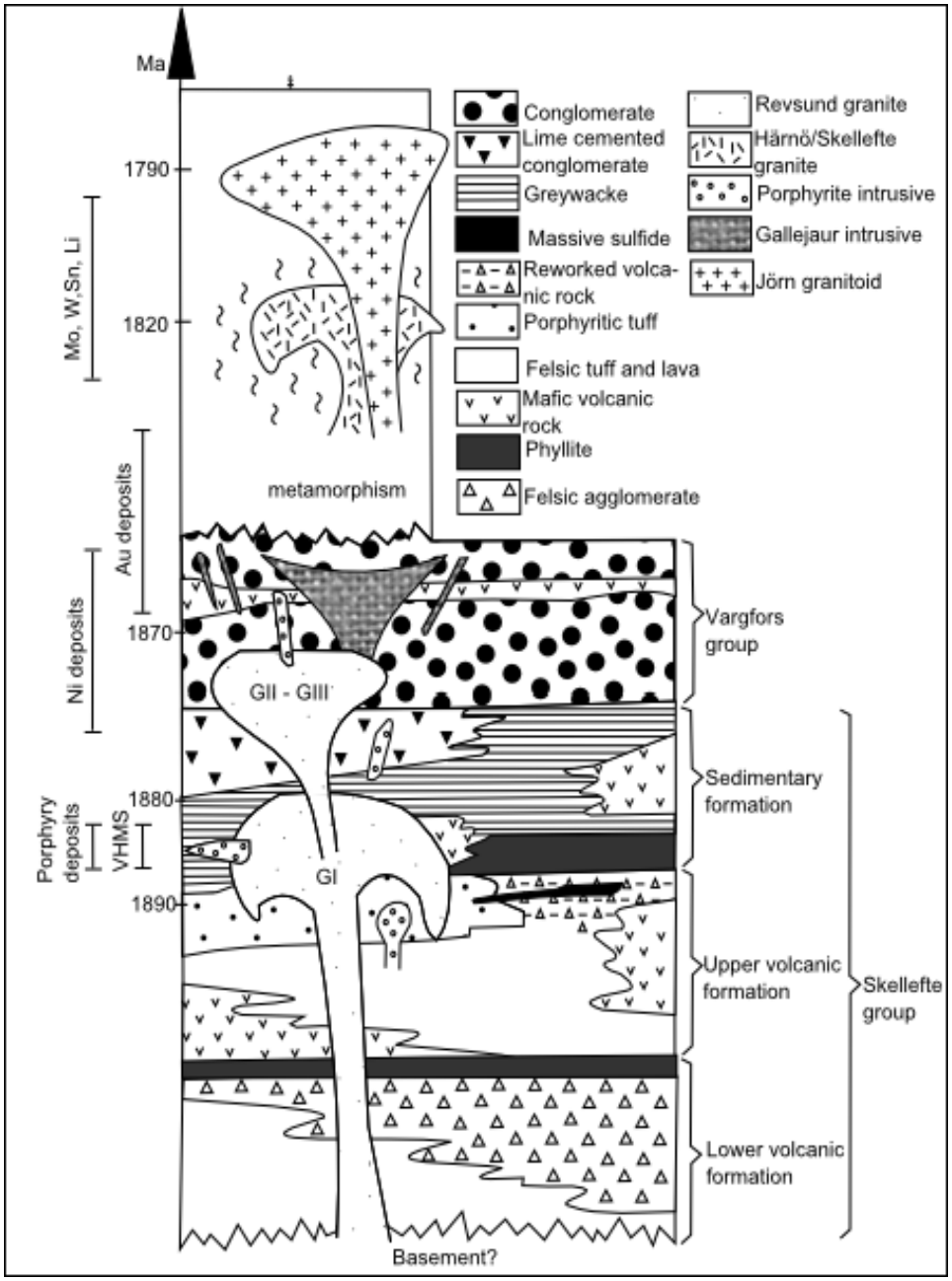

Figure 2: Stratigraphy of the Skellefte district. Based on Weihed et al. (1992).

The VHMS deposits consist of massive lenses or slabs composed primarily of pyrite, pyrrhotite, chalcopyrite and sphalerite. Pyrite is the dominant sulfide in most deposits (Weihed et al. 1992). The ores are rich in Zn and As, with variable amounts of Cu, Pb Ag and Au. Zoning is common, with distal Zn and proximal Cu (Weihed et al. 1992). The massive sulfide deposits are associated with felsic pyroclastic rocks, quartz porphyries and minor mafic volcanics in the footwall and calcareous or graphitic reworked volcanics or tuffitic rocks often occurring in the hanging wall (Weihed et al. 1992). The ore deposits are often accompanied by

hydrothermally altered rocks, though these alterations are often irregular and sometimes absent. The hydrothermal alteration consists of chloritic, sericitic and silicic types, with sericitic type dominating proximal alterations and silicic type prominent in the distal parts of the orebodies. Chloritic alteration tends to be more regional, although it is also common in the proximal alteration aureoles (Berglund 1980; Weihed et al. 1992). Broman (1987) suggested to have found primary fluid inclusions in the massive ore that show the ores were deposited on the sea floor from Ca-Na-Cl solutions during two phases of mineralization, at temperatures of 210 °C and 295 °C, respectively. After their formation the ore deposits have been affected by the regional deformation and metamorphosis, which led to the remobilization of ore minerals and formation of Au±Ag ore-bearing quartz veins (Weihed et al. 1992; Weihed et al. 2002). The fluids involved in the metamorphism and remobilization were of three main types: CO_2-rich fluids, hydrocarbon-rich fluids and saline aqueous solutions (Broman 1998; Weihed 1992). It is likely that sulfide precipitation and remobilization has occurred in several stages from the emplacement of the Skellefte (1.89 Ga) group to the intrusion of the Revsund granite (1.78 Ga) (Weihed et al. 2002).

The relatively low Nb content of the felsic volcanites (10 – 20 ppm measured at the Kristineberg deposit) suggests that the magma was formed in a subduction-related setting (Barrett et al. 2005). However, the extremely felsic nature of many of the volcanic rocks of the Skellefte group does not fit into the model of a primitive island arc (Allen 1997; Weihed 2010). The rocks in the central and eastern parts of the Skellefte district are of calc-alcaline affinity, which is unusual for Archean and Proterozoic VHMS deposits, the majority of which are hosted in tholeitic rocks. However, this signature is typical for modern mature island arcs and nascent back-arc basins. Multiple hypothesis of the tectonic setting in which the volcanic units of the Skellefte group have formed have been proposed, many of which point to the deposits originating in the subduction zone or the intra-arc region of a continental arc or a mature island arc (Weihed et al. 1992; Barrett et al. 2005; Weihed 2010 and references therein). However, the basement of the Skellefte group is not exposed, which has made verifying these hypotheses difficult. The strata of the district is generally moderately to steeply dipping, and

regional and structural trends indicate that it youngs towards south (Barrett et al. 2005, Årebäck et al. 2005).

According to Weihed et al (1992), at least two major phases of deformation have occurred in the Skellefte district. The folds associated with the first deformation phase (D_1) are steep and isoclinal, with NW-SE striking axial surfaces. This NW-SE strike dominates the western and central part of the district but swings through east to northeast in the eastern part of the district. In the central district F_1 folds are upright and tight to isoclinal, but fold axes are variable: most of them plunge at 45º, but a range of plunges between SE and SW has been observed. A steep, WNW-ESE striking, axial planar S_1 cleavage developed during D_1 as a penetrative grain shape foliation in coarser volcanic rocks, but as a spaced crenulation cleavage in laminated tufts and schists. Penecontemporaneous slip along the S_1 cleavage is common, and in some localities may have developed into over 25 km long shear zones. A second deformation phase (D_2) is coaxial with the first folding, and involved open folding with NNE-SSW striking axial planes and subvertical fold axes. A number of N-S striking shear zones in the Skellefte district are interpreted as having formed during D_2 (Weihed et al. 1992; Weihed et al. 2002). Mapping in the Skellefte district by the Geological Survey of Sweden indicates that there was also another deformation phase that occurred at 1.90 – 1.86 Ga, predating the one defined by Weihed et al. (1992) as D_1 (Årebäck et al. 2005, and references therein).

The absolute timing of deformation is poorly constrained. No differences in structural style can be observed between the deepest exposed level in the volcanic pile and the uppermost Vargfors sedimentary units and andesitic lavas. This implies that the D_1 deformation phase was not completed by 1.87 Ga, the age of crystallization of the Gallejaur monzonite and related extrusive andesitic lavas. On the other hand, the deformation must predate the intrusion of the Härno-Skellefte granites, dated at ~1.82 – 1.80 Ga, which are unaffected by it. D_1 is thus established to have taken place between 1.87 Ga and 1.82 Ga (Weihed et al. 1992; Weihed et al. 2002). The N-S striking shear zones which may be associated with S_2 foliation and the second deformation phase appear to be coeval with the Revsund granite (1.78 Ga) (Weihed et al. in press, according to Weihed et al.

2002).

Porphyroblasts of andalusite, cordierite and staurolite have grown across the bedding and S_1 foliation, but are deformed by the S_2 crenulation cleavage, indicating that the peak of metamorphism occurred after the formation of S_1 cleavage but predates the D_2 deformation phase and the formation of S_2 cleavage (Weihed et al. 2002). Peak metamorphism took place under upper greenschist facies conditions, with amphibolite facies reached in some areas close to the southern and western margins of the district, and has been estimated to have taken place at 1.84 – 1.82 Ga. (Weihed et al. 1992; Årebäck et al. 2005).

2.2. Geology of the Storliden deposit

The Storliden deposit itself (Fig. 3) is located in the northwestern area of the district. Its host rocks are composed of felsic to intermediate metavolcanics, mostly of rhyolitic and dacitic composition, with minor andesite. Located immediately southwest of the deposit are mafic to intermediate metavolcanics, mostly basaltic and andesitic, with minor dacite lavas and sills. Both rocks appear to have been deposited mostly in a submarine enviroment, and are of the similar age, 1.89 – 1.87 Ga (Årebäck et al. 2005). The lower part of the deposit's stratigraphy consists of weakly deformed and metamorphosed basaltic and andesistic tuffaceous sandstones and Al-rich porphyritic pillow lavas, while the upper part consists of a bimodal sequence that includes andesitic tuffaceous sandstones, felsic syn-volcanic sills and juvenile resedimented pyroclastic rocks. Both mafic and felsic rocks have Zr/Y ratios of < 4 and flat REE pattern, with $La_n/Yb_n < 2$, indicating tholeiitic sources (Imaña et al. 2005).

The bulk of the ore mineralization occurs between the contact of a thick felsic pumice- and crystal-rich volcanoclastic unit and an overlying andesitic tuffaceous unit. The orebody forms a single flat-lying stratabound lens composed primarily of sphalerite, chalcopyrite, pyrrhotite and calcite, with almost no pyrite. Compared to other VHMS deposits in the district, the sulfide ore at Storliden is very coarse grained. It represents a high-grade Cu-Zn orebody, containing 1.8 Mt of ore, with 10.9 % Zn, 3.5 % Cu, 0.25 g/t Au and 24 g/t Ag (Imaña et al. 2005). Sulfide-bearing remobilization veins are found in and around the orebody.

Storliden has an asymmetric alteration system, which consists of six metamorphosed alteration facies. The innermost zone is composed of intensely silicified rocks, surrounded by a layer of spinel-orthoamphibole-humite. The outer zones are composed of spotted cordierite-anthophyllite, cordierite-phlogopite and biotite-muscovite assemblages. Skarn alteration is common, primarily where inner alteration zones overprint diagenetic pods of calcitic alteration. Fracture-controlled alteration zones are well developed near the central part of the orebody. Relict silicified volcanoclastics in the orebody suggest that the ore formed by replacement of volcanoclastic sedimentary rocks (Imaña et al. 2005). A younger vein system with calcite and sulfides crosscuts the host rocks, massive ore and remobilization veins.

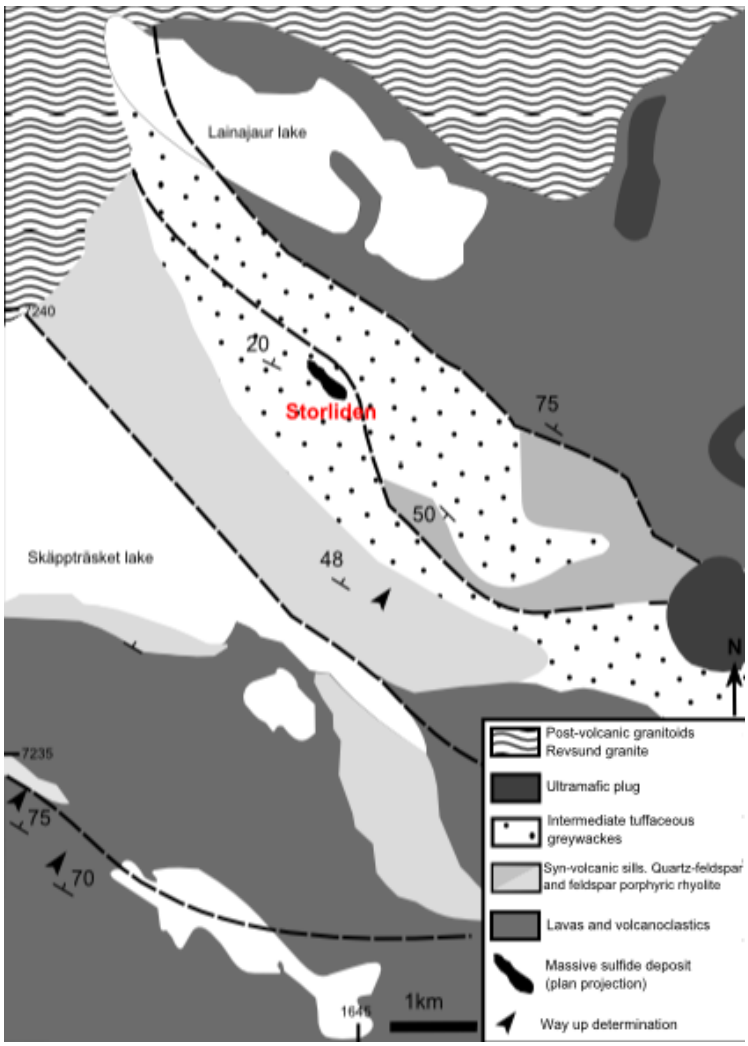

Figure 3: Geological map of the area surrounding the Storliden deposit. Based on Imaña et al. (2005).

3. MATERIALS

The materials for the project consisted of 56 samples, 44 of which were collected from the Storliden mine and 12 of which were collected from drill cores. All samples are listed in the appendix (Table 10). The samples consisted of meta-volcanic and meta-sedimentary rocks with sulfide-, quartz- and calcite veins, as well as sections of massive sulfide ore. The samples included ore sections (28 mine samples and 6 drill core samples), which contained sections of massive ore and vein rocks, and thin sections (18 mine samples and 6 drill core samples), which were taken from the host rock of the orebody as well as from quartz- and calcite-bearing veins. Whole rock samples and cut-off blocks were also available from most samples. Five cut off blocks from quartz veins and one from a calcite vein were cut into 300 µm thick doubly polished sections for use in fluid inclusion studies. In addition to the samples, oxygen isotope data from selected quartz vein samples had been measured prior to the project and was available for use.

4. METHODS

4.1. Petrography

The samples were first analyzed using an optical microscope, using both transmitted and reflected light microscopy, in order to determine the textures of the mineralizations, common mineral assemblages and internal structures.

4.2. Electron microprobe analysis

The selected samples were analyzed with an electron microprobe. The microprobe used was a JXA-8600 Jeol superprobe.

In order to ascertain the identity of some minerals and to prepare the fully qualitative analysis, ten samples were investigated with quantitative EDS (energy dispersive spectroscopy)-analysis. The purpose of this analysis was to identify the elements present in the minerals and to calculate qualitative mineral formulas which might help in determining minerals that could not be identified with optical

microscopy. The acceleration voltage used was 15 kV for analysis of silicate minerals and 20 kV for samples that also contained ore minerals. The probe current used was 1 nA. Prior to analysis the samples were carbon coated with a vacuum evaporator. The proper thickness of the coating (~20 nm) was ensured by observing a brass standard.

Following the EDS-analysis, samples were selected for a fully quantitative WDS (wavelenght dispersive spectroscopy)-analysis, the aim of which was to determine the composition of the minerals (sphalerite, arsenopyrite and tetrahedrite-tennantite) for possible use in geothermobarometry, as well as to confirm minerals that could not be conclusively determined with optical microscope or EDS-analysis. Furthermore, WDS-analysis was used to characterize the differences in composition between the massive sulfide ore and the remobilized sulfides. Ten samples, four from the remobilization veins and six others (massive ore and host rocks of the orebody that contained large amounts of ore minerals), were selected based on the presence of mineral assemblages suitable for geothermobarometry (sphalerite-pyrite-pyrrhotite and arsenopyrite-pyrite-pyrrhotite), tetrahedrite-tennantite and of the unknown minerals. Analyzed spots in each sample were selected based on optical microscope images before the samples were carbon coated in the same manner as the samples used for the EDS-analysis. The analyses were done with focused beam (1 – 2 μW beam size), with acceleration voltage of 20 kV and beam current of 20 nA. Three analyses were performed on each selected spot in order to minimize the effect of errors during measurement. The composition of chlorite in 10 samples was analyzed for use in geothermometry. One of the samples also contained large arsenopyrite grains which, although without a sulfur fugacity buffering assemblage, were nevertheless analyzed to gain more data for geothermometry. Like the ore mineral analyses, the chlorite analyses were done with focused beam. The acceleration voltage and beam current used were 15 kV and 15 nA, The list of analyzed elements, the standards used and the analyzed energy-lines for each element for both ore mineral and chlorite analyses are listed in Table 1.

Table 1: Analyzed elements, the standards used and energy lines analyzed.

Ore minerals			Chlorite		
Element	**Standards**	**Energy-line**	**Element**	**Standards**	**Energy-line**
S	pyrite, sphalerite, galena	K-α	Na	albite	K-α
Mn	rhodonite	K-α	Si	biotite	K-α
Fe	pyrite	K-α	K	biotite	K-α
Ni	Ni-sulfide	K-α	Cr	Cr-oxide	K-α
Cu	cuprite	K-α	Fe	hematite	K-α
Zn	sphalerite	K-α	Mg	periclase	K-α
As	Ga-arsenide	L-α	Al	plagioclase	K-α
Se	Bi-selenide	L-α	Ca	plagioclase	K-α
Ag	silver	L-α	Mn	rhodonite	K-α
Cd	cadmium	L-α	Ti	rutile	K-α
Sn	cassiterite	L-α	Beam size: 1 – 2 µW		
Sb	stibnite	L-α	Current (ore): 20 kV		
Te	Sb-telluride	L-α	Voltage (ore): 20 nA		
Au	gold	L-α	Current (chlorite): 15 kV		
Hg	cinnabar	L-α	Voltage (chlorite): 15 nA		
Bi	Bi-selenide	L-α			
Pb	galena	M-α			

4.3. Geothermobarometry

In order to determine the temperature and pressure condition during ore formation, the samples were examined for sulfide minerals that could be used as geothermometers and -barometers. For geothermobarometry to give reliable results, the necessary minerals must be in chemical equilibrium with mineral assemblages that can buffer chemical potentials that control their composition (eg. sulfur and oxygen fugacity). Equilibrium between minerals is typically achieved if they are in grain contact, so the samples were searched for places were the necessary minerals were found in contact with each other.

Of the sulfides found in the samples, sphalerite is established to function as a geobarometer (Scott, 1976) and arsenopyrite as a geothermometer (Kretchmar and Scott, 1976), so these minerals were chosen to be used as such in this study. The FeS-content of sphalerite correlates with pressure when the FeS-activity is being buffered by pyrite and hexagonal pyrrhotite, with the Mol% FeS of the sphalerite decreasing as pressure increases. Combined with the abundance of sphalerite in most sulfide deposits and its rather refractory nature, this makes it an extremely useful geobarometer in sulfide ores (Scott, 1976). Similarly, the As/S ratio of

arsenopyrite correlates with temperature when the sulfur activity is being buffered by other a(S_2)-dependent iron- or arsenic sulfides, including pyrite and pyrrhotite (Kretchmar and Scott, 1976), allowing temperatures to be determined from the As concentration in arsenopyrite. Similarly to sphalerite, arsenopyrite is common in many types of sulfide ores and is the most refractory of the common sulfides.

In addition to the sulfide minerals, chlorite was also used as a geothermometer. The "traditional" empirical chlorite geothermometer is based on the tetrahedral Aluminum (Al^{IV}) content of chlorite, which increases as a function of temperature (Cathelineu 1988, Jiang et al. 1994, López-Munguira et al. 2002, Vidal et al. 2007). However, this method is often unreliable as there is also a strong correlation between chlorite composition and the MgO (and FeO) content of the host rock (López-Munguira et al. 2002). Furthermore, study by Jiang et al. (1994) suggests that the measured Al^{IV}-content may be greatly affected by even small amount of contamination by other minerals such as kaolinite or muscovite, causing inaccurate results. The use of octahedral vacancies (□) in chlorite, the amount of which decreases as a function of temperature, instead of Al^{IV} has been shown to give more accurate geothermometric results that are less affected by factors other than the temperature (Lanari et al. 2014a).

Bourdelle et al. (2013) and Lanari et al. (2014a) have developed more accurate chlorite thermometers using thermodynamic activity-composition models based on several chlorite end-members: Mg- and Fe- end-members of 'Al-free chlorite S' ($(Mg, Fe)_6Si_4O_{10}(OH)_8$), sudoite ($(Mg_2(AlFe^{3+})_3Si_3AlO_{10}(OH)_8$) and amesite ($Mg_6Al_2(Si,Al)_2O_{10}(OH)_8$) in the former, and amesite, sudoite, chlinochlore ($(Mg, Fe^{3+})_5Al(Si_3, Al)O_{10}(OH)_8$) and daphnite ($AlFe_5Si_3AlO_{10}(OH)_8$) in the latter, which take into account all major crystalochemical substitutions that occur in chlorite: Fe^{2+} - Mg substitution, Tschermak substitution ($Al^{IV}Al^{VI} = Si(Mg,Fe^{2+})$) and di/trioctahedral substitution ($3(Mg,Fe^{2+}) = □ + 2Al^{VI}$). These models produce more accurate results than a purely empirical thermometer (Bourdelle et al., 2013, Lanari et al., 2014a).

The thermometers by Lanari et al. have been shown to give accurate results over P-T range of 100 – 500 °C and 1 – 20 kbar, while the thermometer by Bourdelle et al. has been calibrated in the range of T < 350 °C and P < 4 kbar. The

paper by Lanari et al. (2014) presents two version of their thermometer, Chl (1), which requires knowledge of $Fe^{3+}/\Sigma Fe$ ratio in chlorite, and Chl(2), which assumes all iron is Fe^{2+}. As the ratio of ferrous to ferric iron can not be determined using EMPA analysis, this study used the Chl(2)-version.

5. RESULTS

5.1. Petrography

The host rock of the ore minerals is a fine-grained grey meta-volcanic rock composed primarily of quartz, feldspar and mafic minerals (primarily biotite and other micas) and their alteration products (primarily chlorite) (Fig. 4 A). Samples form skarn rocks, such as STO-24 (Fig. 4 B), have slightly larger grain sizes and less micas and chlorite. They also contain larger amounts of calcite, visible as white spots in some of the samples. Samples from shear zones, such as STO-4, contain more mafic minerals with larger grain size. The ore minerals in the host rock are primarily found disseminated as small grains with diameter of ~1 mm or less. Larger grains are also found in varying amounts in many samples. The massive ore lenses (Fig. 4 C) contain massive inclusions of ore surrounded by large amounts of disseminated ore mineral grains. The ore is primarily composed of chalcopyrite and pyrrhotite, with large amounts of sphalerite inclusions, especially inside chalcopyrite.

The remobilizations veins are present in two distinct types. First type is composed of quartz- or calcite veins with varying amounts of disseminated ore minerals (Fig. 4 D). The amount of ore minerals in the veins ranges from few small disseminated grains, to coarse grains with diameters of ~10 mm and large amounts of smaller grains. The ore minerals in the veins are primarily chalcopyrite, pyrrhotite and galena. The quartz veins consist mostly of heterogranular subhedral to anhedral quartz grains with small amounts of minor minerals. Quartz grains possess textures typical for recrystallization, with sutured grain boundaries and irregular grain shapes. Grain size varies between samples, but is generally around 1 mm. The grains in calcite veins are polygonal, unlike the irregularly shaped quartz grains. Calcite grains typically have well-defined

cleavages and in some samples they exhibit polysynthetic twinning.

The second type of veins is composed primarily of remobilized sulfides. Their mineralogy and internal structures range from very simple, such as sample STOB-98051-123.8 (Fig. 4 E), where the vein consists of a pyrrhotite core and chalcopyrite margin, to a more complex assemblage of minerals, such as sample STO-28 (Fig. 4 F), which contains large amounts of chalcopyrite, pyrrhotite, galena and arsenopyrite, both massive inclusions and partially to wholly intact grains of varying sizes. While some veins have a mineralogy similar to massive ore (i.e., mostly composed of chalcopyrite and pyrrhotite), others are composed primarily out of galena and other Pb-sulfosalts, which commonly form symplectitic intergrowth. More details of the mineral assemblages and textures are given in chapter 5.2.

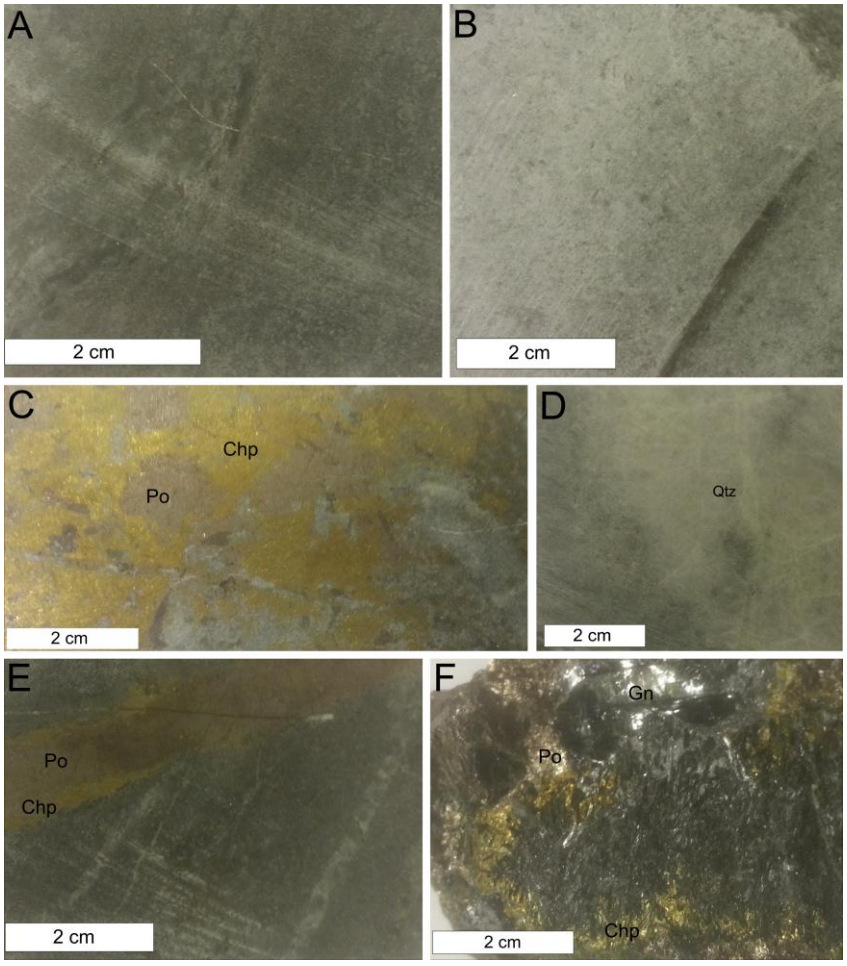

Figure 4: Photographs of hand samples. A: STOB-98070-105.6: host rock with chlorite-biotite and disseminated ore minerals. B: STO-24: host rock with skarn alteration. C: STOB98051-144.6: Massive chp-po ore. D: STO-5: quartz vein with minor amount of disseminated ore minerals. E: STOB95041-123.8: sulfide-rich vein with chp and po. F: STO-28: sulfide-rich vein with chp, po, gn and smaller amounts of other ore minerals. chp=chalcopyrite, gn=galena, po=pyrrhotite, qtz=quartz.

5.1.1. Internal structures of the samples

The samples were largely devoid of pre-metamorphic internal structures, likely because any traces of them having been obliterated during metamorphism.

The most obvious syn-metamorphic structures are the remobilization veins. Samples taken from the host of the massive ore also contain small cracks and veinlets which likely have a shared origin with the large remobilization veins. The massive ore sample STO-4A also shows signs of microscale remobilization, with a crack in massive pyrrhotite that was filled by chalcopyrite seemingly derived from a chalcopyrite mineralization next to the pyrrhotite.

Evidence of ductile deformation are present in several samples, primarily in the remobilization veins. These are most apparent as bending and microscale folding in the more massive portions of galena in the veins, but in parts of sample STO-37 sphalerite and gangue minerals also show microscale folding and in STO-34 multiple chalcopyrite inclusions in sphalerite have in some areas of the sample been stretched out and aligned along the same direction. The micas in samples STOB-98070-105.6 and STOB-98070-107.6 have a banded structure, which is likely to have been formed by mica crystals aligning normal to the direction low stress. However, as the original position of the samples in unknown, the direction of the stress field could not be determined.

Additionally some ore samples showed signs of brittle deformation, such as cracks in the host rock of the ore in several samples and large amounts of cracks and fractures in arsenopyrite in sample STOB-98070-93.4. Given the relatively low temperature at which most sulfides except pyrite pass the brittle-ductile transition (around 200 – 350 °C) (Marshall and Gilligan 1987), the cracks in STOB-98070-93.4 are likely either retrograde or post-metamorphic in origin.

5.1.2. Fluid inclusions

Fluid inclusions (FI) occur both in quartz and calcite veins. They most commonly occur as trails of small inclusions that are likely associated with healed microcracks. Most of these trails of inclusions are confined to single grains (and therefore more likely to be pseudosecondary) running from one grain border to another grain border or through the interior of the grain (Fig. 5 A). Secondary trails that cross over grain boundaries were also observed (Fig. 5 B), as were trails

that run along grain boundaries (Fig. 5 C), although these are rarer. Some inclusions are found in unidentifiable positions, often clustered together, but they are rarer than the trails or the inclusions aligned along grain boundaries. These are likely trails of inclusions that were at a high angle to the direction the think sections were cut.

Most inclusions have a diameter of about 2 – 5 µm. Few large inclusions were observed, but they are rare. Recrystallization of the quartz grains has likely destroyed any larger primary inclusions. The largest inclusions are irregularly shaped, usually considerably longer along one direction than the other (for example 5 µm in one direction and 20 µm in the other one) (Fig. 5 D). Considering the direction of elongation, such FI are typically aligned parallel to other inclusions in the trail. The calcite vein contains some larger (close to 50 µm size) inclusions that are more regularly shaped. The samples contain both aqueous and CO_2-rich inclusions. Some inclusions have a bubble indicating presence of multiple phases (likely H_2O-NaCl or H_2O-CO_2-NaCl). Such inclusions are found in the quartz vein samples (Fig. 5 E), but are larger and more common in the calcite vein samples (Fig. 5 F). Unfortunately, the small size of most inclusions and the observed evidence of necking down of most of the larger ones meant that the vast majority of inclusions would be too small for microthermometric measurements.

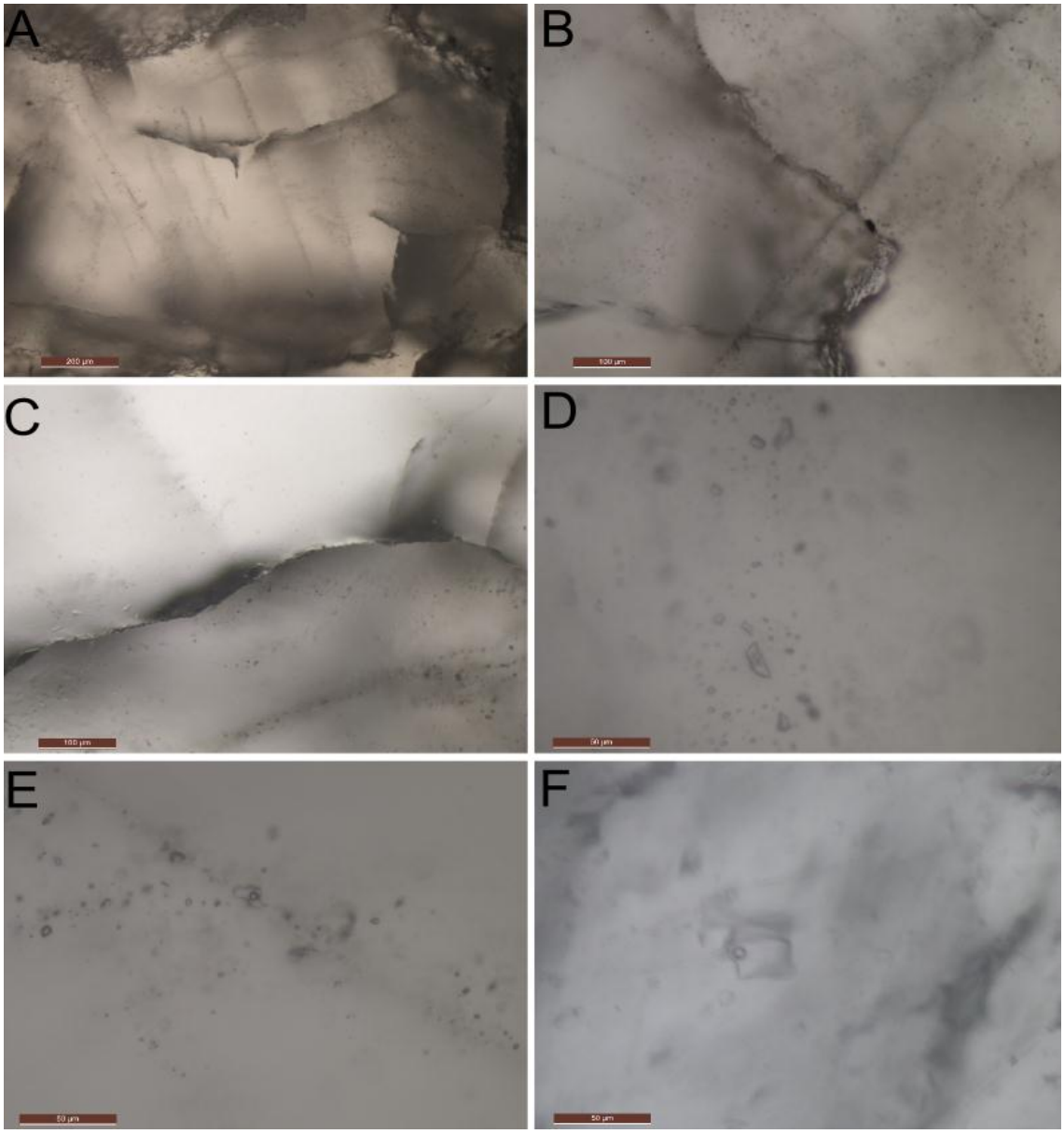

Figure 5: Fluid inclusions. A: Intragranular inclusion trails, sample STO-6B. B: Intergranular inclusion trail, sample STO-5. C: Inclusion trail running parallel to grian border, sample STO-5. D: Close-up on an inclusion trail, sample STO-42. E: Inclusion with a gas bubble in quartz vein, sample STO-5. F: Large inclusion with a gas bubble in calcite vein, sample STO-35.

5.2. Mineralogy

5.2.1. Massive ore

The massive ore consists primarily of pyrrhotite and chalcopyrite with large amounts of sphalerite inclusions, especially inside chalcopyrite (Fig. 6 B and C). All three minerals possess anhedral textures and commonly contain inclusions of the other two minerals. The ratio of pyrrhotite to chalcopyrite varies between samples, from dominantly pyrrhotite to dominantly chalcopyrite. Sphalerite inclusions vary widely in size, but they usually have small blebs and needle-

shaped inclusions of chalcopyrite inside them (the so-called “chalcopyrite disease”). While sphalerite is primarily found as inclusions in chalcopyrite-rich samples, there are some samples that consist mostly out of massive sphalerite with inclusions of pyrrhotite and chalcopyrite.

Arsenopyrite is a common minor phase in the massive ore, occurring as subhedral or euhedral inclusions and porphyroblasts in multiple samples. The largest of these are several hundreds of μm in diameter. The sample STOB-98070-93.4 (Fig. 6 D) in particular contains large amounts of arsenopyrite. This sample is unusual in that it contains almost no pyrrhotite, but instead contains large amounts of coarse-grained arsenopyrite as a major phase. In most samples, arsenopyrite shows little signs of damage or deformation, but in STOB-98070-93.4 it contains large amounts of crosscutting fractures.

Pyrite is mostly absent from the samples, or only occurs as a few very small grains. Three samples, however, contain large amounts of pyrite: STO-14 (Fig. 6 A and B) (which contains some large pyrite porphyroblasts, the largest of which is more than 1,000 μm in size, as well as fine-grained pyrite grains), STOB-98070-101.8 (Fig. 6 E) (which contains large amounts of pyrite grains, ranging from tens to a few hundred μm in diameter, in contact with sphalerite and pyrrhotite) and STOB-98070-93.4 (which has pyrite coexisting with large amounts of arsenopyrite). Despite pyrite coexisting with both arsenopyrite and pyrrhotite in different samples, no sample contains notable amounts of all three minerals.

Hematite and ilmenite are present as minor phases in several samples, occurring as small grains (rarely more than 10 μm in diameter). In several samples the minerals are closely associated, although there are some samples which only contain one of the two minerals.

Additionally, while primarily occurring in the remobilization veins, galena occurs in small amounts in some massive ore samples. These may represent small veinlets with remobilized sulfides that are crosscutting the massive ore. The sample STO-07c (Fig. 6 E), however, contains notable amounts of coarse-grained galena. STO-07c is also the only massive ore sample that contains notable amounts of tetrahedrite-tennantite ($(Cu,Fe)_{12}Sb_4S_{13}$ – $(Cu,Fe)_{12}As_4S_{13}$), a phase that in other massive ore samples only occurs as a few small grains, if at all.

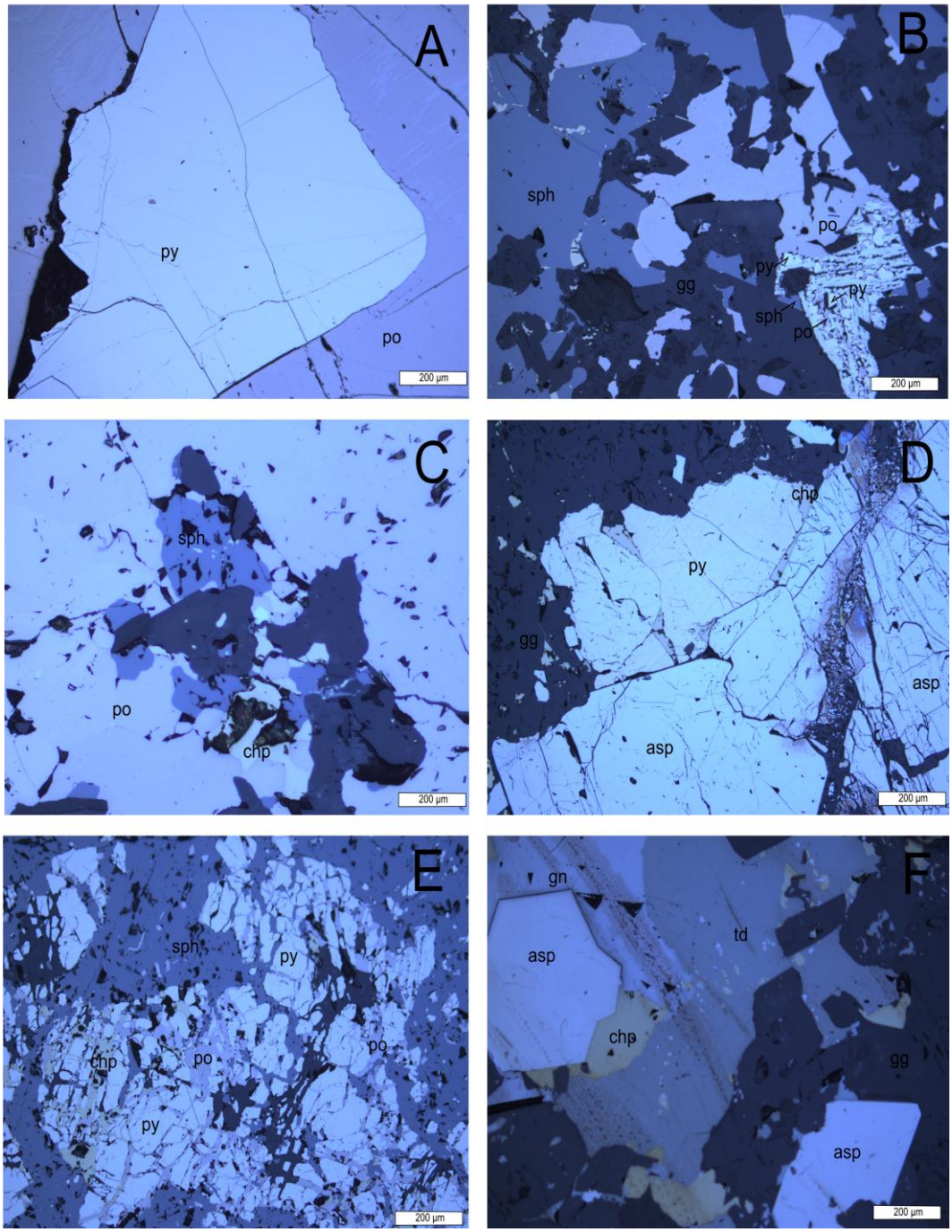

Figure 6: Ore minerals and texture of massive ore. A: STO-14, py porphyroblast in massive po. B: ST-14, small py grains with po and sph. C: STO-37, massive po with sph and chp inclusions. D: STOB-98070-93.4, coarse-grained asp and py. E: STOB-98070-101.8, py and po in massive asp. F: STO-07c, massive td and ga. asp=arsenopyrite, chp=chalcopyrite, gg=gangue, gn=galena, po=pyrrhotite, py=pyrite, sph=sphalerite, td=tetrahedrite.

5.2.2 Remobilization veins

The samples from the remobilization veins can be grouped into different types: pyrrhotite-chalcopyrite sulfide veins, galena-bournonite sulfide veins and sulfide-poor quartz and calcite veins.

The ore minerals in the pyrrhotite-chalcopyrite veins consist primarily of pyrrhotite and chalcopyrite (Fig. 7 F). Sphalerite inclusions are also common, especially inside chalcopyrite. Gangue minerals consist mostly of quartz, although sample STO-19b also contains notable amounts of chlorite. In some veins the ore minerals are hosted inside quartz veins, while other veins, such as the one in sample STOB-98051-123.8, are composed entirely out of ore minerals. Minor amounts of ilmenite, hematite, arsenopyrite, galena and/or tetrahedrite occur in some of the samples. The sample STOB-98051-123.8 is unusual in that it contains multiple unusually large (a few hundred μm in diameter) hematite inclusions inside pyrrhotite and chalcopyrite. The same sample also contains fine grained arsenopyrite, primarily along the vein margins, and a few extremely small grains of cassiterite.

The ore minerals in the galena-bournonite veins consist primarily of galena, bournonite ($PbCuSbS_3$), gudmundite (FeSbS) and tetrahedrite-tennantite (Fig. 7 , B, C, D and E). Gangue minerals consist primarily of quartz. As with the pyrrhotite-chalcopyrite veins, some of the veins are composed entirely out of ore minerals, while others consist of inclusions of ore minerals in a quartz matrix. The textures and mineralogy of these veins are more complex than in the pyrrhotite-chalcopyrite veins. Galena and bournonite are the most common minerals in these veins, and are closely associated with each other. Galena occurs with both massive coarse grained texture (often with bournonite inclusions) and as symplectitic intergrowths with bournonite. The ratio of galena to bournonite varies between samples from dominantly galena to dominantly bournonite. Gudmundite is usually found as small subhedral inclusions associated with galena and bournonite. Sample STO-28a (Fig. 7 C)contains large amounts of gudmundite, mostly as a rim around bournonite-galena mineralizations, while sample STO-6a is noteworthy for containing more gudmundite inclusions than bournonite in massive galena. Tetrahedrite occurs in these veins as large anhedral grains, including grains of more than 1 cm in size in sample STO-6a (Fig. 7 A). The grains are often surrounded by a rim of galena, bournonite and gudmundite.

Several minor phases occur in the galena-bournonite veins as well, some occurring in multiple samples, while others only in a single one. Pyrrhotite,

chalcopyrite and sphalerite occur in varying amounts in multiple samples. Arsenopyrite occurs in some samples, most notably in the STO-28 samples (which contain multiple arsenopyrite grains of varying sized,) and sample STO-50, which contains a large (about 1,000 µm in size) arsenopyrite porphyroblast (Fig. 7 E). Sample STO-50 also contains notable amounts of boulangerite ($Pb_5Sb_4S_{11}$) (Fig. 7 D), a sulfosalt that was not encountered in any other sample. It is present as inclusions of varying size along with galena and bournonite. Additionally, small amounts of native Bi are present as inclusions in bournonite in sample STO-28c.

The sulfide-poor quartz veins and calcite veins are composed mostly of quartz and calcite, respectively, with epidote as a common accessory mineral. Some quartz veins also contain small amounts of calcite, and calcite veins small amounts of quartz. Small amounts of chlorite occur as aggregates of small needle-shaped crystals in samples STO-18 and STO-28c. Sample STO-40 contains larger amounts of chlorite along the contact of the quartz vein and the host rock. Only minor amounts of disseminated sulfides (most commonly pyrrhotite+chalcopyrite±sphalerite and/or galena, but some samples also contain arsenopyrite, bournonite and/or tetrahedrite) are found in these veins. In most of the samples sulfide minerals occur as few small disseminated grains, but some, such as sample STO-39, also contain larger (a few hundred µm in size) sulfide mineralizations. The calcite veins are more sulfide-poor than quartz veins. Sample STO-18 contained an unrecognized Cal-Al silicate with notable amounts of Ce and Nd in close association with grains of ilmenite. This most likely conforms to allanite ($(Ce,Ca,Y)_2(Al,Fe)_3Si_3O_{12}(OH)$), a REE-bearing epidote-group mineral that is often found in Ca-bearing rocks of low- to medium metamorphic grade. Comparison of the semi-quantitative EDS analysis of the mineral with microprobe analyses of allanite and epidote from greenschist to low amphibole fascies conditions done by Janots et al. (2008) reveals that the composition is similar given the large interval involved with the EDS analysis (Table 2). The Al-, Ca-, Fe and REE-content of the mineral falls between those of the allanites and epidotes measured by Janots et al., with Al- and Ca-content being higher and Fe- and REE-content lower than that of the allanites. It appears the mineral in STO-18 is a solid

solution with a composition between the pure allanite and epidote end-members.

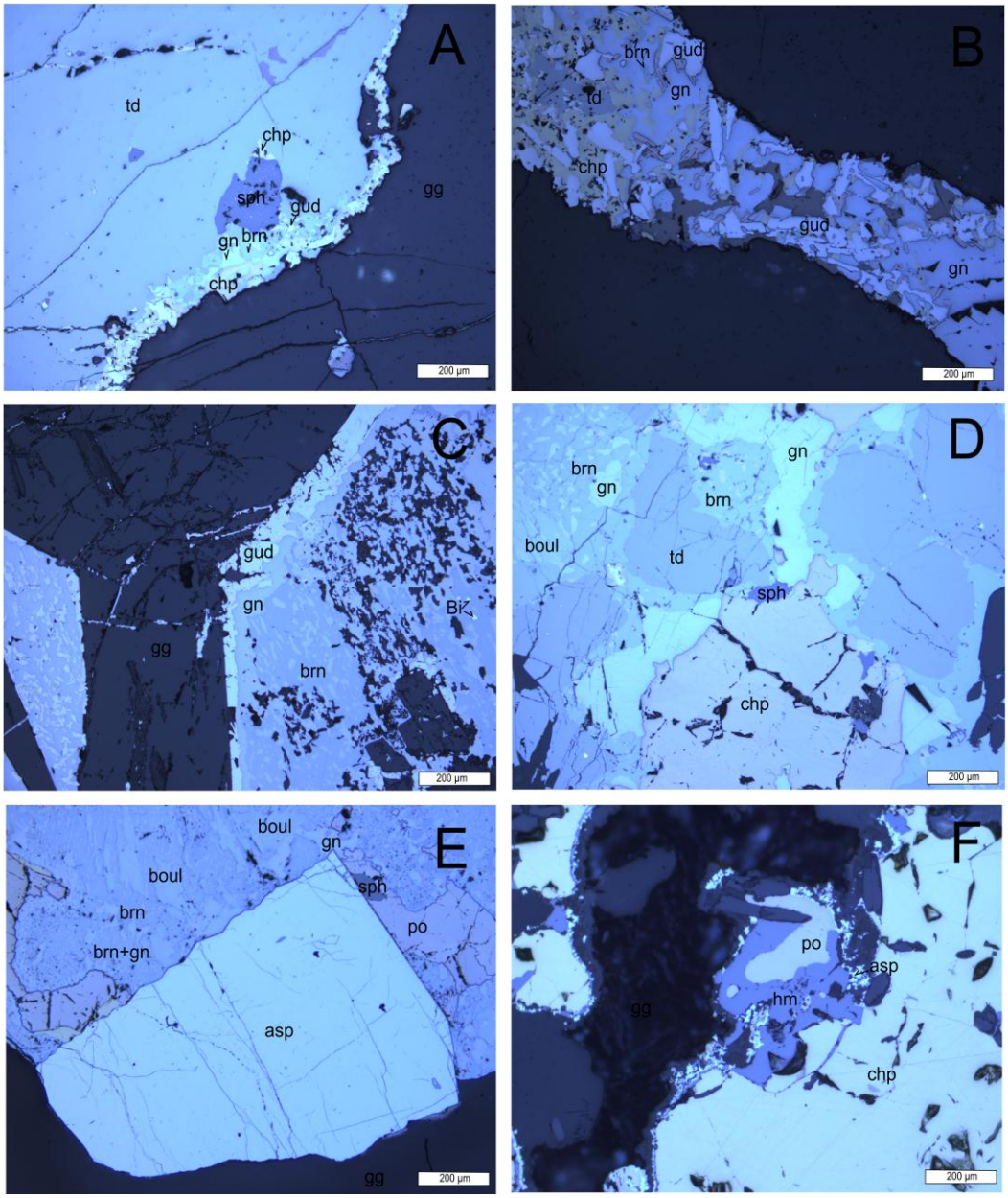

Figure 7:Minerals and textures of sulfide-rich remobilization veins. A: STO-6a, massive gn with gud inclusions. C: STO-28a, symplectitic gn and brn with gud rim. D: STO-50, boul and td inclusion in gn+brn. E: STO-50, asp porphyroblast in symplectitic gn and brn. F: STOB-98051-123.8: remobilized chp with po, hm and asp inclusions. asp=arsenopyrite, boul=boulangerite, brn=bournonite, chp=chalcopyrite, gg=gangue, gn=galena, gud=gudmundite, hm=hematite, po=pyrrhotite, py=pyrite, td=tetrahedrite.

Table 2: Comparison of microprobe analyses from the unknown mineral in sample STO-18 and from allanites and epidotes from cental Alps, taken by Janots et al. (2008).

Ox%	STO-18	MF482 Aln	MF482 Aln	MF131 Aln	MF131 Aln	MF307 Aln	MF307 Aln	MF307 Ep1	MF307 Ep2	MF94 Aln	MF94 Aln	MF94 Ep1	MF161 Aln	MF161 Ep1
MgO	1.62	0.07	0	0.09	0.07	0.13	0.09	0.06	0	0.12	0.09	0.13	0.42	0.2
Al_2O_3	24.14	21.21	20.86	22.45	20.39	21.86	22.64	25.48	26.54	23.10	23.14	26.46	23.61	27.85
SiO2	39.52	34.28	33.45	36.14	34.3	34.44	34.53	36.89	37.22	33.76	34.62	37.16	34.42	36.85
CaO	17.22	12.68	11.62	13.16	11.4	13	13.52	19.28	22.66	13.06	13.08	18.05	13.12	17.97
FeO	7.71	10.86	10.57	11.83	11.08	9.99	9.19	4.78	1.05	8.09	8.49	5.83	8.03	5.9
Ce_2O_3	4.29	7.04	6.37	8.45	9.79	7.06	8.69	0.73	0.08	9.77	8.29	1.12	9.07	1.38
Nd_2O_3	4.41	2.49	8.14	1.55	5.96	6.34	3.74	0.38	0.05	2.4	5.6	0.46	3.19	0.52

5.2.3 Host rock

Most of the host rock is altered and composed largely of quartz, chlorite and biotite, with muscovite and possibly other while mica phases present in smaller amounts, along with epidote and plagioclase. Calcite also occurs in notable amounts in some samples. Small amounts of titanite and apatite occur as accessory minerals in multiple samples. Special attention was paid to chlorite due to its application in geothermometry. Chlorite occurs in needle-like or platy crystals, often in large aggregates, and as massive areas with no clear internal structures. Most chlorite in the samples is pale or brown in color, but some samples also contain chlorite with dark green color. In some samples the green chlorite crystals are found is round spots, surrounded by quartz or chlorite of different color. These may be pseudomorphs of chlorite replacing another mineral, likely garnet. Disseminated ore minerals occur in the host rock, primarily near the contact of the host rock and the massive ore or veins. The abundance of different ore minerals generally reflect their abundance in the massive ore or veins; pyrrhotite, chalcopyrite and sphalerite are the most common disseminated ore minerals in most samples but, for example, the host rock around arsenopyrite-rich sample STOB.98070-93.4 contains larger amounts of disseminated arsenopyrite. Away from the contact of the host rock and massive ore or veins, minor amounts of disseminated ore minerals are present in many samples, usually between grain borders of quartz grains. These grains mostly consist of pyrrhotite+chalcopyrite±sphalerite, but grains of arsenopyrite, galena tetrahedrite, ilmenite and hematite occur in multiple samples as well. Pyrite occurs in small amounts in some samples. Sample STOB-98070-91.5 also contains small amounts of what may be marcasite (a polymorph of pyrite).

Skarn rocks contain a different mineral assemblage than the other host rock samples, indicative of them having been subjected to considerably higher temperatures. They are primarily composed of quartz, plagioclase, clinopyroxene (both Mg- and Fe-rich, with Mg-rich clinopyroxene being more common) and calcite. Ca-Fe garnet, Mg-rich amphibole (most likely actinolite, but EDS-analysis revealed that at least some grains have composition more similar to Mg-hornblende) and spinel occur in notable amounts in multiple samples. Apatite and

titanite occur in small amounts in multiple of these samples as well. Orthopyroxene occurs in some samples, but in much smaller amounts than clinopyroxene. Chlorite and micas, however, are rare. The garnet in the samples is zoned, with variation in Al- Fe- and Ca-content from core to rim (Table 3). Disseminated ore minerals in the skarn samples are generally similar to those of other host rock samples, occurring as small grains among the gangue minerals with grain size and abundance increasing near contact of the host rock and the orebody. The most common ore minerals are pyrrhotite+chalcopyrite±sphalerite, but galena and arsenopyrite occur in most samples as well. Small amounts of tetrahedrite, hematite and ilmenite occur in multiple samples. Sample STO-44 contains small amounts of marcasite as small (around 10 - 20 µm in size) roughly rectangular crystals with dark cracks parallel to the long side. Sample STO-12b may also contain marcasite.

Table 3: weight percentages of elements, measured from core, rim, and midway between core and rim, of a garnet porphyroblast in sample STO-12b with semi-quantitative EDS-analysis.

wt%	Core	Midway	Rim
O	36.57	38.55	36.67
Al	0.29	3.77	0.17
Si	18.16	18.88	18.39
Ca	24.35	24.48	24.35
Fe	20.63	14.53	20.42

5.3. Mineral chemistry

5.3.1. Ore minerals

The results of the WDS-analyses with total weight percentage of below 96 % or above 100.5 % were discarded as unreliable, and the remaining results were normalized to calculate the chemical formulas of the analyzed minerals. The tables containing the weight percentages of analyzed elements and formulas of the ore minrals calculated from the samples are located in the appendix (Tables 11 – 22).

Figure 8 shows the negative correlation between Zn- and Fe-content of sphalerite, and sphalerite from the remobilization veins always show lower Fe-content (and consequently higher Zn-content) than that from the massive ore. Figures 9 and 10 contain histograms of Fe-content of sphalerite in masisve ore and veins, respectively. Sphalerite from the vein samples also has considerably

higher Cd-content than the massive ore samples (Fig. 11 and 12) (mean of 0.73 wt% compared to 0.21 wt%). Sample STO-50 in particular contains notable amounts of Cd in sphalerite (average Cd-content of 1 wt%). Vein samples also contain some measurements with higher Cu-content, most notably samples STO-6a and STO-50, with up to 0.6 and 0.9 wt% Cu, repectively (with mean of 0.3 and 0.4 wt%, respectively). The average Cu-content measured from sphalerite in the massive ore is 0.1 wt%. The measured Mn-content does not show as clear differences between veins and massive ore. While data from massive ore samples STO-14 and STO-33a show higher wt% of Mn than other samples and data from vein sample STO-6a contain no Mn, the remaining vein and massive ore samples all have similar Mn-content (0.1 – 0.2 wt%).

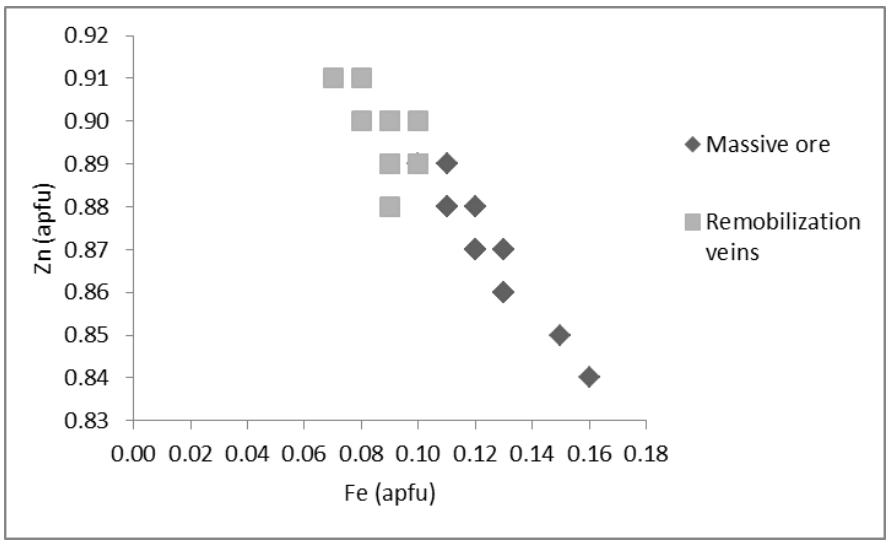

Figure 8: Fe-Zn ratios in sphalerite. Apfu=atoms per formula unit.

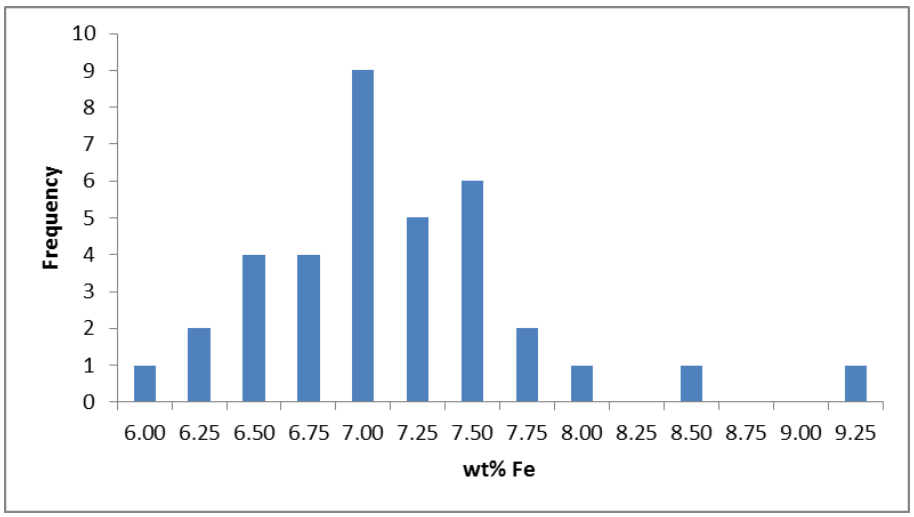

Figure 9: Histogram of wt% Fe in sphalerite from the massive ore samples.

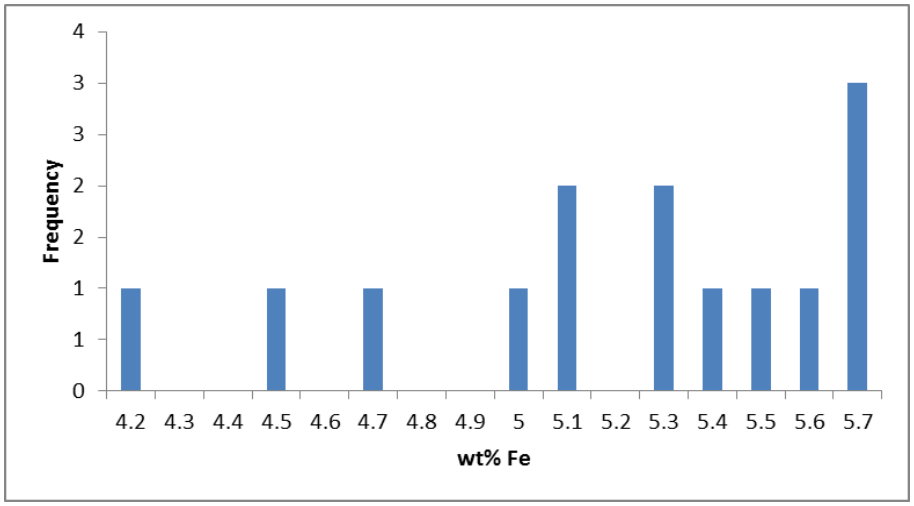

Figure 10: Histogram of wt% Fe in sphalerite from the remobilization vein samples.

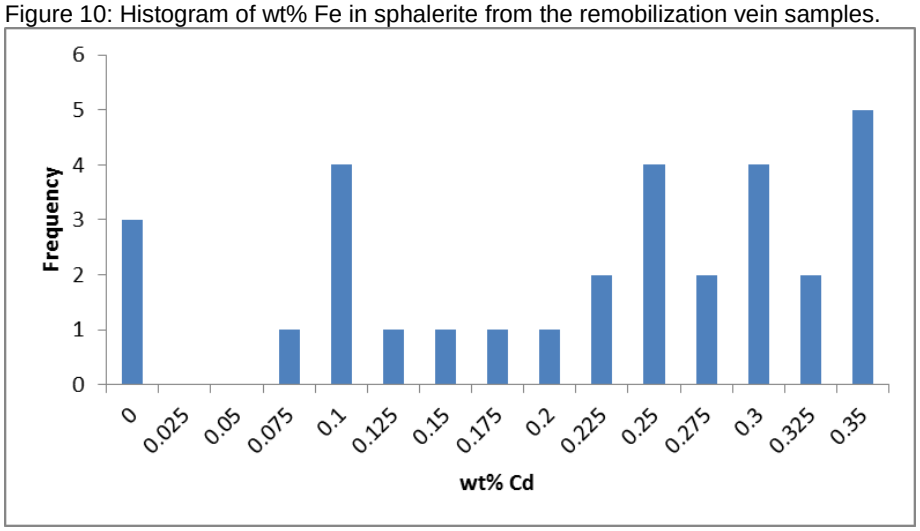

Figure 11: Histogram of wt% Cd in sphalerite from the massive ore samples.

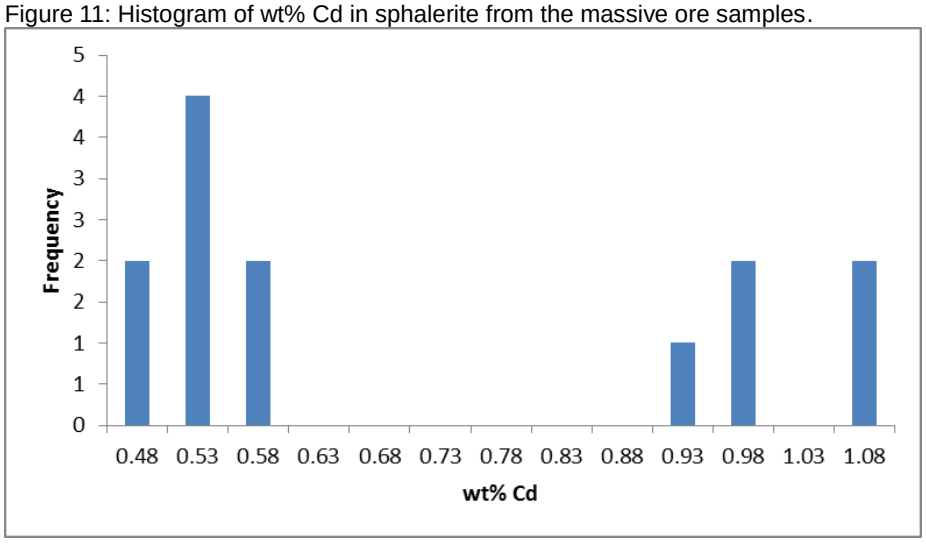

Figure 12: Histogram of wt% Fe in sphalerite from the remobilization vein samples.

The measured composition of tetrahedrite-tennantite is closer to the tetrahedrite end-member, and has an Cu-rich composition (average 34.4 wt% Cu). Tetrahedrite from sample STO-50 also contains notable amounts of Ag (5.3 – 6.1 wt%,

whereas other samples contain less than 3 wt% Ag). The tetrahedrite from sample STO-7c (the only massive ore sample containing notable amounts of tetrahedrite) has a clearly different composition from other measured tetrahedrite compositions, having a notably higher As-content (mean of 2.2 wt% As, whereas the vein samples contain 0.3 – 1.1 wt% As) and lower Fe/(Fe+Zn) ratio (Fig.13 and 14). The tetrahedrite in STO-7c also has slightly higher amount of Zn than the tetrahedrite in the veins, although the difference is less than 0.5 wt% in most cases. Only two measurements from STO-7c had a total wt% higher than 96 %.

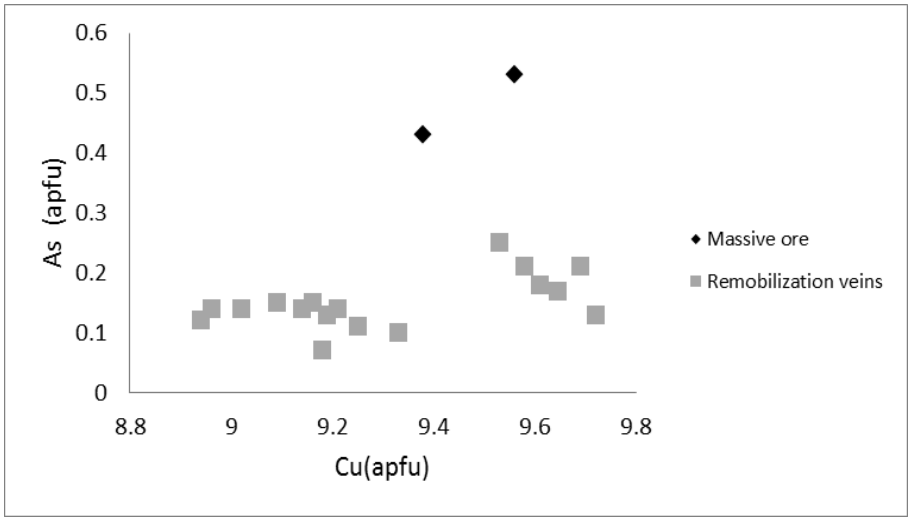

Figure 13: Cu-As ratios of tetrahedrite-tennentite. Apfu=atoms per formula unit.

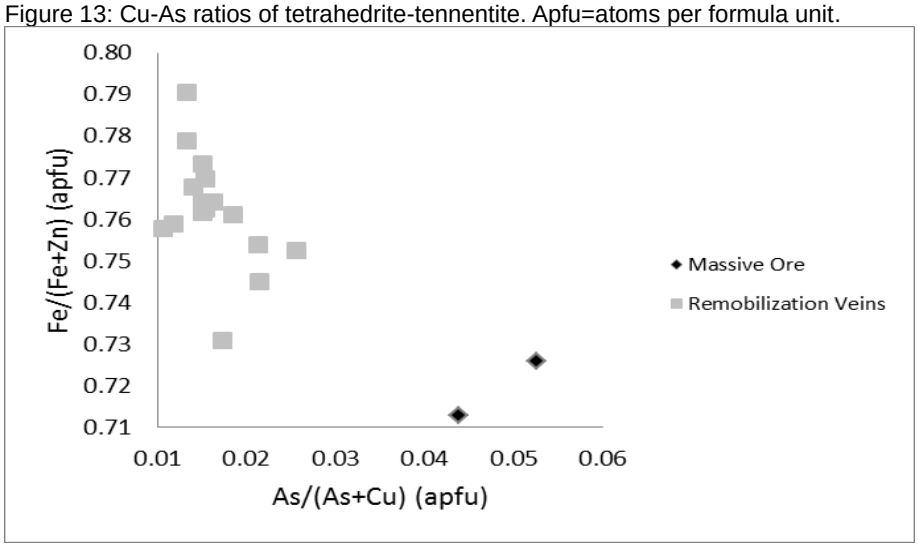

Figure 14: As/(As+Cu) to Fe/(Fe+Zn) ratios in tetrahedrite. Apfu=atoms per formula unit.

The Fe/As ratio of arsenopyrite does not show a clear differences between the massive ore and the remobilization veins (Fig. 15). The average ratio of Fe to As is 1.04 in both the veins and the massive ore. Of the massive ore samples,

STOB-98070-93.4 contains both the lowest and the highest Fe/As ratios measured (lowest being 0.93 and highest 1.13). The low Fe/As ratios are measured from coarse-grained arsenopyrite in contact with pyrite, while the high ratios are measured from small disseminated grains in the gangue. In the remobilization veins, the lowest Fe/As ratios (lowest being 0.94, with multiple results of 0.98 – 0.99) are measured from sample STO-50, from a large porphyroblast in contact with galena, although the measurements from other spots in the same porphyroblast also yield higher ratios (1.05 – 1.08). The highest Fe/As ratios in the veins (highest being 1.10) are measured from sample STO-28a, from grains in contact with chalcopyrite. The arsenopyrite in sample STO-28a also contains notably higher amounts of Co than other samples, with amean of 0.4 wt%, and 0.7 wt% measured at one spot. Other samples contain 0.0 wt% Co, aside from a few spots where concentrations of 0.1 wt% were measured. . The arsenopyrite in sample STO-28c, on the other hand, contains no notable amounts of Co, but instead all but one measurement from the sample contain 0.2 wt% Se, an element which was not measured in quantities above detection limit from the other samples.

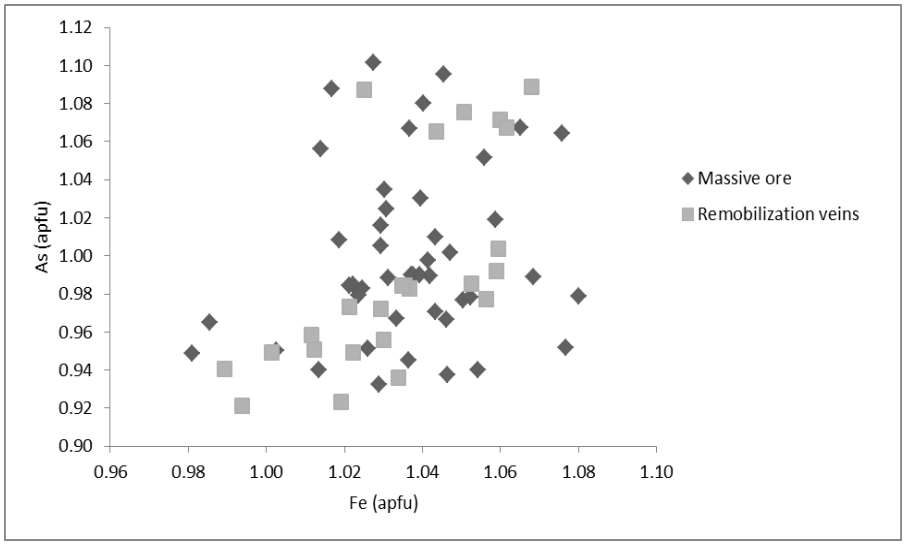

Figure 15: Fe-As ratios in arsenopyrite. Apfu=atoms per formula unit.

The Boulangerite in sample STO-50 contains an average of 0.6 wt% Bi. Most analyzed spots contain Bi, with the highest amount measured at 1.1 wt%. Additionally, minor amounts of Cu, Hg and As were measured from some spots.

Of the analyzed bournonite grains, only the ones in sample STO-50 had high

enough total weight percentages to not be discarded. The Cu-content measured from them varies from 11.8 to 13.0 wt%. Multiple analyzed spots contain 0.3 – 0.4 wt% As. One spot (STO-50, spot 1b-3c) also contained 0.6 wt% Bi and 0.4 wt% Se.

The analysed chalcopyrite grains contained very little trace elements. Data from samples STO-33a and STO-37 contained 1.7 and 0.9 wt% Zn, respectively. Minor variations in Cu/Fe ratio occur between samples, with Cu/Fe ranging from 1.1 to 1.3 in the analyzed samples.

Some of the analyzed galena grains, especially the ones from sample STO-6a, contain minor amounts of Cu and Se. The highest Cu- and Se-content measured are 0.7 and 0.4 wt%, respectively, from STO-6a. No notable compositional differences were measured between galena from the massive ore and from the remobilization veins.

All analyzed gudmundite grains contain over 1 wt% As (average 1.4 wt%, with highest As-content of 1.7 wt% measured from samples STO-28a and STO-6a). Two of the analyzed spots in sample STO-50 also contain over 1 wt% Cu and one spot from the same sample contains 0.9 wt% Zn. These elements are found in some of gudmundite grains in other samples as well, but in smaller amounts (highest Cu-content outside sample STO-50 is 0.6 wt% and highest Zn-content 0.1 wt%).

Multiple pyrite grains in sample STOB-98070-101.8 (one of the two samples where notable amounts of pyrite coexist with pyrrhotite) contain notable amounts of Co, with average Co-content of 0.5 wt%. The highest Co-content measured from other samples is 0.1 wt%. The pyrite grains in STOB-98070-101.8 that are in contact with chalcopyrite have much lower Co-content (only 0.1 wt%) than the grains that occur as inclusions in sphalerite (where several grains have Co-content of 0.5 wt% or higher, with 1.9 wt% being the highest measured). Pyrite grains from this sample also contain elevated amounts of Zn, up to 0.5 wt% in the grains inside sphalerite.

Data from pyrrhotite from sample STOB-98070-101.8 contains over 2.1 wt% Zn. The measurements are taken from pyrrhotite filling a crack in pyrite. A pyrrhotite inclusion in sphalerite from sample STO-33a also contains 3.6 wt% Zn,

but similar inclusions in STOB-98070-101.8 only contain up to 0.6 wt% Zn. Pyrrhotite grains from sample STOB-98051-123.8, which are inclusions in hematite, do not contain Zn. STOB-98051-123.8 is a remobilization vein while the two other samples are from the massive ore, but the difference in Zn-content is more likely related to the minerals pyrrhotite is in contact with. Other than the difference in Zn-content, there are no notable differences in the composition of pyrrhotite between the samples.

5.3.2. Chlorite

The results of the WDS-analyses of chlorite samples were normalize to 14 water-free oxygen atoms. Any results that showed obvious signs of contamination (primarily large amounts of K, which indicates contamination with biotite) were discarded, as were any results with total oxide percentage of less than 95%. The table showing measured oxide percentages and calculated formulas from all analyzed samples is included in the appendix (Tables 23 – 26). Table 4 contains the average composition of analyzed chlorite, compared to different chlorite end-members.

The composition of chlorite varies between samples and slightly between different spots in the same sample, but in all cases chlorite has a low Fe/Mg ratio (Fig. 16) and low amount of octahedral vacancies (around 0.10 to 0.20 per 14 O). Samples from quartz veins have lower Fe/Mg ratios than the ones from the host rock, as well as higher amounts of Si and vacancies, and lower amounts of Al^{IV} (Fig. 17 and 18). Based on the composition, the chlorite in the samples consists mostly of clinochlore-daphnite solid solution, although there are sudoite and amesite components present as well.

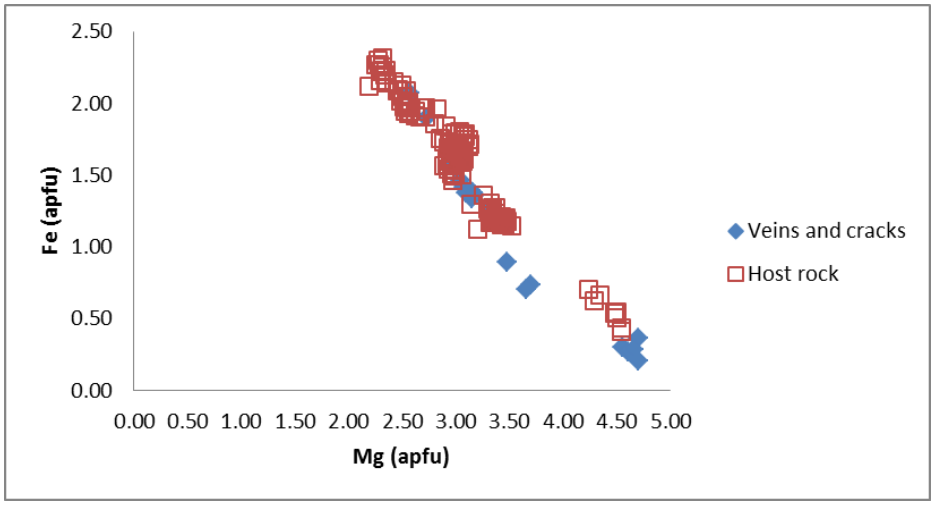

Figure 16: Fe-Mg ratios in chlorite, normalized to 14 O. Apfu=atoms per formula unit.

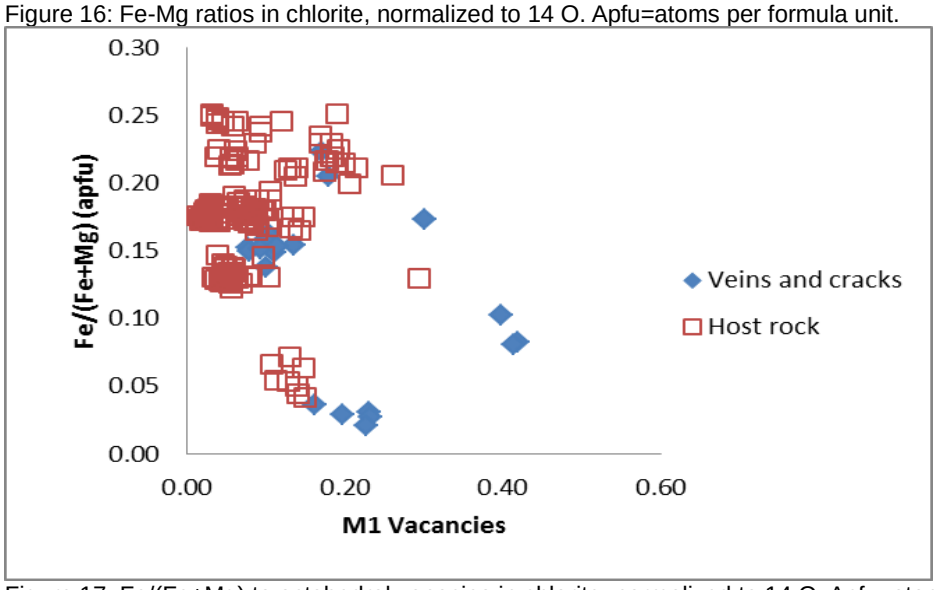

Figure 17: Fe/(Fe+Mg) to octahedral vanacies in chlorite, normalized to 14 O. Apfu=atoms per formula unit.

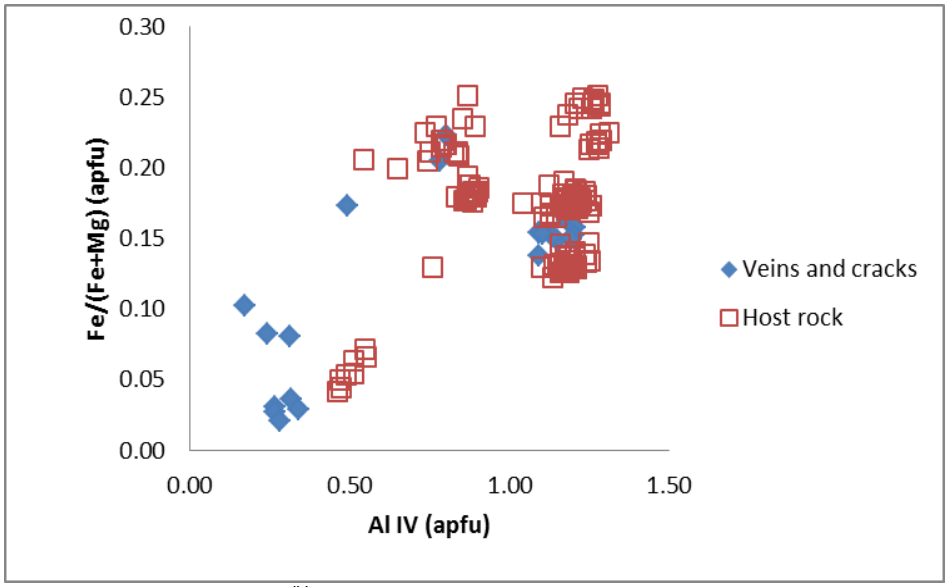

Figure18: Fe/(Fe+Mg) to Al^{IV} in chlorite, normalized to 14 O. Apfu=atoms per formula unit.

Table 4: Average composition of chlorite from the analyzed samples (average from all samples, chlorite from veins, and from the host rock) in comparison to different chlorite end-members.

Based on (O=14)	Samples (average all)	Samples (average veins)	Samples (average host)	Clinochlore[1] (pure)	Daphnite[1] (pure)	Amesite[1] (Mg)	Amesite[1] (Fe)	Sudoite[1] (Fe)	Sudoite[1] (Mg)
Si	2.98	3.27	2.93	3.00	3.00	2.00	2.00	3.00	3.00
Al (VI)	1.02	0.73	1.07	1.00	1.00	2.00	2.00	1.00	1.00
Al (IV)	1.22	1.12	1.23	1.00	1.00	2.00	2.00	3.00	3.00
Mg	3.09	3.53	3.03	5.00	0.00	4.00	0.00	0.00	2.00
Fe	1.54	1.08	1.60	0.00	5.00	0.00	4.00	2.00	0.00
Vacancies	0.10	0.19	0.08	0.00	0.00	0.00	0.00	1.00	1.00
OH*	8.00	8.00	8.00	8.00	8.00	8.00	8.00	8.00	8.00
Fe/(Fe+Mg)	0.33	0.23	0.35	0.00	1.00	0.00	1.00	1.00	0.00

[1] Based on Lanari et al. (2014a)

5.3.3. Stable isotopes

The $\delta^{18}O$- values measured from the vein samples are listed in Table 5. Histogram of $\delta^{18}O$-values (SMOW-standard) from the quartz veins can be seen in Figure 19. δ18O in quartz ranges from 8.8 to 12.5 ‰, with mean of 11.11 ‰ and mode of 12 ‰. All mine samples show $\delta^{18}O$-values of 10.10 ‰ or higher, while the single drillcore sample (STOB-00134-71.5) has a noticeably lower $\delta^{18}O$-value of 8.8 ‰. Devolatilization and isotope fractionation during metamorphosis leads to metamorphic fluids being enriched in ^{18}O compared to bulk rock (Hoefs 1997), which is in line with the positive $\delta^{18}O$-values measured from the remobilization veins. The quartz veins do not display any trend between measurements taken from the margin and the center of the veins, as depending on the sample the $\delta^{18}O$-value can be higher, lower or the same in the margin compared to the center.

Table 5: Oxygen isotope data from quartz veins in the Storliden deposit.

Conventional oxygen isotope data: Storliden deposit (n=15)			
Sample No.	Mineral	Description	$d^{18}O$ (SMOW)
STO-5a	quartz	quartz vein, margin	12.2
STO-5b	quartz	quartz vein, center	12.1
STO-6a	quartz	quartz vein	11.9
STO-6b	quartz	quartz vein	11.8
STO-18a	quartz	quartz vein, center	11.8
STO-18b	quartz	quartz vein, margin	11.5
STO-32a	quartz	quartz vein, margin	10.1
STO-32b	quartz	quartz vein, center	10.1
STO-35a	quartz	quartz vein	11.1
STO-35b	quartz	quartz vein	10.8
STO-40	quartz	quartz vein	12.5
STO-41a	quartz	quartz vein	10.3
STO-41b	quartz	quartz vein, margin	10.3
STO-42	quartz	quartz vein	11.4
STOB-00134-71.5	quartz	quartz vein	8.8

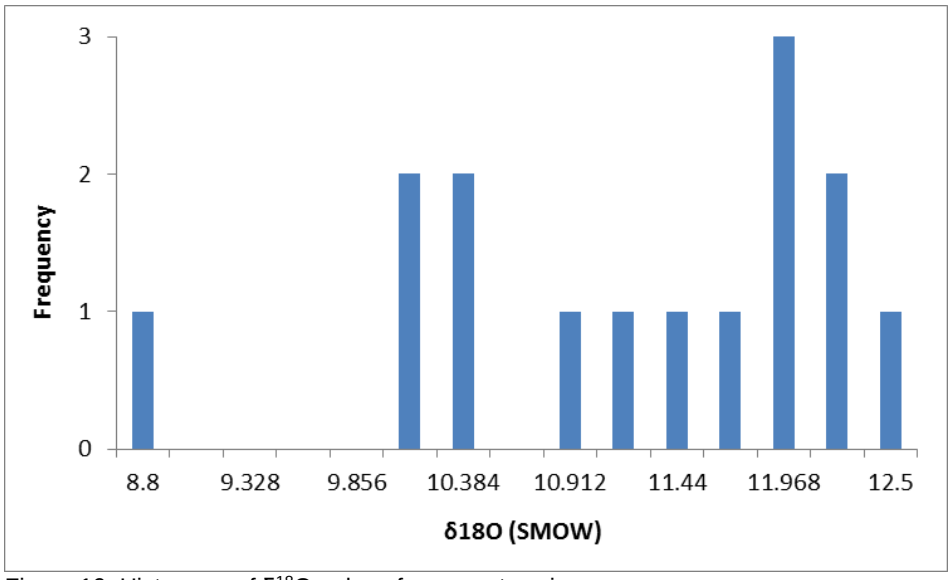

Figure 19: Histogram of $\delta^{18}O$-values from quartz veins.

5.4. Pressure-temperature conditions

5.4.1 Arsenopyrite thermometry

The temperatures are based on Mol% of As in relation with the pyrite-pyrrhotite coexistence curve in the arsenopyrite phase stability diagram, and were calculated with a program based on the results from Kretchmar and Scott (1976). The calculated temperatures are listed in Table 6. The temperatures range from 325 to 479 °C in the vein samples and 350 to 479 °C in the massive ore samples. While the highest measured temperature is identical for both, most temperatures

obtained from the remobilization veins are lower than the ones taken from the massive ore. The mean temperature measured from the veins is 412±43 °C, while massive ore gave a mean temperature of 425 ±41 °C. Figure 20 contains a histogram of temperatures measured from the massive ore and the remobilization veins. The temperatures would appear consistent with regional metamorphic conditions of greenschist to low amphibole facies. However, it must be noted that while some samples have arsenopyrite coexisting with large amounts of pyrrhotite or pyrite, the full buffering assemblage of all three minerals was not found in any of the analyzed samples, and therefore there is no guarantee that the arsenopyrite has preserved the composition it had during ore formation.

Table 6: Mol% As measured from arsenopyrite, along with corresponding temperatures based on py-po coexistance curve.

Massive Ore								
Sample/Spot:	STO-7c/2-1a	STO-7c/2-1b	STO-7c/2-1c	STO-7c/3-1a	STO-7c/3-1b	STO-7c/3-1c	STOB-98070-93.4/2a-4a	STOB-98070-93.4/2a-4b
Mol% (As)	31.88	32.59	31.73	30.79	31.78	32.00	32.53	32.59
T (C°)	420	465	410	350	413	427	461	465
Sample/Spot:	STOB-98070-93.4/2b-1a	STOB-98070-93.4/2b-1b	STOB-98070-93.4/2b-1c	STOB-98070-93.4/2b-2a	STOB-98070-93.4/2b-2b	STOB-98070-93.4/2b-2c	STOB-98070-93.4/2b-3a	STOB-98070-93.4/2b-3b
Mol% (As)	31.65	30.78	30.78	32.06	31.83	32.33	31.43	31.13
T (C°)	405	350	350	431	416	448	391	372
Sample/Spot:	STOB-98070-93.4/2b-3c	STOB-98070-93.4/2b-4a	STOB-98070-93.4/2b-4b	STOB-98070-93.4/2b-4c	STOB-98070-101.8/Pos1a-1a	STOB-98070-101.8/Pos1a-1b	STOB-98070-101.8/Pos1a-1c	STOB-98070-101.8/Pos1a-2a
Mol% (As)	31.88	32.59	31.21	30.94	32.56	32.50	32.81	32.80
T (C°)	420	465	377	360	463	459	479	478
Sample/Spot:	STOB-98070-101.8/Pos1a-2b	STOB-98070-101.8/Pos1a-2c	STOB-98070-101.8/Pos1b-1a	STOB-98070-101.8/Pos1b-1c				
Mol% (As)	32.20	32.59	32.53	32.36				
T (C°)	440	465	461	450				
Remobilization Veins								
Sample/Spot:	STO-28a/2a-1a	STO-28a/2a-1b	STO-28a/2a-1c	STO-28a/2a-2a	STO-28a/2a-2b	STO-28a/2a-2c	STO-28a/2a-3a	STO-28a/2a-3b
Mol% (As)	30.64	31.28	30.74	31.55	30.40	31.34	31.47	31.73
T (C°)	341	381	347	399	325	385	393	410
Sample/Spot:	STO-28a/2a-3c	STO-50/3-5a	STO-50/3-5b	STO-50/3-5c	STO-28c/2-1a	STO-28c/2-1b	STO-28c/2-2a	STO-28c/2-2b
Mol% (As)	31.43	31.98	32.81	32.43	32.21	32.36	32.43	32.43
T (C°)	391	426	479	455	441	450	455	455
Sample/Spot:	STO-28c/2-3a	STO-28c/2-3b						
Mol% (As)	32.09	32.29						
T (C°)	433	446						

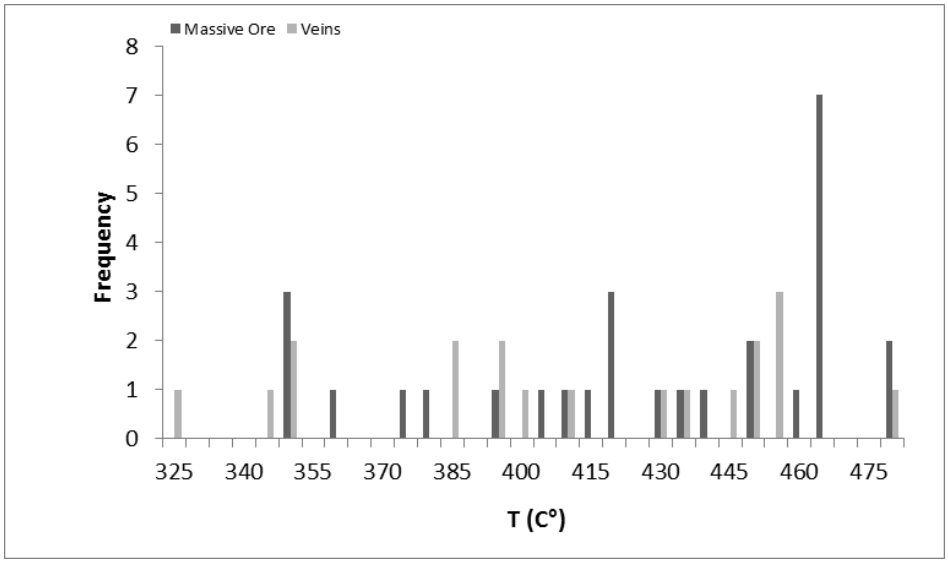

Figure 20:Histogram of temperatures measured using arsenopyrite thermometry.

5.4.2. Sphalerite barometry

Figures 21 and 22 contain histograms of mol% FeS from sphalerite in the massive ore and the remobilization veins, respectively. Figure 23 shows the Mol% FeS projected onto the FeS-ZnS join of sphalerite+pyrite+pyrrhotite isobars (based on Scott 1976).

Only two massive ore samples were found to contain the full assemblage of sphalerite+pyrite+pyrrhotite required for buffering the composition of sphalerite; STO-14 (which contained small sphalerite grains surrounded by pyrite and small amounts of pyrrhotite) and STOB-98070-101.8 (which contained massive sphalerite with large amounts of pyrite and pyrrhotite inclusions). However, despite lacking the full buffering assemblage, the measurements from the other samples show little variance, suggesting that the massive ore has a very homogenous composition, or that the entire orebody behaved essentially isochemically during metamorphosis and sphalerite composition was buffered by pyrite+pyrrhotite elsewhere in the orebody.

Data from sample STO-14 showed anomalously high amounts of FeS compared to other massive ore samples, especially those from spot 2a-4, with highest measurement of 16 Mol%. This is likely due to the small size of the analyzed sphalerite grains (while the sample did contain massive sphalerite, the only sphalerite in contact with both pyrite and pyrrhotite were few small grains), which may have led to contamination by the pyrite grains next to the sphalerite. Additionally, the small amount of pyrrhotite near the sphalerite grains may not

have been sufficient to buffer the sulfur fugacity. Sample STOB-98070-101.8, on the other hand, contains large amounts of all three minerals and therefore should be properly buffered and give accurate geobarometric data. The measurements from this sample give results that are mostly similar to those from the unbuffered samples, with all but one falling between 11.3 and 13.1 Mol% FeS, with mean of 12.1±0.9 (ignoring one anomalous result that is likely result of contamination). Figure 24 contains a histogram of Mol% FeS measured from sample STOB-98070-101.8 only. Using the values for pressure and Mol% FeS of buffered sphalerite assemblages presented by Scott (1976), it can be calculated that change of sphalerite composition of 1 Mol% FeS corresponds to pressure change of 1.25 kbar. Based on this, the pressures measured from the massive ore samples range from 6.3 to 8.5 kbar, with mean of 7.5 ±1.1 kbar.

Measurements taken from the vein samples show very low Fe-content (7.3 to 10.0 Mol% FeS), resulting in unreasonably high pressures (lowest measurement being close to 10 kbar) compared to the massive ore. No vein sample was found with the full sulfur fugacity buffering assemblage, so the results indicate that the sphalerite in the remobilization veins was not in equilibrium with pyrite+pyrrhotite.

From Fig.22 it can be seen that most of the data from the massive ore plots between 11 and 13 Mol% FeS, corresponding to pressure of roughly 6.5 – 8.5 kbar (indicating burial depth of around 18 – 24 km), with a mean of 12.1 Mol% and mode of 12 Mol% or 7.6 kbar.

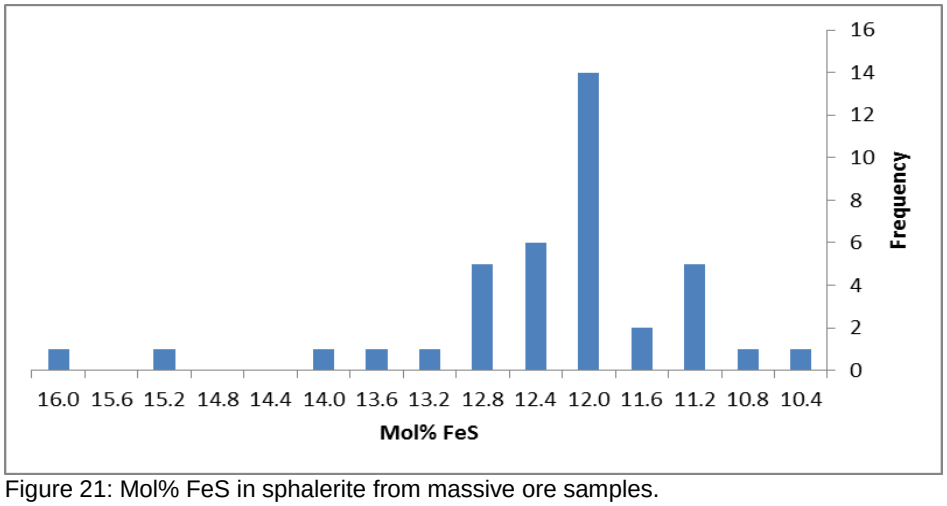

Figure 21: Mol% FeS in sphalerite from massive ore samples.

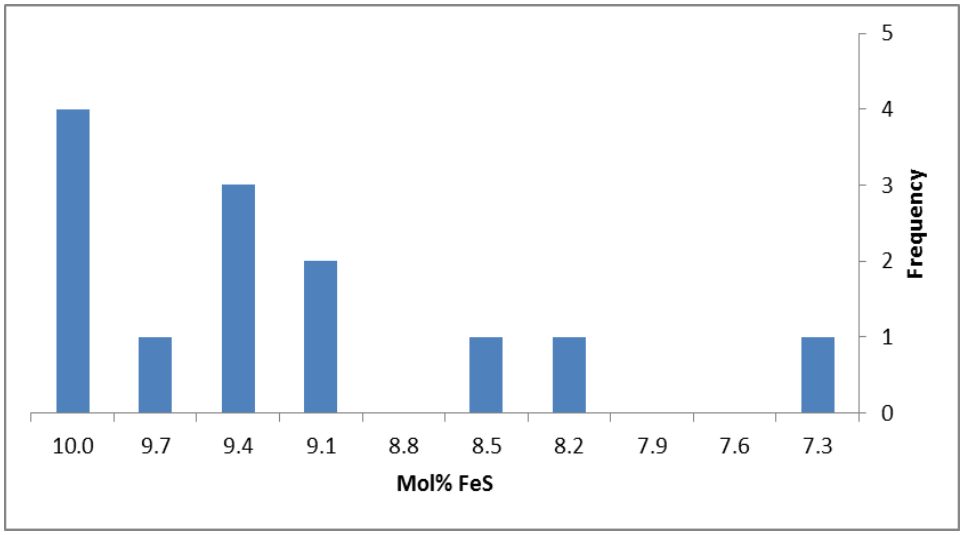

Figure 22: Mol% FeS in sphalerite from remobilization veins.

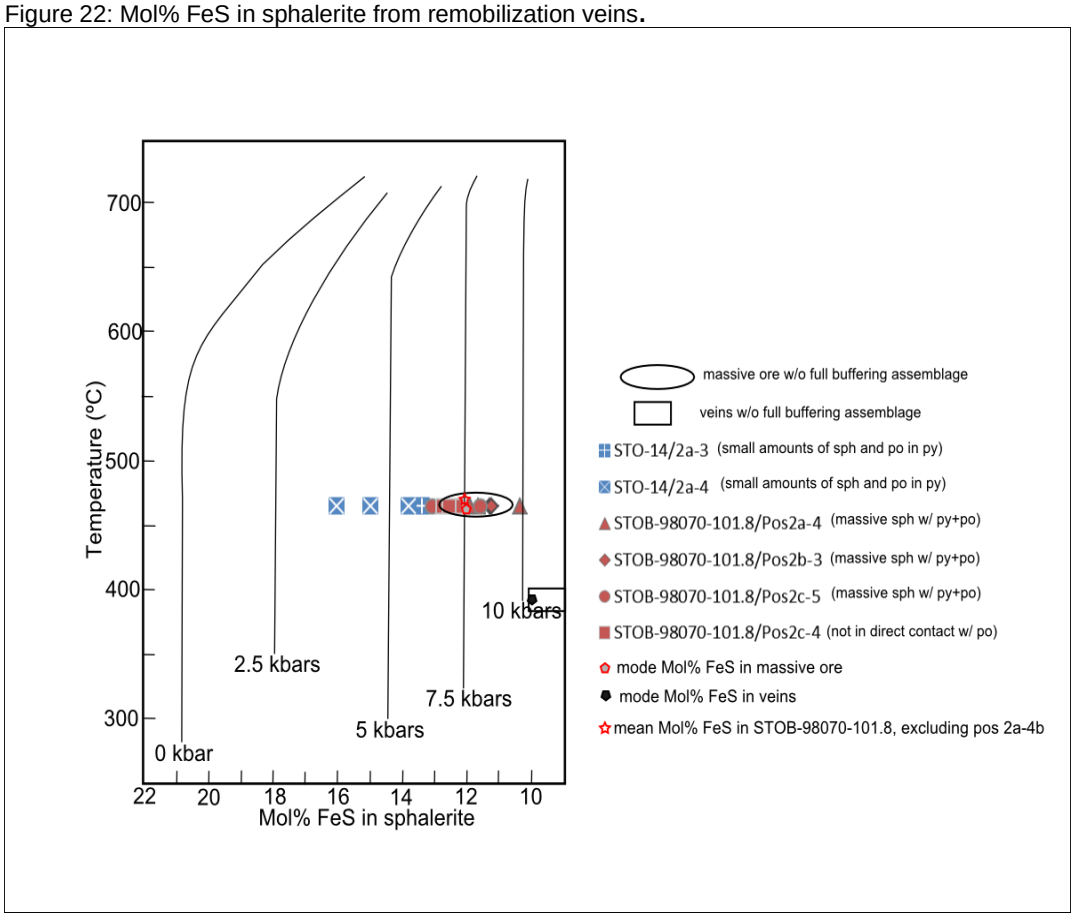

Figure 23: Mol% FeS in sphalerites projected onto FeS-ZnS join of sphalerite+pyrite+hexagonal pyrrhotite isobars. Based on Scott (1976).

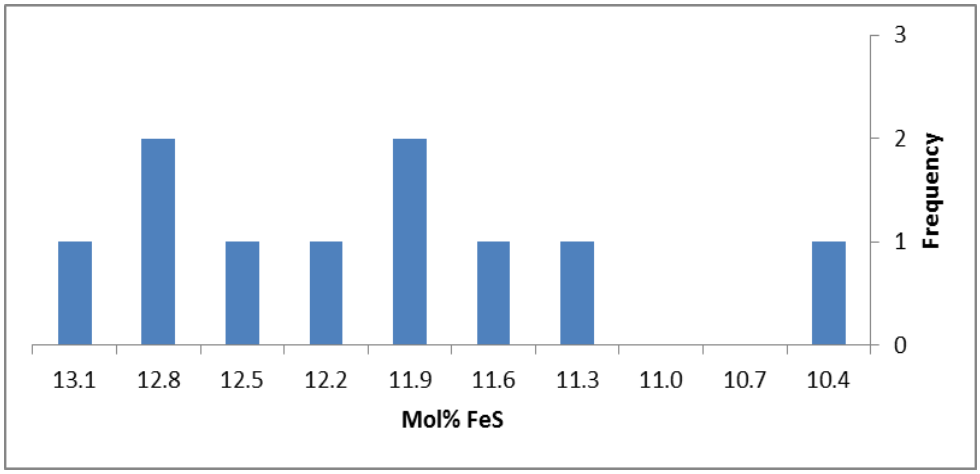

Figure 24: Mol% FeS in sphalerite from sample STOB-98070-101.8.

5.4.3. Chlorite thermometry

Temperatures from chlorite composition were calculated using the semi-empirical thermometers of Bourdelle et al. (2013) (Eq.1) and Lanari et al. (2014a) (Eq.2), as well as the empirical thermometers of Cathelineau and Nieva (1985) (Eq. 3), Cathelineau (1988) (Eq. 4) and Jowett (Eq. 51). The original equation given for the chlorite thermometer by Lanari et al. (2014a) in their paper contained a typographical error, which has been corrected in a subsequently published erratum (Lanari et al. 2014b). Eq. 2 is the corrected version. As the thermometer presented by Lanari et al. (2014a) requires the pressure conditions during the formation of chlorite to be known, four separate calculations were made using P of 2.5 kbar, 5.0 kbar, 7.5 kbar (the pressure measured from the sphalerite in sample STOB-98070-101.8) and 10 kbar. The full list of temperatures calculated from the samples is listed in the appendix (Table 27).

$$T_{Chlorite}(^{\circ}C)=\frac{-9400}{Log(K)-23.4}-273.15 \quad (1)$$

$$T_{Chlorite}(^{\circ}C)=\frac{203093+4996.99P(kbar)}{-Rln(K)+455.782}-273.15 \quad (2)$$

$$T_{Chlorite}(^{\circ}C)=212.31*n(Al^{IV})+17.54 \quad (3)$$

$$T_{Chlorite}(^{\circ}C)=321.98*n(Al^{IV})-62.92 \quad (4)$$

$$T_{Chlorite}(^{\circ}C)=319*n(Al^{IV})+\frac{0.1*n(Fe^{2+})}{n(Fe^{2+})+n(Mg)}-69 \quad (5)$$

Data obtained with the Bourdelle et al. (2013) thermometer (Fig. 25) yields high values for the standard deviation in both host rock and vein samples

(314±118 °C in the host rock and 164±92 °C in veins). Using the Lanari et al. (2014a) thermometer (Fig. 26 – 29) yields a high standard deviation for the host rock samples but lower standard deviation for the vein samples, while the opposite is true for the empirical thermometers. The three empirical thermometers (Fig.29 – 32) yield lower temperatures than the Bourdelle at al. (2013) and Lanari et al. (2014a) thermometers. Some temperatures calculated from the vein samples (sample STO-28c in particular) with these thermometers yield unphysical values, despite temperatures calculated from the same samples using the chlorite activity thermemeters not differing notably from ones calculated from the other samples.

Regardless of the thermometer used, however, the measurements from most samples show a broad range of temperatures. An example is shown Figure 33, which uses the temperatures measured from the host rock using the Lanari et al (2014a). thermometer as an example. This suggests that the chlorites in the same sample have either formed during different temperatures or that they have party undergone re-equilibration during retrograde metamorphism.

Furthermore, the temperatures obtained for the vein samples are in most thermometers unrealistically low for even low-grade metamorphic conditions, indicating that chlorite has undergone re-equilibration or alteration in hydrothermal conditions. The temperatures measured from the host rock appear to show a bimodal distribution of temperatures, with two separate peaks visible in in the histograms (best visible in the Lanari et al. (2014a) thermometer at higher pressures, and in the empirical thermometers). The lower temperature peak consists of measurements from samples STO-4a, STO-13, STOB-98070-100.3 and STOB-98070107.6. The higher temperature peak consists of measurements from samples STO-4a, STO-36b, STO-22b, STOB-98070-105.6 and STOB-98070-107.6. Additionally the Bourdelle et al (2013). and Lanari et al (2014a). thermometers contain a spike at the low end of the temperature scale which corresponds almost entirely to measurements from sample STO-19b and one datapoint form sample STOB-98070-107.6.

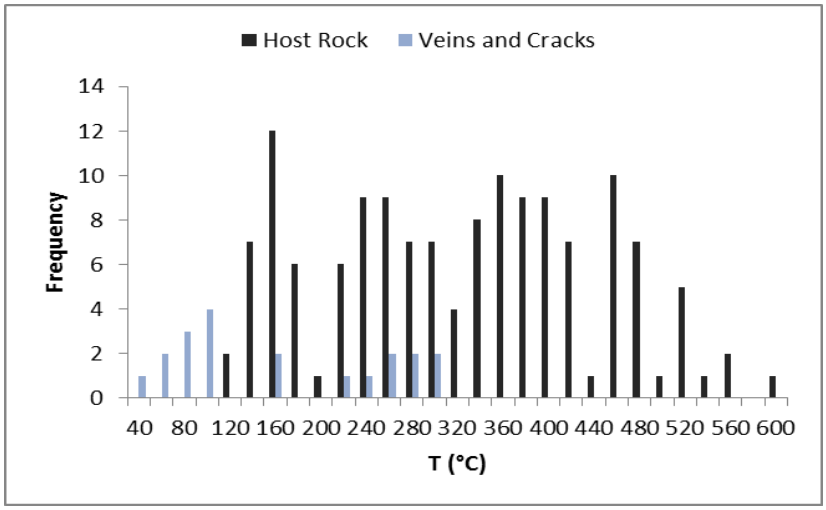

Figure 25: Histogram of temperatures obtained from chlorite samples using thermometry based on Bourdelle et al. (2013). Mean temperature is 314 ±118 °C for the host rock and 164±92 °C for the veins.

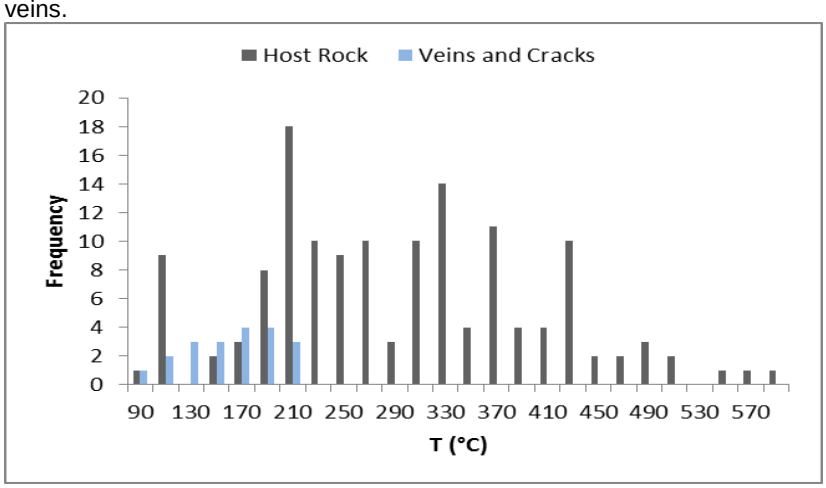

Figure 26: Histogram of temperatures obtained from chlorite samples using thermometry based on Lanari et al. (2014). P=2.5 kbar. Mean temperature is 287±107 °C for the host rock and 152±36 °C for the veins.

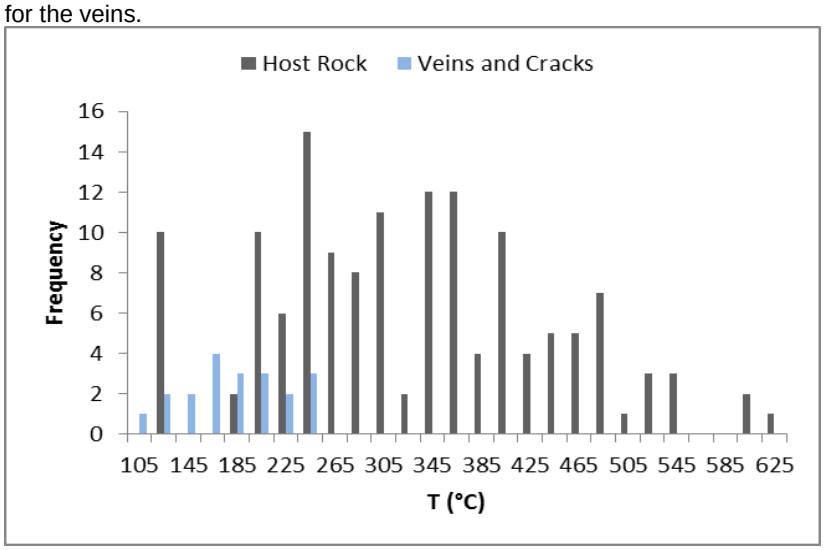

Figure 27: Histogram of temperatures obtained from chlorite samples using thermometry based on Lanari et al. (2014). P=5.0 kbar**.** Mean temperature is 319 ±113 °C for the host rock and 176 ±38 °C for the veins.

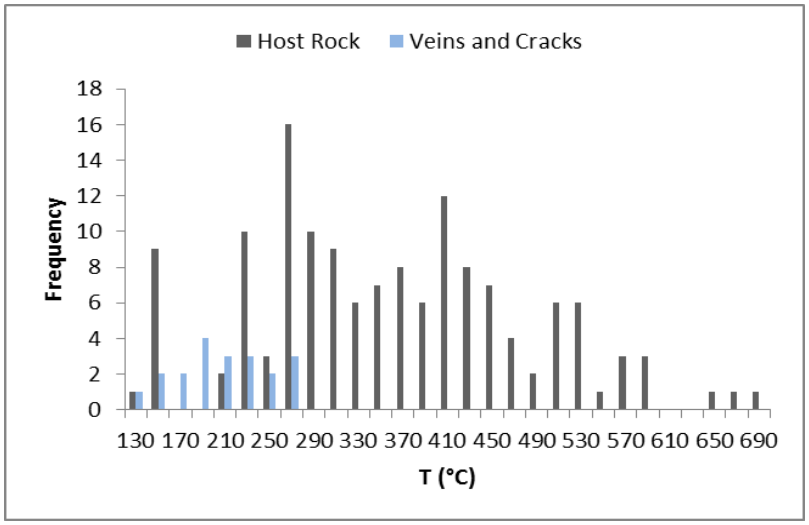

Figure 28: Histogram of temperatures obtained from chlorite samples using thermometry based on Lanari et al. (2014). P=7.5 kbar. Mean temperature is 351±120 °C for the host rock and 201±40 °C for the veins.

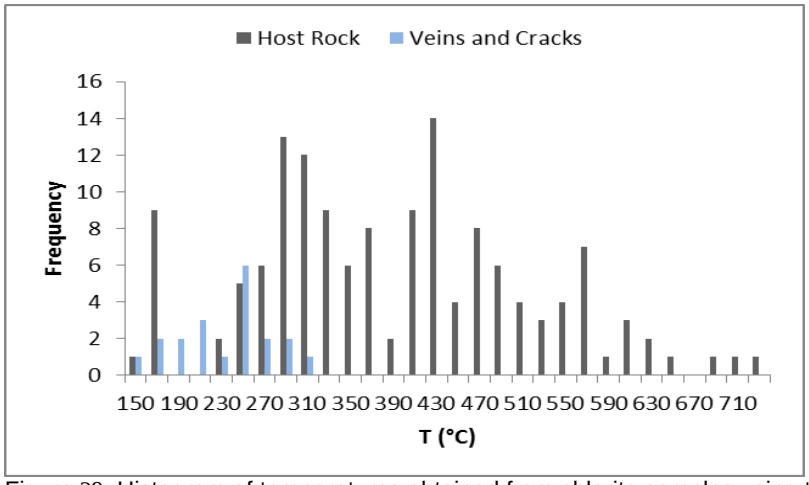

Figure 29: Histogram of temperatures obtained from chlorite samples using thermometry based on Lanari et al. (2014). P=10 kbar. Mean temperature is 384 ±127 °C for the host rock and 225±42 °C for the veins.

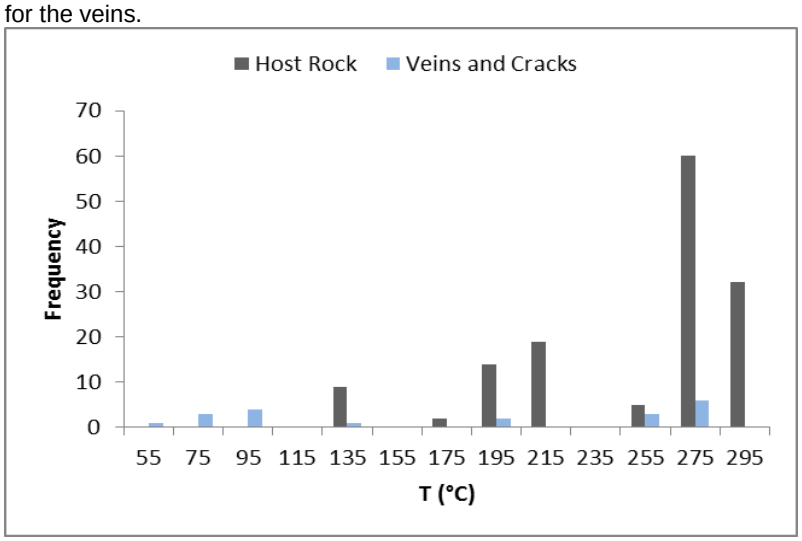

Figure 30: Histogram of temperatures obtained from chlorite samples using thermometry based on Cathelineau and Nieva (1985). Mean temperature is 243±46 °C for the host rock and 173±87 °C for the veins.

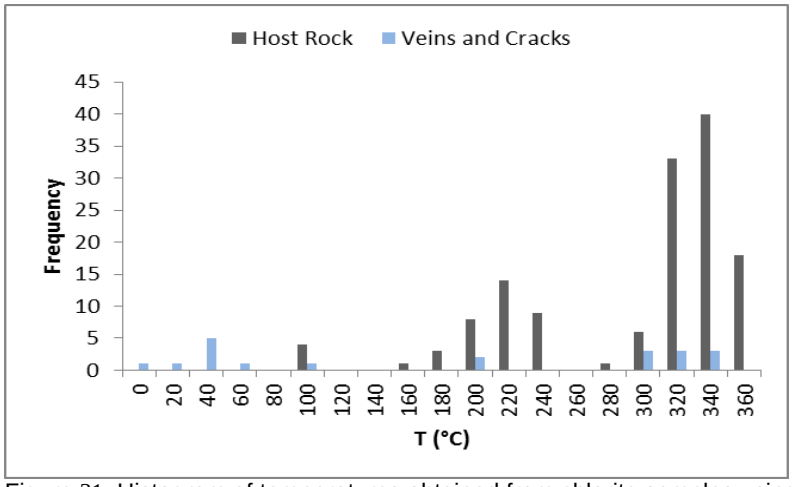

Figure 31: Histogram of temperatures obtained from chlorite samples using thermometry based on Cathelineau (1988). Mean temperature is 281±70 °C for the host rock and 173±131 °C for the veins.

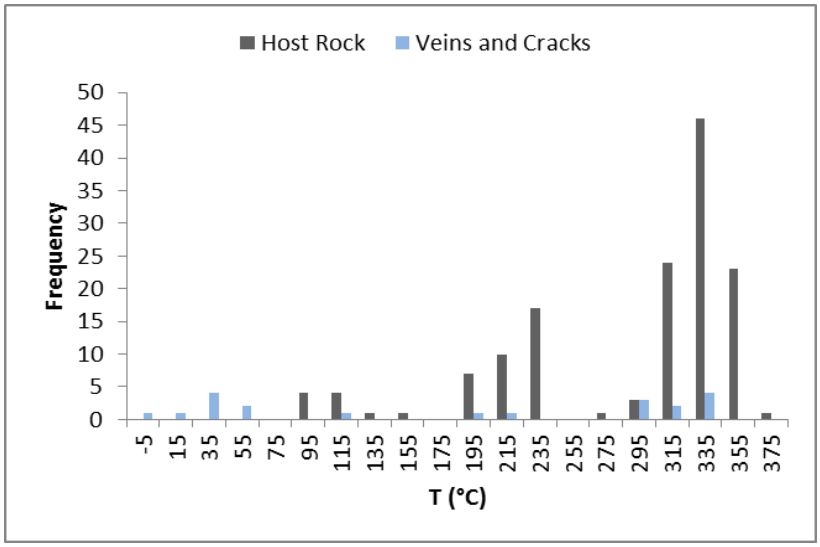

Figure 32: Histogram of temperatures obtained from chlorite samples using thermometry based on Jowett (1991). Mean temperature is 282±71 °C for the host rock and 172±133 °C for the veins.

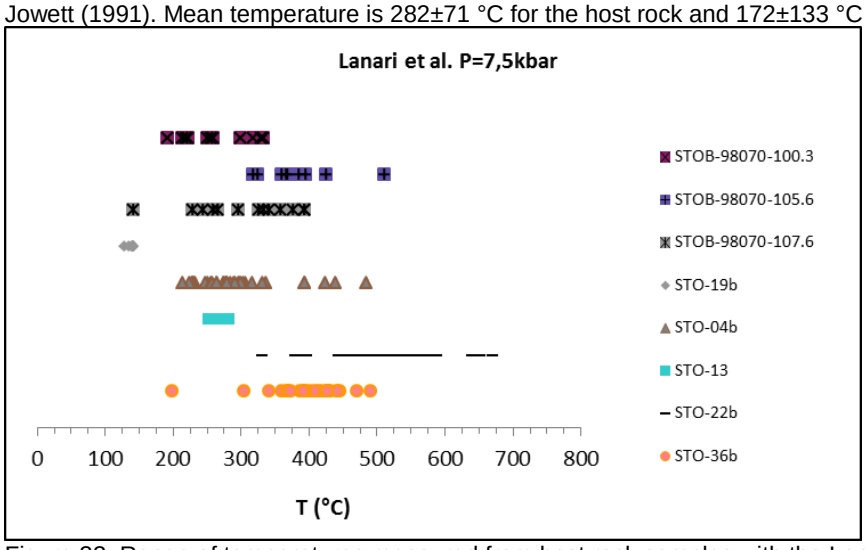

Figure 33: Range of temperatures measured from host rock samples with the Lanari et al. thermometer at P=7.5 kbar. Note the wide distribution in all samples but STO-19b and STO-13.

5.5. Stable isotope composition of the fluid phase

The oxygen isotope data obtained from the quartz veins was used to calculate the $\delta^{18}O$-values for the fluid phase the veins precipitated from. The fractionation factor for oxygen isotopes for a mineral-water pair is determined with the equation $1000 \ln \alpha = a + b\ 10^3\ 1/T + c\ 10^6\ 1/T^2 + d\ 10^9\ 1/T^3$, where α is the fractionation factor, T the temperature (in K) and a, b, c and d are constants that depend on the mineral. Using these equations, one can calculate δ-values, as $1000 \ln \alpha_{A\text{-}B} = \delta_A - \delta_B$, where δ_A and δ_B are the δ-values of two coexisting chemical compounds, such as two minerals or mineral and water. The values of the constants for the oxygen isotope fractionation factors between quartz and water were obtained from Matsuhita et al. (1979). As no temperature measurements existed from the samples the stable isotope data was taken from (this at least partly reflects that some coarse grained quartz vein samples did not contain much sulfides), the $\delta^{18}O$-values for the quartz veins were calculated using the temperatures obtained from other vein samples using arsenopyrite geothermometry, with T of 410±10 °C (412 °C being the mean temperature measured form the veins). The results are listed in Table 7.

Table 7: $\delta^{18}O$-values for water calculated from the $\delta^{18}O$ of SiO^2 in the quartz veins. Calculation based on Matsuhita et al. (1979).

Skellefte Sample No.	$\delta^{18}O$ SiO_2 (SMOW)	$\delta^{18}O$ H_2O T=400°C	$\delta^{18}O$ H_2O T=410 °C	$\delta^{18}O$ H_2O T=420 °C
STO-5a	12.2	8.1	8.3	8.5
STO-5b	12.1	8.0	8.2	8.4
STO-6a	11.9	7.8	8.0	8.2
STO-6b	11.8	7.7	7.9	8.1
STO-18a	11.8	7.7	7.9	8.1
STO-18b	11.5	7.4	7.6	7.8
STO-32a	10.1	6.0	6.2	6.4
STO-32b	10.1	6.0	6.2	6.4
STO-35a	11.1	7.0	7.2	7.4
STO-35b	10.8	6.7	6.9	7.1
STO-40	12.5	8.4	8.6	8.8
STO-41a	10.3	6.2	6.4	6.6
STO-41b	10.3	6.2	6.4	6.6
STO-42	11.4	7.3	7.5	7.7
STOB-00134-71.5	8.8	4.7	4.9	5.1
Average	11.1	7.0	7.2	7.4

The calculated $\delta^{18}O$-values for water in quartz veins range from 4.7 to 8.8 ‰. The mean $\delta^{18}O$ -value is 7.2 ‰, with a standard deviation ±1 ‰. Aside from those measured from sample STOB-00134-71.5, the values fit the range of $\delta^{18}O$-values in metamorphic waters (5 – 25 ‰) (Hoefs, 1997) (Fig. 34). Given the uncertainty in the results, STOB-00134-71.5 may actually also be within the range. Most of the $\delta^{18}O$-values are close to those of primary magmatic water, which has an estimated $\delta^{18}O$ of 6±1 ‰ (Hoefs, 1997). They are considerably higher than $\delta^{18}O$-values of meteoric water (which are usually strongly negative) or oceanic water (which has average $\delta^{18}O$ of 0).

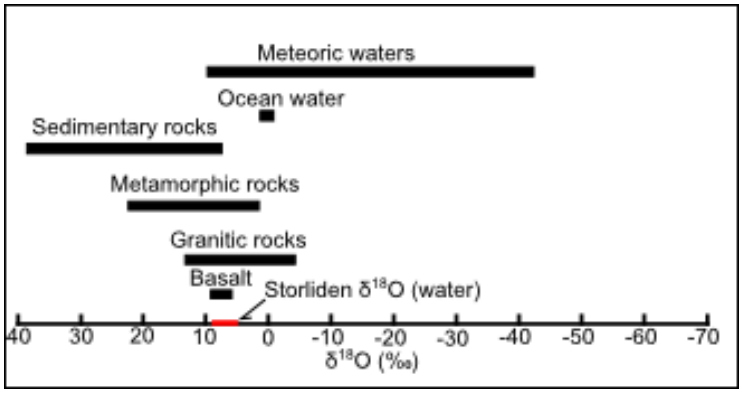

Figure 54: δ18O-values for different reservoirs of water compared to the data from the Storliden quartz veins. Based on Hoefs (1997).

6. DISCUSSION

6.1. Review of data on P-T condition in the Skellefte district

Berglund and Ekström (1980) used arsenopyrite geothermometry and sphalerite geobarometry to determine the temperatures and pressures from several deposit in the Skellefte district, and concluded that the mineral assemblages mainly indicate a temperature range of 300 – 500 °C and a pressure of 5 – 7 kbar. This corresponds to low-grade metamorphism in the conditions of the greenschist facies. The composition of exsolved Ag-Sb minerals in galena indicates that the minimum temperature for ore formation in the Skellefte district was about 250 °C (Amcoff 1976; Berglund and Ekström 1980). The occurrence of Andalusite in the Långseke and Boliden deposits indicates pressures of less than 4 kbar (Holdaway 1971; Berglund and Ekström 1980). However, the andalusite may not be synmetamorphic in origin. The temperatures obtained by Berglund and Ekström

(1980) are in agreement with the mineral assemblages of the orebodies and the bedrock, although there are reports of rocks with mineral assemblages that indicate higher metamorphic grade (Berglund and Ekström 1980 and references therein), including the skarn rocks in this study.

Fluid inclusion studies by Broman (1987) indicate that the ore-bearing quartz veins formed at two phases of mineralization, at temperatures of 210 and 295 °C, respectively. However, temperatures measured from ore-bearing quartz veins in Boliden (Wagner and Jonsson 2001) Vinliden (Broman et al. 1995) deposits indicate higher temperatures of 350 – 400 °C. According to Åberg (1995), however, the minimum formation temperature for arsenopyrite-bearing quartz veins at Boliden is around 200 °C. Broman also used data from fluid inclusions to calculate pressures from quartz veins in the Björkdal (Broman et al. 1994) and Vinliden (Broman et al. 1995) deposits, obtaining pressures of ≤1.8 kbar from the initial quartz veins and about 0.5 kbar from the vein-hosted ore in Björkdal and 1 – 5 kbar from the initial quartz veins and about 0.5 kbar from the vein-hosted ore in Vinliden.

6.2. Discussion on the obtained data

The values obtained for pressure and temperature acquired with the arsenopyrite thermometer and sphalerite barometer (for massive ore) in this study are broadly in agreement with the regional metamorphic conditions and the gangue mineral assemblage observed in most samples, matching the conditions of upper greenschist facies. However, the skarn assemblage in some samples indicates that much higher temperatures have been reached, at least locally. The analysed mineral assemblages, particularly the chlorite, may also have recorded, at least partly, retrograde conditions.

As the arsenopyrite mostly lacks a complete buffering assemblage, it may not be in equilibrium with its surroundings and the temperatures given by the thermometer may be inaccurate. While the measured temperatures seem reasonable, caution is advised when using the thermometric data to make assumptions on the conditions of ore formation or metamorphism. It should be noted however, that arsenopyrite is a very refractory mineral, which makes it

resistant to re-equilibration during the retrograde stages of the metamorphism (Kretchmar and Scott 1976). Therefore it can maintain the composition it obtained during peak metamorphosis.

Massive ore sample STOB-98070-101.8 contains enough sphalerite, pyrite and pyrrhotite in contact with each other to justify the assumption of being buffered and the pressures derived from that sample to be reliable. Most of the massive ore samples without the full buffering assemblage gave similar pressure estimates as STOB-98070-101.8, which suggests that they have not fully re-equilibrated during retrograde metamorphosis despite lacking one of the buffer minerals.

The values for pressure acquired from the remobilization veins, however, are unrealistically high, exceeding the conditions of the regional metamorphic facies. Given that none of the vein samples were found to contain the full buffering assemblage, it can be assumed that the sulfur fugacity was not buffered by the pyrite+pyrrhotite assemblage. The sphalerite composition from the remobilization veins is therefore unsuitable for use as a barometer.

The results of chlorite thermometry, regardless of the thermometer used, yields a large range in temperatures in most samples. This likely indicates that the chlorite has been at least partially re-equilibrated during retrograde phase of metamorphosis. Of the thermometres used, the one based on Lanari et al. (2014a) seems to give the most reliable results. The one based on Bourdelle et al. (2013) gives similar results for the measurements form the host rock, but lower temperatures for the veins and higher standard deviation for both veins and host rock. Furthermore, the Bourdelle et al. (2013) thermometer has been calibrated for low temperatures and pressures ($T < 350°$ C and $P < 4$ kbar) (Bourdelle et al. 2013), which lower than the ones obtained from the samples through arsenopyrite geothermometry and sphalerite geobarometry. However, if the chlorite records retrograde conditions, the P-T-conditions may have been within the calibration range of the Bourdelle et al. (2013) thermometer. The thermometers of Cathelineau and Nieva (1985), Cathelineau (1988) and Jowett (1991) are less accurate, as they are purely empirical, being based on only the composition of the chlorite rather than activities of different chlorite end members. The results they give for the temperature in vein samples include data that are too low or even

unphysical and the measurements from the host rock samples are also lower than the data obtained using the semi-empirical thermometers. Lanari et al. (2014a) model, despite also giving wide ranges of temperatures within a single sample, gives standard deviations for the temperature in vein samples that are comparable in magnitude to the standard deviation produced by the arsenopyrite thermometer. However, the mean temperatures it gives for the veins are lower than would be expected for greenschist facies conditions, and considerably lower than the results given by the arsenopyrite thermometer (around 200 °C compared to 410 °C). In fact, all thermometers yield temperatures from the vein chlorites that are much lower than the temperatures produces by arsenopyrite thermometry. This may reflect chlorite formation during retrograde stage of metamorphism (which in agreement with presence of what appears to be chlorite pseudomorphs of garnet) or late-stage alteration of chlorite under hydrothermal conditions (which would be consistent with the large amount of recrystallization visible in the veins), possibly due to injection of another, lower temperature fluid in the already crystallized quartz veins. In any case large variance of temperatures measured from most samples indicate that the chlorites have likely undergone partial re-equilibration during late retrograde stage of them metamorphism, which makes the results gained form the chlorite thermometers unreliable. The measurements from the host rock produce results that are more in line the information about local metamorphic conditions (greenschist to low amphibole facies), though the mean temperatures are still lower. The standard deviation is also higher than the results produced by the arsenopyrite thermometer, indicating that the chlorite in the host rock may also have undergone at least partial re-equilibration.

The results obtained from arsenopyrite thermometry and sphalerite barometry were compared to thermometric and barometric data obtained from other deposits in the Skellefte district, as well as the Vihanti deposit in Finland, which is a VHMS deposit of similar age and possesses similar geology (Table 8). The temperatures obtained from the massive ore and ore-bearing veins are within similar range than those presented by the other studies (around 300 – 500 °C). The only major difference are the temperatures of roughly 220 °C obtained from fluid inclusions in sulfide and gold ore in the quartz veins in the Björkdal deposit

(Broman et al. 1994). However, according to Broman et al. (1994) the sulfide minerals and gold deposited after a second fluid was injected into the quartz veins. This temperature is quite close to the temperatures obtained from vein chlorites in this study (average T of around 150 – 225 °C, depending on the thermometer used). The temperatures obtained from the early quartz veins in the Björkdal deposit are similar to the values obtained from arsenopyrite in remobilization veins in this study. This may indicate that the chlorite in the Storliden deposit was also deposited from or altered by fluids that were injected into the veins after ore formation took place. The temperature obtained from remobilized sphalerite form the Vihanti deposit is higher than those measured from any of the Skellefte deposits.

It should be noted that the pressures obtained from this study and the ones from Berglund and Ekström (1980) use different methods for determining pressure. This study uses the sphalerite barometer calibrations from Scott (1976), while Berglund and Ekström used an earlier calibrations form the same author (Scott 1973). The average iron content of sphalerite measured by Berglund and Ekström and the one measured in this paper are both around 12 Mol% Fe. Thus if the same values for the relation of sphalerite iron content to pressure would be used for both studies, the pressures obtained would be essentially identical. The pressures obtained from the Vihanti deposits also lie within a similar range, with the average being 0.7 kbar lower than the one measured in this study. As no accurate barometric data could be obtained from the veins in this study, comparisons between them and the pressures measured from the quartz veins by Broman et al. (1994, 1995) could not be made. The results from Broman et al. (1994) confirm that the pressure results obtained from the sphalerite in the veins are rather inaccurate, as they show very low pressures. Figure 35 shows the pressure- and temperature data plotted onto a P-T diagram Data from Berglund and Ekström (1980) has been recalculated with calibrations from Scott (1976). Fig. 34 also contains an illustration of a possible P-T path the rocks in Storliden may have taken (assuming a clockwise P-T gradient typically associated with orogeny-related metamorphism). It should be noted that the illustrated path is by no means a reliable, and exists primarily to give the reader an idea of the changes in

pressure and temperature conditions the rocks may have undergone.

Table 8: Comparison of the results of geothermometry and -barometry with other studies. asp=arsenopyrite, qtz=quartz, sfs=sulfosalts, sph=sphalerite.

Deposit	Storliden	Storliden	Storliden	Storliden	Näsliden[1]	Rakkejaur[1]	Kankberg[1]	Långsele[1]
Type	massive ore	qtz veins w/asp	host rock chlorite	vein chlorite	asp+sph ore	asp+sph ore	asp+sph ore	asp+sph ore
T (°C)	350 - 480 (avg. 425)	325 - 480 (avg. 410)	~300	~200	360 - 420	360 - 425	360 - 475	~400
P (kbar)	6.3 - 8.5 (avg. 7.5)	-	-	-	5.1 - 7.75*	~6*	~6*	~6*
Deposit	Boliden[1]	Boliden[2]	Vinliden[3]	Vinliden [3]	Björkdal[4]	Bjjörkdal[4]	Skellefte	Vihanti
Type	asp+sph ore	sfs veins	qtz veins, initial	vein ore	qtz veins, initial	vein ore	average[1]	sph ore
T (°C)	~430	350 - 450	>400	350 - 400	~375	~220	300 - 500	570[5]
P (kbar)	~6*	-	1 - 5	~0.5	≤1.8	~0.5	5 - 7*	5.8 - 8.0 (avg. 6.8)[6]

[1]Berglund. and Ekström (1980) [2]Wagner and Jonsson (2001) [3]Broman et al. (1995) [4]Broman et al. (1994) [5]Rouhunkoski (1968) [6]Törnroos (1982)
*Berglund and Ekström (1980) use values from Scott (1973) for P, this study uses Scott (1976).

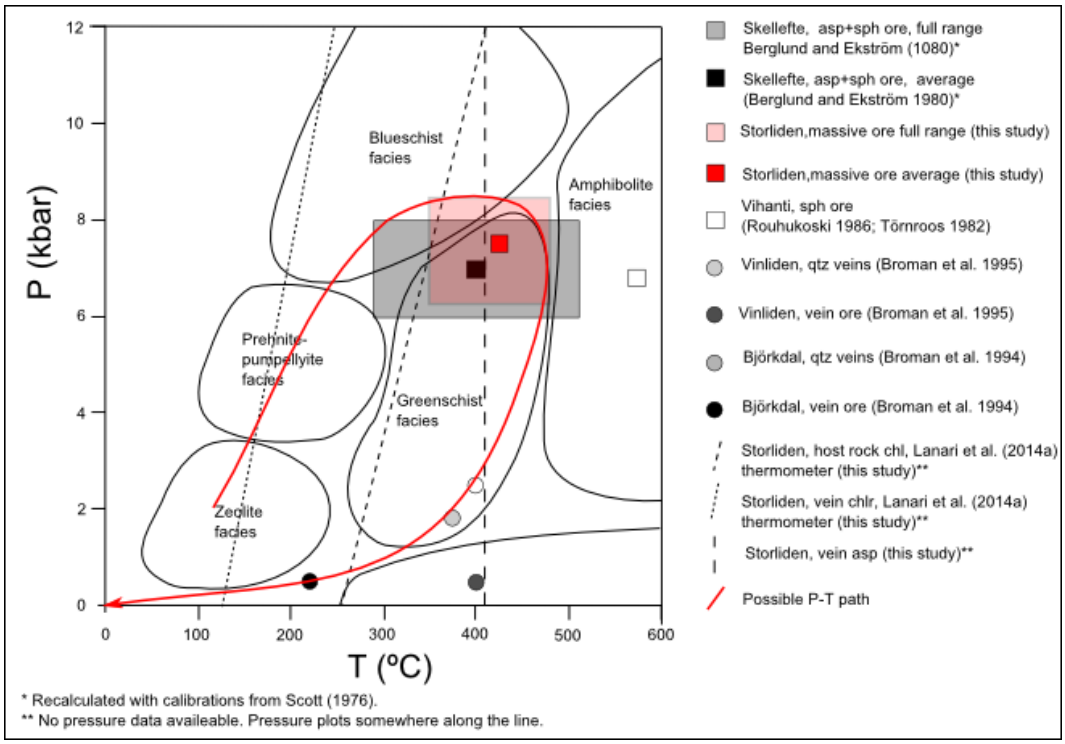

Figure 6:P-T diagram showing the positions of P-T-data from the Skellefte district in a P-T field, and a possible P-T path the rocks in Storliden may have taken.

While the focus of the study was to establish the condition of ore formation in the remobilization veins, the vein samples themselves generally lacked mineral assemblages suitable for geothermobarometry. The majority of the vein samples did not contain chlorite and sphalerite. Large arsenopyrite porphyroblasts do occurs in some vein samples, but arsenopyrite is also more common in massive ore. As such, the massive ore samples yielded more reliable geothermobarometric data and the results from them are likely more accurate.

As no thermometric data existed for the vein samples from which the oxygen

isotope data is taken, the temperatures used to calculate $\delta^{18}O$ for water were based on the mean temperature calculated to the remobilization veins. This increases the interval compared to what it would be if temperatures could have been obtained directly from the samples. Within the range of one σ standard deviation, the interval is not very large, but if the whole range of temperatures would be used, the difference in $\delta^{18}O_{water}$ calculated from the lowest and highest temperature measured would be 3.5 ‰. Comparing the calculated $\delta^{18}O$-values for water to the ones calculated by Broman (1994) from quartz veins in the Björkdal deposit (Table 9), another VHMS deposit in the Skellefte district shows a similar range of $\delta^{18}O$-values. The values calculated from the veins in the Storliden deposit range from 4.7 to 8.5 ‰, with a mean of 7.2 ‰, while the ones calculated from the Björkdal deposit range from 3.7 to 11.6 ‰, with a mean of 6.6 ‰. The data from Broman (1994) has a larger variance than the data from this study, but the difference between in mean $\delta^{18}O$ is only 0.6. The values from both deposits are within the composition range of $\delta^{18}O$ in metamorphic H_2O.

Table 9: Comparison between $\delta^{18}O$-values of water calculated in this study compared to ones calculated from quarz veins in the Björkdal deposit by Broman (1994).

Skellefte	$\delta^{18}O$ H_2O	$\delta^{18}O$ H_2O	$\delta^{18}O$ H_2O	**Björkdal**, Broman (1994)	
Sample No.	T=400°C	T=410 °C	T=420 °C	Sample No.	$\delta^{18}O$ H_2O
STO-5a	8.1	8.3	8.5	Bd-1-87	11.6
STO-5b	8.0	8.2	8.4	Bd-2-87	7.6
STO-6a	7.8	8.0	8.2	Bd-101-89	6.5
STO-6b	7.7	7.9	8.1	Bd-102-89	6.8
STO-18a	7.7	7.9	8.1	Bd-103-89B1	5.9
STO-18b	7.4	7.6	7.8	Bd-103-59B2	3.7
STO-32a	6.0	6.2	6.4	Bd-104-89	6.5
STO-32b	6.0	6.2	6.4	Bd-105-89	6.3
STO-35a	7.0	7.2	7.4	Bd-106-89	4.5
STO-35b	6.7	6.9	7.1	Bd-108-89	6.0
STO-40	8.4	8.6	8.8	Bd-109-89	4.2
STO-41a	6.2	6.4	6.6	Bd-Qz-1	6.1
STO-41b	6.2	6.4	6.6	Bd-85: 3	9.7
STO-42	7.3	7.5	7.7	Average	6.6
STOB-00134-71.5	4.7	4.9	5.1		
Average	7.0	7.2	7.4		

7. CONCLUSIONS

The P-T conditions measured from the massive ore in the Storliden deposit indicate that the ore minerals were subjected to metamorphism at temperature of 350 – 480 °C (with mean T of 425 °C), and pressure of 6.3 – 8.5 kbar (with mean P of 7.5 kbar). This is consistent with thermobarometric results from other deposits in the Skellefte district. Data from remobilization veins using arsenopyrite thermometry give similar temperatures as those from the massive ore, with temperature of 325 – 480 °C (with mean T of 412 °C). Temperatures obtained with chlorite thermometers are lower, with mean T of around 200 °C or less for the veins and around 300 °C for the host rock (exact temperature depending on the geothermometer used). The lower range of temperatures likely reflects formation or re-equilibration during the retrograde stage of the metamorphism. The large standard deviation measured from the chlorites may indicate several generations of chlorite, or that not all of the chlorite even within the same sample underwent re-equilibration at the same conditions. The $\delta^{18}O$-values for water obtained from the quartz veins range from 4.7 to 8.8 ‰ with mean $\delta^{18}O$ of 7.2 ‰, which is within the range of $\delta^{18}O$ of metamorphic waters.

8. AKNOWLEGEMENTS

Sincere thanks to Thomas Wagner, the professor of economic geology of the University of Helsinki faculty of geosciences and geography, who acted as the supervisor for this project, as well as Mr. Radoslaw Michallik, who performed all the microprobe analyses.

9. REFERENCES

Allen, R.L., Weihe, P. and Svenson, S. (1997). Setting of Zn-Cu-Au-Ag Massive Sulfide Deposits in the Evolution and Facies Architetcture of a 1.9 Ga Marine Volcanic Arc, Skellefte District, Sweden. Economic Geology 91, pp. 1022 – 1053.

Amcoff, Ö. (1976). Solubility of antimony and silver in galena. N Jb Miner Mh 6. pp 247 – 261.

Barrett, T.J., MacLean, W.H. and Årebäck, H. (2005). The Paleoproterozoic Kristineberg VMS deposit, Skellefte district, northern Sweden. Part II: chemostratigraphy and alteration. Mineralium Deposita 40, pp. 368 – 395.

Berglund, S. and Ekström, T. K. (1980). Arsenopyrite and Sphalerite as T-P Indicators in Sulfide Ores from Northern Sweden. Mineral Depisita (Berl.) 15, pp. 175 - 187.

Bourdelle, F., Parra, T., Chopi, C. and Beyssac, O. (2013). A new chlorite geothermometer for diagenetic to low-grade metamorphic conditions.Contrib Mineral Petro 165, pp. 723 – 735.

Broman, C. (1987). Fluid inclusions of the massive sulfide deposits in the Skellefte district, Sweden. Chemical Geology 61, pp. 161 – 168.

Broman, C. (1988). Fluids associated with the genesis of the Skellefte district massive sulfide deposits, Sweden. Proc. Seventh Quadrennial IAGOD symposium, E. Sweizer-bartsche Verlagsbuchhandlung, Stuttgart, 1, pp. 191 – 200.

Broman, C., Billström, K., Gustavsson, K., Fallick, A. E. (1994). Fluid inclusions, stable isotopes and gold deposition at Bjökdal, northern Sweden. Mineralium Deposita 29, pp. 139 - 149.

Broman, C., Bergström U. and Lindblom S. (1995). Fluid evolution in gold-bearing quartz veins associated with feldspar porphyry dikes at Vinliden in the Skellefte District, northern Sweden. GFF vol. 117, pp. 233 - 244.

Cathelineau, M. and Nieva, D. (1985). A chlorite solid solution geothermometer The Los Azufresm(Mexico) geothermal system. Contrib Mineral Petrol 91, pp. 235 – 244.

Cathelineau, M. (1988). Cation site occupation in chlorites and illites as a function of temperature. Clay Minerals 23, pp. 471 – 485.

Claesson, S. and Lundqvist, T. (1990). Swecofennian granites in the Bothnian basin, central Sweden. Abstr. 19th Nordic Geol. Wintermeeting, Stavanger, Norway. Geonytt 17.1, pp. 36.

Deines, P. (2002). The carbon isotope geochemistry of mantle xenoliths. Earth-Science Reviews 58, pp. 247 – 278.

Friedman, I., O'Neil, J.R. (1977). Compilation of stable isotope fractionation factors of geo-chemical interest. In: Fleischer M (ed.) Data of geochemistry. U.S. Geol. Survey Professional Paper 440-KK, 12 pp.

Hoefs, J. (1997). Stable Isotope Geochemistry, 4th ed. Berlin: Springer-Verlag.

Holdaway, M. J. (1971). Stability of andalusite and the aluminium silicate phase diagrams. Am J Sci 271. pp 97 – 131-

Hudson, J. D. (1977). Stable isotopes and limestone lithification. Journal of Geological Society of London, vol. 133, pp 637 – 660.

Imaña, M., Allen, R. and Barret, T. (2005). Volcanic stratigraphy, chemical stratigraphy and alteration system of the Storliden massive sulfide deposit, Skellefte district, northern Sweden. Mineral Deposit Research: Meeting the Global Challenge, pp. 627 – 630

Janots, E., Engi, M., Berger, A., Allaz, J., Schwarz, J.O. and Spandler, C. (2008). Prograde metamorphic sequence of REE minerals in pelitic rocks of the Central Alps: implications for allanite-monazite-xenotime phase relations from 250 to 610 °C. Journal of metamorphic Geolpgy 26, pp. 509 – 526.

Jiang, W., Peacor, R.R. and Buseck, P.R. (1994). Chlorite Geothermometry? – Contamination and Apparent Octahedra Vacancies. Clay and Clay Minerals, vol. 42, no. 5, pp. 593 – 605.

Jowett, E. (1991). Fitting iron and magnesium into the hydrothermal chlorite geothermometer. Program Abstr 16:A62.

Kretschmar, U. and Scott, S.D. (1976). Phase Relations Involving Arsenopyrite in the System Fe-As-S and Their Application. Canadian Mineralogist 14, pp. 364 – 386.

Lanari, P., Wagner, T., Vidal, O. (2014a). A thermodynamic model for di-trioctahedral chlorite from experimental and natural data in the system MgO-FeO-Al_2O_3-SiO_2-H_2O: application to P-T sections and geothermometry. Contrib Mineral Petrol 167:968.

Lanari, P., Wagner, T., Vidal, O. (2014b). Erratum to: A thermodynamic model for di-trioctahedral chlorite from experimental and natural data in the system MgO-FeO-

Al_2O_3-SiO_2-H_2O: application to P-T sections and geothermometry.Contrib Mineral Petrol 168:1039.

López-Munguira, A., Nieto, F. and Morata, D. (2002). Chlorite composition and geothermometry: a comparative HRTEM/AEM-EMPA-XRD study of Cambrian basic lavas from the Ossa Morena Zone, SW Spain. Clay Minerals 36, pp. 267 – 281.

Masrhall, B. and Gilligan, L.B. (1987). An Introduction to Remobilization: Information from Ore-Body Geometry and Experimental Considerations. Ore Geology Reviews 2, pp. 87 – 131.

Matsuhisa, Y., Goldsmith, J.R, Clayton, R.N. (1979). Oxygen isotope fractionation in the system quartz-albite-anorthite-water. Geochim. Cosmochim. Acta, 43, 1131-1140.

Ohmoto, H. and Goldhaber, M.B. (1997). Sulfur and carbon isotopes. Barnes HL (ed.) Geochemistry of hydrothermal ore deposits. 3rd ed., Wiley, New York, pp. 517-611.

Rouhunkoski, P. (1968). On the geology and geochemistry of the Vihanti zinc ore deposit. Bulletin de la Commission Geologique de Finlande 236. 121 p.

Scott, S.D. (1973). Experimental calibrations of the sphalerite geobarometer. Economic Geology 70, pp. 466 – 474.

Scott, S.D. (1976). Application of the sphalerite geobarometer to regionally metamorphosed terrains. American Mineralogist 61, pp. 661 – 670.

Skiöld, T. (1988). Implications of new U-Pb zircon chronology to early Proterozoic crustal accretion in northern Sweden. Precambrian Res. 38, pp. 147 – 164.

Törnroos, R. (1982). Sphalerite geobarometry of some metamorphosed sulfide ore deposits in Finland. Geol. Surv. Finland, Bulletin 343, pp. 7 - 32.

Vidal, O., Baldeyrou, A., Dubac, B., DeAndrade, V., Jullien, M. and Lanson, B. (2007). Thermodynamics of phyllosilicates and low temperature thermometry. Seminarios de la Sociedad Española de Mineralogía vol. 3, pp. 76 – 84.

Wagner, T. and Jonsson, E. (2001). Mineralogy of sulfosalt-rich vein type ores, Boliden massive sulfide deposit, Skellefte district, northern Sweden. The Canadian Mineralogist vol. 39, pp. 855 - 872.

Wagner, T., Boyce A.J., Jonsson, E. and Fallick, A.E. (2004). Laser microprobe sulfur isotope analysis of arsenopyrite: experimental calibration and application to the Boliden Au-Cu-As massive sulfide deposit. Ore Geology Reviews 25, pp. 311 – 325.

Wilso, M.R., Claesson, L.-Å., Sehlstedt, S., Smellie, J.A.T., Aftalion, M. Hamilton, P.J. and Fallic, A.E. (1987). Jörn: And early Proterozoic intrusive complex in a volcanic arc environment. Precambiarn Res. 36, PP. 201 – 225.

Weihed, P., Bergman, J., and Bergström, U. (1992). Metallogeny and tectonic evolution of Early Proterozoic Skellefte district, northern Sweden. Precambrian Research 58, pp. 143 – 167.

Weihed P. Weihed J.B., Sorjonen-Ward P., and Matsson B. (2002). Post-deformation, sulfide-quartz vein hosted gold ore in the footwall alteration zone of the Paleoproterozoic Långdal VHMS deposit, Skellefte District, northern Sweden. GFF 124, pp. 201 – 210.

Weihed P., (2010). Paleoproterozoic mineralized volcanic arc systems and tectonic evolution of the Fennoscandian Shield: Skellefte District Sweden. GFF 132, pp. 83 – 91.

Åberg, A. (1995). Fluid evolution in the gold lode oreas at Boliden; a key to metallo-genesis in the Boliden deposit. Swedish National Board for Industrial and Technical Development, Report of the National Ore Geology Research Programme. pp. 93 – 135.

Årebäck, H., Barrett T.J., Abrahamsson S. (2005). The Paleoproterozoic Kristineberg VMS deposit, Skellefte district, northern Sweden. Part I: Geology. Mineralium Deposita 40, pp. 351 – 367.

10. APPENDIX

The tables that were too large to fit in among the text are included in the appendix. The appendix contains the full sample list (Table 10), the composition of ore minerals (Tables 11 – 22) and chlorite (Tables 23 – 26) obtained with the WDS-analysis, and the full list of temperatures calculated from the chlorite composition (Tables 27 – 29).

Table 10: List of samples.

Sample No.	Location	Description	Sections	Analyses
STO-1	Lower West, L300, room 2906	massive coarse-grained sphalerite-chalcopyrite ore	1 ore section	
STO-4	Lower West, L300, room 2906	shear zone with phyllosilicates and chalcopyrite-pyrrhotite veinlets	1 ore section (a), 1 thin section (b)	WDS (b)
STO-5	Lower West, L283, room 14	quartz vein with remobilized sulfides	1 thin section	FI
STO-6	Lower West, L283, room 14	quartz vein with remobilized sulfides	1 ore section (a), 1 thin section (b)	EDS (a), WDS (a), FI (a, b)
STO-7	Lower West, L283, room 14	banded meta-calcsilicate rock with fine-grained sphalerite-galena mineralization	2 thin sections (a,b), 1 ore section (c)	WDS (c)
STO-12	Upper East, L330	altered meta-volcanic rock, with fracture mineralization of calcite, chalcopyrite and epidote	1 ore section (a), 1 thin section (b)	EDS (b)
STO-13	Upper East, L330	altered meta-volcanic rock, with crosscutting fractures filled with sulfides, calcite and chlorite	1 thin section	WDS
STO-14	Upper East, L330	altered meta-volcanic rock, with pyrrhotite-chalcopyrite mineralization	1 ore section	WDS
STO-18	Upper West, L305, room 305, W side	quartz vein crosscutting silicified meta-volcanic rock, contact to shear zone	1 thin section	EDS, WDS
STO-19	Upper West, L325, room 310, E side	shear zone with phyllosilicates and chalcopyrite-pyrrhotite veinlets	1 ore section (a), 1 thin section (b)	WDS (b)
STO-20	Upper West, L305, room 305, W side	massive coarse-grained pyrrhotite ore	1 ore section	
STO-22	Upper West, L305, room 305, W side	altered meta-volcanic rock with biotite-amphibole, disseminated chalcopyrite mineralization	1 ore section (a), 1 thin section (b)	WDS (b)
STO-23	Upper West, L305, room 305, E side	massive coarse-grained sphalerite-chalcopyrite ore	2 ore sections (a,b)	
STO-24	Lower West, L283, room 14	meta-calcsilicate rock, with disseminated chalcopyrite-pyrrhotite mineralization	1 ore section (a), 1 thin section (b)	EDS (b)
STO-26	Lower West, L283, room 14	massive coarse-grained sphalerite-chalcopyrite ore	1 ore section	
STO-28	East, copper lens, L288	remobilization vein, with coarse-grained chalcopyrite, galena, arsenopyrite and sulfosalts	3 ore sections (a,b,c)	EDS (b), WDS (a, c)
STO-29	East, copper lens, L288	remobilization vein, with coarse-grained arsenopyrite, galena and sulfosalts	1 ore section	
STO-33	Central Zone, L301, room Sek2	meta-calcsilicate rock, with pyrrhotite-chalcopyrite mineralization	1 ore section (a), 1 thin section (b)	WDS (a)
STO-34	Central Zone, L301, room Sek2	massive coarse-grained sphalerite-chalcopyrite ore, with visible shear planes	1 ore section	
STO-35	East, copper lens, L288	crosscutting quartz vein, with coarse-grained remobilized chalcopyrite	1 ore section (a), 1 thin section (b)	FI
STO-36	Central Zone, bottom, L255, room 1	semi-massive coarse-grained chalcopyrite-pyrrhotite ore	1 ore section (a), 1 thin section (b)	WDS (b)
STO-37	Central Zone, bottom, L255, room 3	massive coarse-grained chalcopyrite-pyrrhotite ore	1 ore section	WDS
STO-38	Central Zone, bottom, L255, room 3	crosscutting coarse-grained calcite vein, with visible slickenslides at the vein margins	1 thin section	
STO-39	Lower West, L283, room 14	altered meta-volcanic rock, with crosscutting quartz vein, hosting remobilized sulfides	1 thin section	
STO-40	Lower West, L283, room 14	crosscutting quartz vein, with coarse-grained remobilized chalcopyrite, galena and sulfosalts	1 ore section	FI
STO-41	Upper West, L305, room 305, W side	altered meta-volcanic rock, with crosscutting quartz vein, hosting remobilized sulfides	1 ore section	
STO-42	Upper West, L305, room 305, W side	crosscutting quartz vein, with crosscutting remobilized chalcopyrite and pyrrhotite	1 ore section	FI
STO-44	Upper East, L330, room 330	meta-calcsilicate rock, with garnet, diopside and vesuvianite	1 thin section	
STO-47	Upper East, L330, room 330	meta-calcsilicate rock, with garnet, diopside and wollastonite	1 thin section	
STO-50	Upper West, access ramp	remobilization vein, with galena, chalcopyrite, arsenopyrite and sulfosalts	1 ore section	EDS, WDS
STOB-98070-91.5	drillcore STOB-98070	altered meta-volcanic rock with biotite-spinel, disseminated chalcopyrite	1 thin section	
STOB-98070-93.4	drillcore STOB-98070	altered meta-volcanic rock with biotite-chlorite, disseminated chalcopyrite-arsenopyrite	1 ore section	WDS
STOB-98070-94.0	drillcore STOB-98070	altered meta-carbonate rock, with disseminated chalcopyrite-arsenopyrite mineralization	1 thin section	
STOB-98070-95.9	drillcore STOB-98070	altered meta-volcanic rock with amphibole, disseminated chalcopyrite mineralization	1 thin section	
STOB-98070-96.9	drillcore STOB-98070	massive sphalerite-chalcopyrite-pyrrhotite ore	1 ore section	
STOB-98070-97.6	drillcore STOB-98070	altered meta-volcanic rock with chlorite-biotite, fracture-hosted sphalerite-chalcopyrite	1 ore section	
STOB-98070-99.1	drillcore STOB-98070	altered metavolcanic rock with amphibole, semi-massive pyrrhotite-chalcopyrite mineralization	1 ore section	
STOB-98070-100.3	drillcore STOB-98070	altered meta-volcanic rock with chlorite, disseminated pyrrhotite mineralization	1 thin section	WDS
STOB-98070-101.8	drillcore STOB-98070	altered meta-volcanic rock with biotite-chlorite, semi-massive pyrrhotite mineralization	1 ore section	WDS
STOB-98070-105.6	drillcore STOB-98070	altered meta-volcanic rock with chlorite-biotite	1 thin section	WDS
STOB-98070-107.6	drillcore STOB-98070	altered meta-sedimentary rock with chlorite	1 thin section	WDS
STOB-98051-123.8	drillcore STOB-98051	crosscutting remobilization vein, with coarse-grained pyrrhotite and chalcopyrite	1 ore section	WDS

Table 11: Composition of sphalerite in massive ore. anhed.=anhedral, inc.=inclusions, l.=large s.=small, chp=chalcopyrite, po=pyrrhotite, py=pyrite

Sample/Spot:	STO-14/2a-3c	STO-14/2a-4a	STO-14/2a-4b	STO-14/2a-4c	STO-14/2b-4c	STO-14/2b-5a	STO-33a/1b-3a	STO-33a/1b-3b	STO-33a/2a-3a	STO-33a/2a-4b	STO-37/1-4a	STO-37/1-4b	STO-37/1-4c	STO-37/2-5a	STO-37/2-5b
Wt%															
Cu	0.0	0.0	0.0	0.0	0.0	0.0	0.0	0.0	0.0	0.0	0.1	0.1	0.1	0.0	0.0
Fe	7.7	8.0	9.2	8.5	7.3	7.2	6.9	7.2	6.3	6.4	7.0	7.1	6.8	6.3	6.7
Mn	0.4	0.3	0.3	0.4	0.4	0.4	0.3	0.3	0.3	0.2	0.1	0.1	0.1	0.1	0.1
Zn	58.9	59.7	57.8	58.0	59.8	57.3	58.3	58.5	60.5	60.7	57.2	57.1	58.4	57.9	58.2
Cd	0.1	0.1	0.0	0.0	0.1	0.1	0.1	0.1	0.1	0.0	0.3	0.3	0.3	0.4	0.3
Sn	0.0	0.0	0.0	0.0	0.0	0.0	0.0	0.0	0.0	0.0	0.0	0.0	0.0	0.0	0.0
As	0.0	0.0	0.0	0.0	0.0	0.0	0.0	0.0	0.0	0.0	0.0	0.0	0.0	0.0	0.0
S	32.5	32.3	32.3	31.7	32.3	32.7	33.6	33.4	32.5	33.0	34.0	34.2	33.7	33.7	33.5
Se	0.0	0.0	0.0	0.0	0.0	0.0	0.0	0.0	0.0	0.0	0.0	0.0	0.0	0.0	0.0
Te	0.0	0.0	0.0	0.0	0.0	0.0	0.0	0.0	0.0	0.0	0.0	0.0	0.0	0.0	0.0
Total	99.4	100.4	99.7	98.5	100.0	97.7	99.3	99.4	99.6	100.2	98.8	98.9	99.3	98.3	98.7
Formula	$Fe_{0.1}Zn_{0.9}S$	$Fe_{0.1}Zn_{0.9}S$	$Fe_{0.2}Zn_{0.8}S$	$Fe_{0.2}Zn_{0.8}S$	$Fe_{0.1}Zn_{0.9}S$	$Fe_{0.1}Zn_{0.9}S$	$Fe_{0.1}Zn_{0.9}S$	$Fe_{0.1}Zn_{0.9}S$	$Fe_{0.1}Zn_{0.9}S$	$Fe_{0.1}Zn_{0.9}S$	$Fe_{0.1}Zn_{0.9}S_{1.1}$	$Fe_{0.1}Zn_{0.9}S_{1.1}$	$Fe_{0.1}Zn_{0.9}S$	$Fe_{0.1}Zn_{0.9}S_{1.1}$	$Fe_{0.1}Zn_{0.9}S$
Description:	s. grains in py+po	s. grains in py+po	s. grains in py+po	s. grains in py+po	l. anhed. grains	l. anhed. grains	l. anhed. grains	l. anhed. grains	l. inc. in chp	l. inc. in chp	inc. in chp	inc. in chp	inc. in chp	l. inc. in chp	l. inc. in chp
Sample/Spot:	STO-37/2-5c	STO-37/2-6a	STO-37/2-6b	STO-37/2-6c	STO-37/2-7a	STO-37/2-7b	STO-37/3-2a	STO-37/3-2b	STO-37/3-2c	STOB-98070-101.8/Pos2a-4a	STOB-98070-101.8/Pos2a-4b	STOB-98070-101.8/Pos2a-4c	STOB-98070-101.8/Pos2b-3a	STOB-98070-101.8/Pos2b-3c	STOB-98070-101.8/Pos2c-4a
Wt%															
Cu	0.0	0.1	0.0	0.1	0.2	0.2	0.2	0.2	0.0	0.1	0.3	0.1	0.1	0.0	0.1
Fe	7.1	7.0	7.0	6.9	6.8	6.2	6.4	6.2	6.8	6.8	6.0	7.0	6.6	6.6	7.2
Mn	0.1	0.1	0.1	0.1	0.1	0.1	0.1	0.1	0.1	0.2	0.1	0.2	0.2	0.2	0.2
Zn	58.5	58.7	57.8	56.6	58.0	59.4	58.7	57.2	57.4	58.3	60.4	58.5	58.2	59.6	57.5
Cd	0.2	0.3	0.3	0.3	0.3	0.3	0.3	0.3	0.3	0.2	0.2	0.2	0.2	0.2	0.2
Sn	0.0	0.0	0.0	0.0	0.0	0.0	0.1	0.0	0.0	0.0	0.0	0.0	0.0	0.0	0.0
As	0.0	0.0	0.0	0.0	0.0	0.0	0.0	0.0	0.0	0.0	0.0	0.0	0.0	0.0	0.0
S	34.1	33.7	33.6	33.6	33.6	33.5	33.8	33.5	33.8	33.8	33.1	34.3	34.5	33.9	34.7
Se	0.0	0.0	0.0	0.0	0.0	0.0	0.0	0.0	0.0	0.0	0.0	0.0	0.0	0.0	0.0
Te	0.0	0.0	0.0	0.0	0.0	0.0	0.0	0.0	0.0	0.0	0.0	0.0	0.0	0.0	0.0
Total	100.1	99.9	98.8	97.6	99.1	99.7	99.5	97.3	98.4	99.3	100.1	100.3	99.9	100.5	99.9
Formula	$Fe_{0.1}Zn_{0.9}S$	$Fe_{0.1}Zn_{0.9}S$	$Fe_{0.1}Zn_{0.9}S$	$Fe_{0.1}Zn_{0.9}S_{1.1}$	$Fe_{0.1}Zn_{0.9}S$	$Fe_{0.1}Zn_{0.9}S$	$Fe_{0.1}Zn_{0.9}S$	$Fe_{0.1}Zn_{0.9}S_{1.1}$	$Fe_{0.1}Zn_{0.9}S_{1.1}$	$Fe_{0.1}Zn_{0.9}S$	$Fe_{0.1}Zn_{0.9}S$	$Fe_{0.1}Zn_{0.9}S$	$Fe_{0.1}Zn_{0.9}S_{1.1}$	$Fe_{0.1}Zn_{0.9}S$	$Fe_{0.1}Zn_{0.9}S_{1.1}$
Description:	l. inc. in chp	l. inc. in chp	l. inc. in chp	l. inc. in chp	l. inc. in chp	l. inc. in chp	l. inc. in chp	l. inc. in chp	l. inc. in chp	massive w/ py+po	massive w/ py+po	massive w/ py+po	massive w/ py+po	massive w/ py+po	crack fill in py

Sample/Spot:	STOB-98070-101.8/Pos2c-4b	STOB-98070-101.8/Pos2c-4c	STOB-98070-101.8/Pos2c-5b	STOB-98070-101.8/Pos2c-5c
Wt%				
Cu	0.1	0.1	0.1	0.2
Fe	7.4	7.3	7.6	6.7
Mn	0.2	0.2	0.2	0.2
Zn	57.7	57.8	57.1	58.9
Cd	0.2	0.2	0.2	0.3
Sn	0.0	0.0	0.0	0.0
As	0.0	0.0	0.0	0.0
S	34.0	33.6	34.0	33.5
Se	0.0	0.0	0.0	0.0
Te	0.0	0.0	0.0	0.0
Total	99.6	99.1	99.1	99.8
Formula	$Fe_{0.1}Zn_{0.9}S$	$Fe_{0.1}Zn_{0.9}S$	$Fe_{0.1}Zn_{0.9}S_{1.1}$	$Fe_{0.1}Zn_{0.9}S$
Description:	crack fill in py	crack fill in py	massive w/ py+po	massive w/ py+po

Table 12: Composition of sphalerite in remobilization veins. s. inc.=small inclusions, po=pyrrhotite, py=pyrite

Sample/Spot:	STO-6a/1a-7a	STO-6a/1a-7b	STO-6a/1a-7c	STO-6a/1a-8a	STO-6a/1a-8b	STO-6a/1a-8c	STO-6a/1b-2a	STO-6a/1b-2c	STO-50/1a-1a	STO-50/1a-1b	STO-50/1a-1c	STO-50/1b-13a	STO-50/1b-13b	STO-50/1b-13c
Wt%														
Cu	0.2	0.2	0.2	0.5	0.6	0.6	0.3	0.4	0.9	0.1	0.2	0.2	0.1	0.8
Fe	5.7	5.6	5.7	5.7	5.5	5.3	5.4	5.3	5.0	4.5	4.2	5.1	4.7	5.1
Mn	0.0	0.0	0.0	0.0	0.0	0.0	0.0	0.0	0.1	0.1	0.1	0.1	0.2	0.1
Zn	60.5	59.6	60.4	58.9	59.9	59.5	60.3	59.9	59.2	60.5	61.7	61.1	60.4	57.0
Cd	0.5	0.5	0.5	0.6	0.5	0.5	0.5	0.5	1.0	0.9	1.0	1.0	1.1	1.1
Sn	0.0	0.0	0.0	0.0	0.0	0.0	0.0	0.0	0.0	0.0	0.0	0.0	0.0	0.0
As	0.0	0.0	0.0	0.0	0.0	0.0	0.0	0.0	0.0	0.0	0.0	0.0	0.0	0.0
S	33.2	32.8	32.9	33.2	33.5	33.0	33.0	32.9	32.8	32.9	32.9	32.9	33.5	32.7
Se	0.0	0.0	0.0	0.0	0.0	0.0	0.0	0.0	0.0	0.0	0.0	0.0	0.0	0.0
Te	0.0	0.0	0.0	0.0	0.0	0.0	0.0	0.0	0.0	0.0	0.0	0.0	0.0	0.0
Total	99.9	98.7	99.7	98.9	100.0	98.9	99.4	99.0	99.0	99.0	100.1	100.4	100.0	96.8
Formula	$Fe_{0.1}Zn_{0.9}S$	$Fe_{0.1}Zn_{0.9}S$	$Fe_{0.1}Zn_{0.9}S$	$Fe_{0.1}Zn_{0.9}S$	$Fe_{0.1}Zn_{0.9}S$	$Fe_{0.1}Zn_{0.9}S$	$Fe_{0.1}Zn_{0.9}S$	$Fe_{0.1}Zn_{0.9}S$	$Fe_{0.1}Zn_{0.9}S$	$Fe_{0.1}Zn_{0.9}S$	$Fe_{0.1}Zn_{0.9}S$	$Fe_{0.1}Zn_{0.9}S$	$Fe_{0.1}Zn_{0.9}S$	$Fe_{0.1}Zn_{0.9}S$
Description:	inclusion in td	inclusion in td	inclusion in td	inclusion in td	inclusion in td	inclusion in td	inclusion in td	inclusion in td	s. inc. in po	s. inc. in po	s. inc. in po	s. inc. in po	s. inc. in po	s. inc. in po

Table 13: Composition of tetrahedrite-tennantite. STO-7c/2-4a and STO-7c/2-5a are from the massive ore, the rest of the date from remobilization veins. inc.=inclusions, l. **anhed.=large anhedral. brn=bournonite, gn=galena.**

	Massive ore		Remobilization veins							
Sample/Spot:	STO-7c/2-4a	STO-7c/2-5a	STO-6a/1a-1a	STO-6a/1a-1b	STO-6a/1a-9b	STO-6a/1b-1c	STO-6a/2-1a	STO-6a/2-1b	STO-50/1a-2a	STO-50/1a-2b
Wt%										
Cu	36.0	34.4	35.3	35.3	36.2	35.5	36.4	35.8	32.5	33.6
Ag	1.8	1.7	2.5	2.6	2.7	2.5	2.8	2.8	5.8	5.9
Fe	4.7	4.7	4.8	4.8	4.8	4.9	5.3	5.1	5.3	5.0
Zn	2.1	2.2	1.9	1.9	1.9	2.1	1.8	1.9	1.6	1.7
Au	0.0	0.0	0.0	0.0	0.0	0.0	0.0	0.0	0.0	0.0
Hg	0.0	0.0	0.0	0.0	0.0	0.0	0.0	0.0	0.0	0.0
Pb	0.0	0.0	0.0	0.0	0.0	0.0	0.0	0.0	0.0	0.0
As	2.4	1.9	0.9	1.1	0.9	0.7	0.6	0.8	0.5	0.3
Sb	26.4	27.4	26.8	27.2	26.6	26.3	26.0	26.5	27.3	26.6
Bi	0.0	0.0	0.0	0.0	0.0	0.0	0.0	0.0	0.0	0.0
S	24.2	24.9	24.1	23.7	23.0	24.0	23.6	23.9	24.4	23.5
Se	0.0	0.0	0.0	0.0	0.0	0.0	0.0	0.0	0.0	0.0
Te	0.0	0.0	0.0	0.0	0.0	0.0	0.0	0.0	0.0	0.0
Total	97.5	97.0	96.4	96.6	96.1	96.0	96.6	96.8	97.4	96.6
Formula	$Cu_{9.6}Ag_{0.3}Fe_{1.4}Zn_{0.5}As_{0.5}Sb_{3.7}S_{12.8}$	$Cu_{9.4}Ag_{0.3}Fe_{1.4}Zn0_{.6}As_{0.4}Sb_{3.9}S_{13.4}$	$Cu_{9.6}Ag_{0.4}Fe_{1.5}Zn_{0.5}As_{0.2}Sb_{3.8}S_{13}$	$Cu_{9.5}Ag_{0.4}Fe_{1.5}Zn_{0.5}As_{0.3}Sb_{3.8}S_{12.7}$	$Cu_{9.7}Ag_{0.4}Fe_{1.5}Zn_{0.5}As_{0.2}Sb_{3.7}S_{12.2}$	$Cu_{9.6}Ag_{0.4}Fe_{1.5}Zn_{0.6}As_{0.2}Sb_{3.7}S_{12.9}$	$Cu_{9.7}Ag_{0.4}Fe_{1.6}Zn_{0.5}As_{0.1}Sb_{3.6}S_{12.5}$	$Cu_{9.6}Ag_{0.4}Fe_{1.6}Zn_{0.5}As_{0.2}Sb_{3.7}S_{12.7}$	$Cu_{8.9}Ag_{0.9}Fe_{1.7}Zn_{0.4}As_{0.1}Sb_{3.9}S_{13.3}$	$Cu_{9.2}AgFe_{1.6}Zn_{0.4}As_{0.1}Sb_{3.8}S_{12.7}$
Description:	l. anhed. grain	l. anhed. grain	l. anhed. grain	l. anhed. grain	l. anhed. grain	l. anhed. grain	inclusion in gn	inclusion in gn	inc. in gn+brn	inc. in gn+brn
Sample/Spot:	STO-50/1a-2c	STO-50/1a-3a	STO-50/1a-3b	STO-50/1a-3c	STO-50/1b-8a	STO-50/1b-8b	STO-50/1b-8c	STO-50/1b-12a	STO-50/1b-12b	STO-50/1b-12c
Wt%										
Cu	33.4	34.1	35.2	34.2	33.7	33.1	33.8	33.1	33.6	33.1
Ag	6.0	5.5	5.6	5.3	5.9	6.1	5.8	5.8	5.9	5.7
Fe	4.8	4.8	4.9	4.8	4.9	4.8	4.8	5.0	4.8	5.1
Zn	1.7	1.8	1.8	1.8	1.7	1.7	1.7	1.8	1.8	1.8
Au	0.0	0.0	0.0	0.0	0.0	0.0	0.0	0.0	0.0	0.0
Hg	0.0	0.0	0.0	0.0	0.0	0.0	0.0	0.0	0.0	0.4
Pb	0.0	0.0	0.0	0.0	0.0	0.0	0.0	0.0	0.0	0.0
As	0.6	0.5	0.4	0.6	0.6	0.6	0.6	0.6	0.6	0.6
Sb	26.6	26.9	27.2	27.6	26.4	26.7	26.9	27.4	26.7	27.6
Bi	0.0	0.0	0.0	0.0	0.0	0.0	0.6	0.0	0.0	0.0
S	23.0	22.9	23.9	22.8	23.7	24.2	23.4	24.0	23.5	24.0
Se	0.0	0.0	0.0	0.0	0.0	0.0	0.0	0.0	0.0	0.0
Te	0.0	0.0	0.0	0.0	0.0	0.0	0.0	0.0	0.0	0.0
Total	96.1	96.4	99.1	97.0	96.8	97.2	97.6	97.7	96.8	98.3
Formula	$Cu_{9.1}AgFe_{1.5}Zn_{0.4}As_{0.1}Sb_{3.8}S_{12.5}$	$Cu_{9.3}Ag_{0.9}Fe_{1.5}Zn_{0.5}As_{0.1}Sb_{3.8}S_{12.3}$	$Cu_{9.3}Ag_{0.9}Fe_{1.5}Zn_{0.5}As_{0.1}Sb_{3.8}S_{12.5}$	$Cu_{9.2}Ag_{0.8}Fe_{1.5}Zn_{0.5}As_{0.1}Sb_{3.9}S_{12.2}$	$Cu_{9.2}Ag_{0.9}Fe_{1.5}Zn_{0.5}As_{0.1}Sb_{3.2}S_{12.8}$	$Cu_{9.1}AgFe_{1.5}Zn_{0.5}As_{0.2}Sb_{3.8}S_{13.2}$	$Cu_{9.1}Ag_{0.9}Fe_{1.5}Zn_{0.5}As_{0.1}Sb_{3.8}S_{12.6}$	$Cu_{9}Ag_{0.9}Fe_{1.5}Zn_{0.5}As_{0.1}Sb_{3.9}S_{13}$	$Cu_{9.2}AgFe_{1.5}Zn_{0.5}As_{0.2}Sb_{3.8}S_{12.7}$	$Cu_{9}Ag_{0.9}Fe_{1.6}Zn_{0.5}As_{0.1}Sb_{3.9}S_{12.9}$
Description:	inc. in gn+brn	inc. in gn+brn	inc. in gn+brn	inc. in gn+brn	inc. in gn+brn	inc. in gn+brn	inc. in gn+brn	inc. in gn+brn	inc. in gn+brn	inc. in gn+brn

Table 14: Composition of arsenopyrite in massive ore. c. grained=coarse-grained, p-blast=porphyroblast, s. grain= small grain. gg=gangue, gn=galena, py=pyrite.

Sample/Spot:	STO-7c/2-1a	STO-7c/2-1b	STO-7c/2-1c	STO-7c/2-6a	STO-7c/2-6b	STO-7c/2-6c	STO-7c/3-1a	STO-7c/3-1b	STO-7c/3-1c	STOB-98070-93.4/1-1a	STOB-98070-93.4/1-1b	STOB-98070-93.4/1-1c	STOB-98070-93.4/1-2a	STOB-98070-93.4/1-2b	STOB-98070-93.4/1-2c
Wt%															
Cu	0.1	0.0	0.0	0.0	0.0	0.0	0.0	0.0	0.0	0.0	0.0	0.0	0.0	0.0	0.0
Fe	35.2	34.3	35.2	34.4	34.7	33.7	35.2	36.2	35.0	34.7	35.1	34.7	33.4	33.4	34.1
Mn	0.0	0.0	0.0	0.0	0.0	0.0	0.0	0.0	0.0	0.0	0.0	0.0	0.0	0.0	0.0
Co	0.0	0.0	0.0	0.0	0.0	0.0	0.0	0.0	0.1	0.0	0.0	0.0	0.0	0.0	0.0
Ni	0.0	0.0	0.0	0.0	0.0	0.0	0.0	0.0	0.0	0.0	0.0	0.0	0.1	0.1	0.1
Zn	0.0	0.0	0.0	0.0	0.0	0.0	0.0	0.0	0.0	0.0	0.0	0.0	0.0	0.0	0.0
As	43.9	43.9	43.6	44.6	44.8	44.8	42.8	44.0	43.7	46.4	46.6	46.7	47.9	48.0	47.9
Sb	0.0	0.0	0.0	0.0	0.0	0.0	0.0	0.0	0.0	0.0	0.0	0.0	0.0	0.0	0.0
S	20.0	19.2	19.9	18.7	18.5	18.8	21.0	19.7	19.6	17.9	17.5	17.5	17.2	16.8	16.9
Se	0.0	0.0	0.0	0.0	0.0	0.0	0.0	0.0	0.0	0.0	0.0	0.0	0.0	0.0	0.0
Te	0.0	0.0	0.0	0.0	0.0	0.0	0.0	0.0	0.0	0.0	0.0	0.0	0.0	0.0	0.0
Total	99.2	97.4	98.7	97.7	98.0	97.3	99.0	99.9	98.4	99.1	99.2	98.9	98.6	98.3	99.0
Formula	FeAsS	FeAsS	FeAsS	FeAsS	$Fe_{1.1}AsS$	FeAsS	$FeAs_{0.9}S_{1.1}$	$Fe_{1.1}AsS$	$Fe_{1.1}AsS$	$Fe_{1.1}As_{1.1}S_{0.9}$	$Fe_{1.1}As_{1.1}S_{0.9}$	$Fe_{1.1}As_{1.1}S_{0.9}$	$FeAs_{1.1}S_{0.9}$	$FeAs_{1.1}S_{0.9}$	$FeAs_{1.1}S_{0.9}$
Description:	p-blast w/gn	p-blast w/gn	p-blast w/gn	p-blast in gg	p-blast in gg	p-blast in gg	s.grain in gn	s.grain in gn	s. grain in gn	c. grained w/py	c. grained w/py	c. grained w/py	c. grained w/py	c. grained w/py	c. grained w/py
Sample/Spot:	STOB-98070-93.4/1-3a	STOB-98070-93.4/1-3b	STOB-98070-93.4/1-3c	STOB-98070-93.4/2a-2a	STOB-98070-93.4/2a-2b	STOB-98070-93.4/2a-2c	STOB-98070-93.4/2a-4a	STOB-98070-93.4/2a-4b	STOB-98070-93.4/2a-4c	STOB-98070-93.4/2b-1a	STOB-98070-93.4/2b-1b	STOB-98070-93.4/2b-1c	STOB-98070-93.4/2b-2a	STOB-98070-93.4/2b-2b	STOB-98070-93.4/2b-2c
Wt%															
Cu	0.0	0.0	0.0	0.0	0.0	0.0	0.0	0.0	0.0	0.0	0.0	0.0	0.0	0.0	0.0
Fe	33.8	34.2	33.7	34.4	34.0	34.4	34.8	34.8	34.1	33.5	35.1	35.0	34.6	33.1	33.1
Mn	0.0	0.0	0.0	0.0	0.0	0.0	0.0	0.0	0.0	0.0	0.0	0.0	0.0	0.0	0.0
Co	0.0	0.0	0.0	0.0	0.0	0.0	0.0	0.0	0.0	0.0	0.0	0.0	0.0	0.0	0.0
Ni	0.0	0.0	0.0	0.0	0.0	0.0	0.0	0.0	0.0	0.0	0.0	0.0	0.0	0.0	0.0
Zn	0.0	0.0	0.0	0.0	0.0	0.0	0.0	0.0	0.0	0.0	0.0	0.0	0.0	0.0	0.0
As	47.1	47.1	47.1	45.5	45.8	45.7	44.3	44.5	44.6	42.6	41.9	42.1	43.2	43.0	43.4
Sb	0.0	0.0	0.1	0.0	0.0	0.0	0.0	0.0	0.0	0.0	0.0	0.0	0.0	0.0	0.0
S	17.2	17.7	18.0	18.9	18.3	18.4	19.4	19.4	18.9	20.2	20.2	20.4	19.3	20.4	19.9
Se	0.0	0.0	0.0	0.0	0.0	0.0	0.0	0.0	0.0	0.0	0.0	0.0	0.0	0.0	0.0
Te	0.0	0.0	0.0	0.0	0.0	0.0	0.0	0.0	0.0	0.0	0.0	0.1	0.0	0.0	0.0
Total	98.1	98.9	98.8	98.7	98.1	98.5	98.4	98.7	97.6	96.3	97.2	97.5	97.2	96.5	96.5
Formula	$FeAs_{1.1}S_{0.9}$	$FeAs_{1.1}S_{0.9}$	$FeAs_{1.1}S_{0.9}$	FeAsS	FeAsS	FeAsS	FeAsS	FeAsS	FeAsS	FeAsS	$FeAs_{0.9}S_{1.1}$	$FeAs_{0.9}S_{1.1}$	$Fe_{1.1}AsS$	$FeAs_{0.9}S_{1.1}$	FeAsS
Description:	c. grained w/py	c. grained w/py	c. grained w/py	grain in gg	grain in gg	grain in gg	s. grains in gg	s. grains in gg	s. grains in gg	s. grains in gg	s. grains in gg	s. grains in gg	s. grains in gg	s. grains in gg	s. grains in gg
Sample/Spot:	STOB-98070-93.4/2b-3a	STOB-98070-93.4/2b-3b	STOB-98070-93.4/2b-3c	STOB-98070-93.4/2b-4a	STOB-98070-93.4/2b-4b	STOB-98070-93.4/2b-4c	STOB-98070-101.8/Pos1a-1	STOB-98070-101.8/Pos1a-1	STOB-98070-101.8/Pos1a-1	STOB-98070-101.8/Pos1a-2a	STOB-98070-101.8/Pos1a-2b	STOB-98070-101.8/Pos1a-2c	STOB-98070-101.8/Pos1b-1a	STOB-98070-101.8/Pos1b-1b	
Wt%															
Cu	0.0	0.0	0.0	0.0	0.0	0.0	0.0	0.0	0.1	0.0	0.0	0.0	0.0	0.0	
Fe	34.7	34.9	34.3	33.9	34.3	36.1	34.3	34.5	34.5	34.2	35.5	34.0	34.0	33.5	
Mn	0.0	0.0	0.0	0.0	0.0	0.0	0.0	0.0	0.0	0.0	0.0	0.0	0.0	0.0	
Co	0.0	0.0	0.0	0.0	0.0	0.0	0.1	0.0	0.0	0.0	0.1	0.0	0.1	0.0	
Ni	0.0	0.0	0.0	0.0	0.0	0.0	0.0	0.0	0.0	0.0	0.0	0.0	0.0	0.0	
Zn	0.0	0.0	0.0	0.0	0.0	0.0	0.0	0.0	0.1	0.0	0.0	0.1	0.1	0.0	
As	43.1	42.7	43.1	43.9	42.7	42.8	43.9	44.4	44.2	44.0	44.0	43.7	44.0	44.6	
Sb	0.0	0.0	0.0	0.0	0.0	0.0	0.0	0.1	0.0	0.0	0.0	0.0	0.0	0.0	
S	20.4	20.4	19.7	19.4	20.6	20.2	19.2	19.6	18.9	18.9	19.3	19.1	19.4	18.2	
Se	0.0	0.0	0.0	0.0	0.0	0.0	0.0	0.0	0.0	0.0	0.0	0.0	0.0	0.0	
Te	0.0	0.0	0.0	0.0	0.0	0.0	0.0	0.0	0.0	0.0	0.0	0.0	0.0	0.0	
Total	98.1	98.0	97.1	97.1	97.7	99.0	97.4	98.6	97.8	97.2	98.9	96.9	97.6	96.2	
Formula	FeAsS	$FeAs_{0.9}S_{1.1}$	FeAsS	FeAsS	$FeAs_{0.9}S_{1.1}$	FeAsS	FeAsS	FeAsS	FeAsS	FeAsS	$Fe_{1.1}AsS$	FeAsS	FeAsS	FeAsS	
Description:	s. grains in gg	s. grains in gg	s. grains in gg	s. grains in gg	s. grains in gg	s. grains in gg	s. grains in gg	s. grains in gg	s. grains in gg	s. grains in gg	s. grains in gg	s. grains in gg	s. grains in gg	s. grains in gg	

Table 15: Composition of arsenopyrite in remobilization veins. cont. w/= contact with, l.=large, p-blast=porphyroblast, s.=small, chp=chalcopyrite, gg=gangue, gn=galena.

Sample/Spot:	STOB-98070-101.8/Pos1b-1c	STO-28a/2a-1a	STO-28a/2a-1b	STO-28a/2a-1c	STO-28a/2a-2a	STO-28a/2a-2b	STO-28a/2a-3a	STO-28a/2a-3b	STO-28a/2a-3c	STO-50/3-4a	STO-50/3-4b	STO-50/3-4c
Wt%												
Cu	0.0	0.0	0.0	0.0	0.0	0.0	0.0	0.0	0.0	0.0	0.0	0.0
Fe	34.3	34.1	34.3	35.1	33.9	34.6	34.6	34.2	35.2	32.6	34.2	34.5
Mn	0.0	0.0	0.0	0.0	0.0	0.0	0.0	0.0	0.0	0.0	0.0	0.0
Co	0.1	0.5	0.5	0.4	0.3	0.7	0.3	0.3	0.4	0.0	0.0	0.0
Ni	0.0	0.0	0.0	0.0	0.0	0.0	0.0	0.0	0.0	0.1	0.0	0.0
Zn	0.0	0.0	0.0	0.0	0.0	0.0	0.0	0.0	0.0	0.0	0.0	0.0
As	44.0	42.5	42.7	42.6	43.2	42.0	43.5	43.5	43.8	46.4	46.3	46.6
Sb	0.0	0.0	0.0	0.1	0.0	0.0	0.0	0.0	0.0	0.5	0.4	0.4
S	19.6	21.3	20.2	20.7	20.5	21.0	20.6	20.2	20.5	16.6	17.1	17.3
Se	0.0	0.0	0.0	0.0	0.0	0.0	0.0	0.0	0.0	0.0	0.0	0.0
Te	0.0	0.0	0.0	0.0	0.0	0.0	0.0	0.0	0.0	0.0	0.0	0.0
Total	98.0	98.3	97.6	98.9	97.8	98.3	99.0	98.4	99.9	96.1	97.9	98.8
Formula	FeAsS	$FeAs_{0.9}S_{1.1}$	$FeAs_{0.9}S_{1.1}$	$FeAs_{0.9}S_{1.1}$	$FeAs_{0.9}S_{1.1}$	$FeAs_{0.9}S_{1.1}$	FeAsS	FeAsS	FeAsS	$FeAs_{1.1}S_{0.9}$	$Fe_{1.1}As_{1.1}S_{0.9}$	$Fe_{1.1}As_{1.1}S_{0.9}$
Description:	s. grains in gg	grain, cont. w/ chp	grain, cont. w/ chp	grain, cont. w/ chp	grain, cont. w/ chp	grain, cont. w/ chp	grain, cont. w/ chp	grain, cont. w/ chp	grain, cont. w/ chp	l. p-blast in gn	l. p-blast in gn	l. p-blast in gn
Sample/Spot:	STO-50/3-5a	STO-50/3-5b	STO-50/3-5c	STO-50/3-6a	STO-50/3-6b	STO-50/3-6c	STO-28c/2-1a	STO-28c/2-1b	STO-28c/2-2a	STO-28c/2-2b	STO-28c/2-3a	STO-28c/2-3b
Wt%												
Cu	0.0	0.0	0.0	0.0	0.0	0.0	0.0	0.0	0.0	0.0	0.0	0.0
Fe	35.6	35.0	35.3	33.9	34.4	34.2	34.3	34.5	34.6	34.7	34.8	35.1
Mn	0.0	0.0	0.0	0.0	0.0	0.0	0.0	0.0	0.0	0.0	0.0	0.0
Co	0.0	0.0	0.0	0.0	0.0	0.0	0.0	0.0	0.0	0.0	0.0	0.0
Ni	0.0	0.0	0.0	0.0	0.0	0.0	0.0	0.0	0.0	0.0	0.0	0.0
Zn	0.0	0.0	0.0	0.0	0.0	0.0	0.0	0.0	0.0	0.0	0.0	0.0
As	44.2	44.5	44.3	46.5	47.1	47.0	43.8	43.9	44.2	44.2	44.1	44.1
Sb	0.0	0.0	0.1	0.4	0.4	0.5	0.0	0.0	0.0	0.0	0.0	0.0
S	19.8	18.9	19.3	17.3	16.8	17.2	19.8	19.4	19.4	19.4	19.9	19.3
Se	0.0	0.0	0.0	0.0	0.0	0.0	0.0	0.2	0.2	0.2	0.2	0.2
Te	0.0	0.0	0.0	0.0	0.0	0.0	0.0	0.0	0.0	0.0	0.0	0.0
Total	99.5	98.3	98.9	98.2	98.6	98.8	97.9	97.9	98.4	98.6	98.9	98.9
Formula	$Fe_{1.1}AsS$	$Fe_{1.1}AsS$	$Fe_{1.1}AsS$	$FeAs_{1.1}S_{0.9}$	$Fe_{1.1}As_{1.1}S_{0.9}$	$Fe_{1.1}As_{1.1}S_{0.9}$	FeAsS	FeAsS	FeAsS	FeAsS	FeAsS	$Fe_{1.1}AsS$
Description:	l. p-blast in gn	l. p-blast in gn	l. p-blast in gn	l. p-blast in gn	l. p-blast in gn	l. p-blast in gn	l. grain in gg	l. grain in gg	l. grain in gg	l. grain in gg	l. grain in gg	l. grain in gg

Table 16: Composition of boulangerite. All samples are from remobilization veins. inc.=inclusions, l.=large, symp.=symplectitic, gn=galena

Sample/Spot:	STO-50/1b-1a	STO-50/1b-1b	STO-50/1b-1c	STO-50/1b-2b	STO-50/1b-2c	STO-50/2-1a	STO-50/2-1b	STO-50/2-3a	STO-50/2-3b	STO-50/2-3c	STO-50/2-4b
Wt%											
Cu	0.0	0.0	0.2	0.0	0.1	0.0	0.0	0.0	0.0	0.0	0.0
Ag	0.0	0.0	0.0	0.0	0.0	0.0	0.0	0.0	0.0	0.0	0.0
Fe	0.0	0.0	0.0	0.0	0.0	0.0	0.0	0.0	0.0	0.0	0.0
Zn	0.0	0.0	0.0	0.0	0.0	0.0	0.0	0.0	0.0	0.0	0.0
Au	0.0	0.0	0.0	0.0	0.0	0.0	0.0	0.0	0.0	0.0	0.0
Hg	0.5	0.0	0.0	0.0	0.0	0.0	0.0	0.0	0.0	0.0	0.0
Pb	56.5	56.3	55.4	56.6	57.3	56.8	56.5	56.3	56.5	55.7	56.7
As	0.0	0.0	0.0	0.0	0.0	0.0	0.3	0.0	0.0	0.0	0.0
Sb	22.0	22.1	22.6	22.6	21.8	21.9	22.3	22.2	22.1	22.0	21.7
Bi	0.8	0.7	0.8	0.6	0.0	0.0	0.6	0.8	0.8	1.0	1.1
S	17.4	17.2	17.4	17.6	17.1	17.5	17.6	18.2	17.9	18.1	17.8
Se	0.0	0.0	0.0	0.0	0.0	0.0	0.0	0.0	0.0	0.0	0.0
Te	0.0	0.0	0.0	0.0	0.0	0.0	0.0	0.0	0.0	0.0	0.0
Total	97.1	96.3	96.4	97.3	96.3	96.2	97.2	97.5	97.3	96.7	97.3
Formula	$Hg_{0.1}Pb_{5.3}Sb_{3.5}Bi_{0.1}S_{10.6}$	$Pb_{5.4}Sb_{3.6}Bi_{0.1}S_{10.5}$	$Cu_{0.1}Pb_{5.2}Sb_{3.6}Bi_{0.1}S_{10.6}$	$Pb_{5.3}Sb_{3.6}Bi_{0.1}S_{10.7}$	$Pb_{5.5}Sb_{3.5}S_{10.5}$	$Pb_{5.4}Sb_{3.6}S_{10.8}$	$Pb_{5.3}As_{0.1}Sb_{3.6}Bi_{0.1}S_{10.7}$	$Pb_{5.3}Sb_{3.6}Bi_{0.1}S_{11.1}$	$Pb_{5.4}Sb_{3.6}Bi_{0.1}S_{11}$	$Pb_{5.3}Sb_{3.6}Bi_{0.1}S_{11.2}$	$Pb_{5.4}Sb_{3.5}Bi_{0.1}S_{10.9}$
Description	symp. w/gn	symp. w/gn	symp. w/gn	symp. w/gn	symp. w/gn	symp. w/gn	l. inc. in gn	inc. in gn	inc. in gn	inc. in gn	inc. in gn

Sample/Spot:	STO-50/2-4c	STO-50/2-6a	STO-50/2-6b	STO-50/2-6c	STO-50/3-2a	STO-50/3-2b	STO-50/3-2c	STO-50/3-3a	STO-50/3-3b	STO-50/3-3c
Wt%										
Cu	0.0	0.0	0.0	0.0	0.0	0.0	0.0	0.0	0.0	0.0
Ag	0.0	0.0	0.0	0.0	0.0	0.0	0.0	0.0	0.0	0.0
Fe	0.0	0.0	0.0	0.0	0.0	0.0	0.0	0.0	0.0	0.0
Zn	0.0	0.0	0.0	0.0	0.0	0.0	0.0	0.0	0.0	0.0
Au	0.0	0.0	0.0	0.0	0.0	0.0	0.0	0.0	0.0	0.0
Hg	0.0	0.0	0.0	0.0	0.0	0.0	0.6	0.0	0.0	0.0
Pb	55.7	55.8	55.9	55.9	56.4	55.5	56.0	55.1	55.5	56.3
As	0.0	0.0	0.0	0.0	0.3	0.0	0.0	0.0	0.0	0.0
Sb	21.6	22.5	22.5	22.2	22.6	21.5	22.2	21.9	22.2	22.6
Bi	0.9	0.6	0.0	0.0	0.7	0.9	0.9	0.9	0.7	0.0
S	18.0	18.5	18.3	18.3	18.2	18.3	18.4	18.5	18.3	18.0
Se	0.0	0.0	0.0	0.0	0.0	0.0	0.0	0.0	0.0	0.0
Te	0.0	0.0	0.0	0.0	0.0	0.0	0.0	0.0	0.0	0.0
Total	96.1	97.4	96.7	96.5	98.2	96.2	98.0	96.5	96.8	96.9
Formula	$Pb_{5.4}Sb_{3.5}Bi_{0.1}S_{11.2}$	$Pb_{5.3}Sb_{3.6}Bi_{0.1}S_{11.3}$	$Pb_{5.3}Sb_{3.7}Bi_{0.1}S_{11.3}$	$Pb_{5.4}Sb_{3.6}Bi_{0.1}S_{11.4}$	$Pb_{5.3}As_{0.1}Sb_{3.6}Bi_{0.1}S_{11}$	$Pb_{5.4}Sb_{3.5}Bi_{0.1}S_{11.4}$	$Hg_{0.1}Pb_{5.3}Sb_{3.6}Bi_{0.1}S_{11.3}$	$Pb_{5.3}Sb_{3.6}Bi_{0.1}S_{11.5}$	$Pb_{5.3}Sb_{3.6}Bi_{0.1}S_{11.3}$	$Pb_{5.3}Sb_{3.7}S_{11.1}$
Description	inc. in gn	l. inc. in gn	l. inc. in gn	l. inc. in gn	inc. in gn	inc. in gn	inc. in gn	inc. in gn	inc. in gn	inc. in gn

Table 17: Composition of bournonite. All samples are from remobilization veins. symp.=symplectitic. gn=galena.

Sample/Spot:	STO-50/1b-3c	STO-50/1b-6b	STO-50/1b-9b	STO-50/1b-9c	STO-50/2-5a	STO-50/2-5b	STO-50/2-5c	STO-50/3-1a	STO-50/3-1b	STO-50/3-1c
Wt%										
Cu	11.8	12.5	12.9	12.8	12.6	13.0	12.6	13.2	12.9	12.7
Ag	0.0	0.0	0.0	0.0	0.0	0.0	0.0	0.0	0.0	0.0
Fe	0.0	0.0	0.0	0.0	0.0	0.0	0.0	0.0	0.0	0.0
Zn	0.0	0.0	0.0	0.0	0.0	0.0	0.0	0.0	0.0	0.0
Au	0.0	0.0	0.0	0.0	0.0	0.0	0.0	0.0	0.0	0.0
Hg	0.0	0.0	0.0	0.0	0.0	0.0	0.0	0.0	0.0	0.0
Pb	42.2	41.2	42.2	41.4	41.5	42.1	41.6	40.8	41.2	42.2
As	0.4	0.0	0.0	0.3	0.4	0.0	0.0	0.3	0.0	0.3
Sb	22.6	23.5	23.4	23.1	23.3	23.5	22.6	22.6	23.2	22.4
Bi	0.6	0.0	0.0	0.0	0.0	0.0	0.0	0.0	0.0	0.0
S	18.9	19.1	18.9	19.0	19.5	19.5	19.7	19.7	19.8	19.9
Se	0.4	0.0	0.0	0.0	0.0	0.0	0.0	0.0	0.0	0.0
Te	0.0	0.0	0.0	0.0	0.0	0.0	0.0	0.0	0.0	0.0
Total	96.8	96.3	97.5	96.5	97.2	98.1	96.5	96.5	97.2	97.4
Formula	$CuPbSbS_3$	$CuPbSbS_3$	$CuPbSbS_3$	$CuPbSbS_3$	$CuPbSbS_{3.1}$	$CuPbSbS_3$	$CuPbSbS_{3.1}$	$CuPbSb_{0.9}S_{3.1}$	$CuPbSbS_{3.1}$	$CuPbSb_{0.9}S_{3.1}$
Description:	symp. w/ gn	symp. w/ gn	symp. w/ gn	inc. in gn	symp. w/ gn	symp. w/ gn	symp. w/ gn	symp. w/ gn	symp. w/ gn	symp. w/ gn

Table 18: Composition of chalcopyrite. inc.=inclusions, chp=chalcopyrite, gg=gangue, sph=sphalerite.

	Massive Ore					Remobilization Veins	
Sample/Spot:	STO-33a/1a-1	STO-37/2-2a	STOB-98070-101.8/Pos1a-3a	STOB-98070-101.8/Pos1a-3b	STOB-98070-101.8/Pos1a-3c	STOB-98051-123.8/Pos1-3a	STOB-98051-123.8/Pos1-3b
Wt%							
Cu	32.0	33.0	36.9	37.0	36.7	34.4	34.3
Fe	29.2	28.2	29.6	28.8	28.8	28.5	28.4
Mn	0.0	0.0	0.0	0.0	0.0	0.0	0.0
Co	0.0	0.0	0.0	0.0	0.0	0.0	0.0
Ni	0.0	0.0	0.0	0.0	0.0	0.0	0.0
Zn	1.7	0.9	0.0	0.0	0.0	0.0	0.0
As	0.0	0.0	0.0	0.0	0.0	0.0	0.0
Sb	0.0	0.0	0.0	0.0	0.0	0.0	0.0
S	35.6	34.1	33.8	33.1	33.5	35.5	34.6
Se	0.0	0.0	0.0	0.0	0.0	0.0	0.0
Te	0.0	0.0	0.0	0.0	0.0	0.0	0.0
Total	98.4	96.2	100.3	98.9	98.9	98.4	97.4
Formula	$CuFeZn_{0.1}S_{2.1}$	$CuFeS_{2.1}$	$CuFeS_{1.9}$	$Cu_{1.1}Fe_{0.9}S_{1.9}$	$Cu_{1.1}Fe_{0.9}S_{1.9}$	$CuFeS_{2.1}$	$CuFeS_{2.1}$
Description:	inc. in sph	inc. in sph	small inc. in gg	small inc. in gg	small inc. in gg	massive chp	massive chp

Table 19:Composition of galena. Samples STO-7c and STOB-98070-93.4 are from the massive ore, the rest from remobilization veins. inc.=inclusions, l. anhed.=large anhedra, symp=symplectitic, brn=bournonite, gg=gangue, td=tetrahedrite.

	Massive Ore				Remobilization Veins										
Sample/Spot:	STO-7c/3-2a	STO-7c/3-2b	STO-7c/3-2c	STOB-98070-93.4/2b-5a	STO-6a/1a-4a	STO-6a/1a-4b	STO-6a/1a-6a	STO-6a/1a-6b	STO-6a/1a-6c	STO-6a/1b-5a	STO-6a/1b-5b	STO-6a/1b-5c	STO-6a/2-3a	STO-6a/2-3b	STO-6a/2-3c
Wt%															
Cu	0.0	0.0	0.0	0.0	0.7	0.6	0.0	0.1	0.1	0.3	0.1	0.2	0.0	0.0	0.1
Ag	0.0	0.0	0.0	0.0	0.0	0.0	0.0	0.0	0.0	0.0	0.0	0.0	0.0	0.0	0.0
Fe	0.0	0.0	0.0	0.0	0.1	0.0	0.0	0.0	0.0	0.0	0.0	0.0	0.0	0.0	0.0
Zn	0.0	0.0	0.0	0.0	0.1	0.1	0.0	0.1	0.1	0.0	0.0	0.0	0.0	0.0	0.0
Au	0.0	0.0	0.0	0.0	0.0	0.0	0.0	0.0	0.0	0.0	0.0	0.0	0.0	0.0	0.0
Hg	0.0	0.0	0.0	0.0	0.0	0.0	0.0	0.0	0.4	0.0	0.0	0.0	0.0	0.0	0.0
Pb	85.7	82.9	85.0	83.9	83.5	84.2	84.1	85.6	85.3	85.2	85.7	83.7	83.2	84.5	84.5
As	0.0	0.0	0.0	0.0	0.0	0.0	0.0	0.0	0.0	0.0	0.0	0.0	0.0	0.0	0.0
Sb	0.0	0.0	0.0	0.0	0.0	0.0	0.0	0.0	0.0	0.0	0.0	0.0	0.0	0.0	0.0
Bi	0.0	0.0	0.0	0.0	0.0	0.0	0.0	0.0	0.0	0.0	0.0	0.0	0.7	0.0	0.0
S	12.7	13.1	12.9	13.3	12.5	12.4	12.3	12.4	12.7	13.2	12.9	13.1	13.1	13.2	13.1
Se	0.0	0.2	0.3	0.0	0.4	0.3	0.4	0.3	0.5	0.0	0.2	0.0	0.0	0.0	0.0
Te	0.0	0.0	0.0	0.0	0.0	0.0	0.0	0.0	0.0	0.0	0.0	0.0	0.0	0.0	0.0
Total	98.4	96.3	98.1	97.1	97.3	97.7	96.9	98.5	99.1	98.6	99.0	97.0	97.0	97.7	97.6
Formula	PbS	PbS	PbS	PbS	$PbS_{0.9}$	$PbS_{0.9}$	$PbS_{0.9}$	$PbS_{0.9}$	$PbS_{0.9}$	PbS	PbS	PbS	PbS	PbS	PbS
Description:	l. anhed. grain	l. anhed. grain	l. anhed. grain	inc. in gg	symp. w/ brn	symp. w/ brn	inclusion in td	inclusion in td	inclusion in td	symp. w/ brn	symp. w/ brn	symp. w/ brn	l. anhed. grain	l. anhed. grain	l. anhed. grain
Sample/Spot:	STO-28a/1a-2a	STO-28a/1a-2b	STO-28a/1a-7a	STO-28a/1a-7b	STO-28a/1a-7c	STO-28a/1a-8a	STO-28a/1a-8b	STO-50/1a-4a	STO-50/1a-4b	STO-50/1a-4c	STO-50/1b-5a	STO-50/1b-5b	STO-50/1b-5c	STO-50/2-2b	
Wt%															
Cu	0.0	0.0	0.1	0.2	0.1	0.0	0.0	0.3	0.1	0.2	0.0	0.0	0.0	0.0	
Ag	0.2	0.0	0.2	0.2	0.3	0.0	0.0	0.0	0.0	0.0	0.0	0.0	0.0	0.0	
Fe	0.0	0.0	0.0	0.0	0.0	0.0	0.0	0.0	0.0	0.0	0.0	0.0	0.0	0.0	
Zn	0.0	0.0	0.0	0.0	0.0	0.0	0.0	0.0	0.0	0.0	0.0	0.0	0.0	0.0	
Au	0.0	0.0	0.0	0.0	0.0	0.0	0.0	0.0	0.0	0.0	0.0	0.0	0.0	0.0	
Hg	0.0	0.0	0.0	0.0	0.0	0.0	0.0	0.0	0.0	0.0	0.0	0.0	0.0	0.0	
Pb	82.7	83.5	85.4	83.8	84.4	84.0	84.5	84.8	86.1	85.4	84.7	86.8	86.9	87.1	
As	0.0	0.0	0.0	0.0	0.0	0.0	0.0	0.0	0.0	0.0	0.0	0.0	0.0	0.0	
Sb	0.0	0.0	0.0	0.3	0.0	0.0	0.0	0.0	0.0	0.0	0.0	0.0	0.0	0.0	
Bi	0.9	0.0	0.7	1.2	0.0	0.0	0.0	0.0	0.0	0.0	0.6	0.0	0.0	0.0	
S	13.7	13.1	12.8	13.1	13.3	13.3	13.6	13.3	12.8	12.9	12.9	13.1	13.3	13.0	
Se	0.3	0.2	0.0	0.0	0.2	0.2	0.3	0.0	0.0	0.0	0.2	0.0	0.0	0.2	
Te	0.0	0.0	0.0	0.0	0.0	0.0	0.0	0.0	0.0	0.0	0.0	0.0	0.0	0.0	
Total	97.6	96.8	99.2	98.7	98.2	97.6	98.3	98.4	99.1	98.4	98.4	99.9	100.2	100.3	
Formula	$PbS_{1.1}$	PbS	PbS	PbS	PbS	PbS	PbS	PbS	PbS	PbS	PbS	PbS	PbS	PbS	
Description:	symp. w/ brn	symp. w/ brn	symp. w/ brn	symp. w/ brn	symp. w/ brn	symp. w/ brn	symp. w/ brn	symp. w/ brn	symp. w/ brn	symp. w/ brn	inc. in brn	inc. in brn	inc. in brn	symp. w/ brn	

Table 20: Composition of gudmundite. All samples are from remobilization veins. inc.=inclusions, symp.=symplectititc. brn=bournonite, gn=galena, po=pyrrhotite.

Sample/Spot:	STO-28a/1a-1a	STO-28a/1a-1c	STO-28a/1a-4b	STO-28a/1a-9a	STO-6a/1a-10a	STO-6a/1a-10b	STO-6a/1a-11b	STO-6a/2-4a	STO-6a/2-4b	STO-50/1a-8a	STO-50/1a-8b	STO-50/1b-7
Wt%												
Cu	0.0	0.0	0.1	0.0	0.6	0.4	0.5	0.0	0.0	1.2	1.6	0.0
Fe	25.4	26.0	25.5	26.1	27.1	27.0	26.5	26.5	26.7	26.5	25.2	27.0
Mn	0.0	0.0	0.0	0.0	0.0	0.0	0.0	0.0	0.0	0.1	0.0	0.0
Co	0.0	0.0	0.0	0.0	0.0	0.0	0.0	0.0	0.0	0.0	0.0	0.0
Ni	0.0	0.0	0.0	0.0	0.0	0.0	0.0	0.1	0.0	0.2	0.0	0.0
Zn	0.0	0.0	0.0	0.1	0.0	0.1	0.1	0.0	0.0	0.9	0.2	0.0
As	1.4	1.4	1.7	1.2	1.7	1.4	1.4	1.2	1.3	1.1	1.2	1.4
Sb	57.3	56.5	55.7	55.8	52.8	53.5	53.4	54.7	54.3	51.1	53.7	54.1
S	14.5	14.6	14.2	15.0	14.4	14.0	14.1	14.3	14.6	16.2	14.8	13.9
Se	0.0	0.0	0.0	0.0	0.0	0.0	0.0	0.0	0.0	0.0	0.0	0.0
Te	0.0	0.0	0.0	0.0	0.0	0.0	0.0	0.0	0.0	0.0	0.0	0.0
Total	98.7	98.4	97.2	98.1	96.6	96.5	96.0	96.8	96.9	97.2	96.6	96.3
Formula	FeSbS	FeSbS	FeSbS	FeSbS	$Fe_{1.1}As_{0.1}SbS$	$Fe_{1.1}SbS$	$Fe_{1.1}SbS$	FeSbS	FeSbS	$FeSb_{0.9}S_{1.1}$	$Cu_{0.1}FeSbS$	$Fe_{1.1}SbS$
Description:	rim on gn+brn	rim on gn+brn	inc. in brn	inc. in brn+gn	symp. in gn	symp. in gn	symp. in gn	inc. in gn	inc. in gn	inc. in po	inc. in po	inc. in brn

Table 21: Composition of pyrite. All samples are from massive ore. anhed.=anhedral, cont. w/=contact with, l.=large, p-blast=porphyroblast, s.=small. chp=chalcopyrite, po=pyrrhotite, sph=sphalerite.

Sample/Spot:	STO-14/1-1b	STO-14/1-2c	STO-14/2a-1b	STO-14/2a-2c	STO-14/3-1b	STO-14/3-1c	STO-14/3-3c	STOB-98070-93.4/2a-1a	STOB-98070-93.4/2a-1b	STOB-98070-101.8/Pos2a-1a	STOB-98070-101.8/Pos2a-1b
Wt%											
Cu	0.0	0.0	0.0	0.0	0.0	0.0	0.0	0.0	0.0	0.0	0.0
Fe	47.1	46.1	45.9	46.6	47.2	46.1	45.9	46.8	45.5	45.4	45.5
Mn	0.0	0.0	0.0	0.0	0.0	0.0	0.0	0.0	0.0	0.0	0.0
Co	0.1	0.0	0.0	0.0	0.1	0.1	0.0	0.0	0.0	1.0	0.9
Ni	0.0	0.0	0.0	0.0	0.0	0.0	0.0	0.0	0.0	0.0	0.0
Zn	0.0	0.0	0.0	0.0	0.0	0.0	0.0	0.0	0.0	0.4	0.2
As	0.0	0.0	0.0	0.0	0.0	0.0	0.0	0.0	0.0	0.0	0.0
Sb	0.0	0.0	0.0	0.0	0.0	0.0	0.0	0.0	0.0	0.0	0.0
S	49.3	50.5	50.3	49.6	50.1	49.9	50.6	51.5	51.0	51.5	50.0
Se	0.0	0.0	0.0	0.0	0.0	0.0	0.0	0.0	0.0	0.0	0.0
Te	0.0	0.0	0.0	0.0	0.0	0.0	0.0	0.0	0.0	0.0	0.0
Total	96.4	96.6	96.3	96.2	97.4	96.0	96.5	98.2	96.5	98.3	96.6
Formula	$FeS_{1.8}$	$FeS_{1.9}$	$FeS_{1.9}$	$FeS_{1.9}$	$FeS_{1.8}$	$FeS_{1.9}$	$FeS_{1.9}$	$FeS_{1.9}$	FeS_2	$FeS_{1.9}$	$FeS_{1.9}$
Description:	l. p-blast in po	l. p-blast in po	s. grains w/ po	s. grains w/ po	l. p-blast in po	l. p-blast in po	l. p-blast in po	l. anhed. grain	l. anhed. grain	inclusion in sph	inclusion in sph
Sample/Spot:	STOB-98070-101.8/Pos2a-1c	STOB-98070-101.8/Pos2a-3a	STOB-98070-101.8/Pos2a-3b	STOB-98070-101.8/Pos2a-3c	STOB-98070-101.8/Pos2b-2a	STOB-98070-101.8/Pos2b-2b	STOB-98070-101.8/Pos2b-2c	STOB-98070-101.8/Pos2c-2a	STOB-98070-101.8/Pos2c-2b	STOB-98070-101.8/Pos2c-2c	
Wt%											
Cu	0.0	0.0	0.0	0.0	0.0	0.0	0.1	0.1	0.1	0.1	
Fe	45.1	45.1	45.4	45.3	45.0	45.8	46.6	45.5	46.3	45.4	
Mn	0.0	0.0	0.0	0.0	0.0	0.0	0.0	0.0	0.0	0.0	
Co	1.0	0.3	0.7	0.5	0.5	0.5	0.3	0.1	0.1	0.1	
Ni	0.0	0.0	0.0	0.0	0.0	0.0	0.0	0.0	0.0	0.0	
Zn	0.5	0.3	0.2	0.2	0.4	0.3	0.2	0.1	0.1	0.1	
As	0.0	0.0	0.0	0.0	0.0	0.0	0.0	0.0	0.0	0.0	
Sb	0.0	0.0	0.0	0.0	0.0	0.0	0.0	0.0	0.0	0.0	
S	50.9	51.1	51.0	50.3	50.4	51.1	50.7	50.4	51.6	51.9	
Se	0.0	0.0	0.0	0.0	0.0	0.0	0.0	0.0	0.0	0.0	
Te	0.0	0.0	0.0	0.0	0.0	0.0	0.0	0.0	0.0	0.0	
Total	97.5	96.8	97.3	96.2	96.3	97.7	97.8	96.2	98.1	97.5	
Formula	$FeS_{1.9}$	$FeS_{1.9}$	$FeS_{1.9}$	$FeS_{1.9}$	$FeS_{1.9}$	$FeS_{1.9}$	$FeS_{1.9}$	$FeS_{1.9}$	$FeS_{1.9}$	FeS_2	
Description:	inclusion in sph	inclusion in sph	inclusion in sph	inclusion in sph	inclusion in sph	inclusion in sph	inclusion in sph	in cont. w/ sph+chp	in cont. w/ sph+chp	in cont. w/ sph+chp	

Table 22: Composition of pyrrhotite. Sample STOB-98051-123.8 is from a remobilization vein, the rest from massive ore. inc.=inclusion, hm=hematite, sph=sphalerite.

	Massive Ore				Remobilization Veins			
Sample/Spot:	STO-33a/1b-1	STOB-98070-101.8/Pos2a-2a	STOB-98070-101.8/Pos2b-1c	STOB-98070-101.8/Pos2c-1a	STOB-98070-101.8/Pos2c-1b	STOB-98051-123.8/Pos1-2a	STOB-98051-123.8/Pos1-2b	STOB-98051-123.8/Pos1-2c
Wt%								
Cu	0.0	0.0	0.0	0.0	0.0	0.0	0.0	0.0
Fe	55.3	58.8	57.4	55.8	57.5	58.6	58.8	58.5
Mn	0.0	0.0	0.0	0.0	0.0	0.0	0.0	0.0
Co	0.0	0.0	0.0	0.0	0.0	0.0	0.0	0.0
Ni	0.0	0.0	0.0	0.0	0.0	0.0	0.0	0.0
Zn	3.6	0.3	0.6	2.4	2.1	0.0	0.0	0.0
As	0.0	0.0	0.0	0.0	0.0	0.0	0.0	0.0
Sb	0.0	0.0	0.0	0.0	0.0	0.0	0.0	0.0
S	40.5	38.1	38.5	37.8	37.9	39.2	40.0	40.2
Se	0.0	0.0	0.0	0.0	0.0	0.0	0.0	0.0
Te	0.0	0.0	0.0	0.0	0.0	0.0	0.0	0.0
Total	99.4	97.1	96.4	96.0	97.6	97.8	98.8	98.7
Formula	$Fe_{0.8}S$	$Fe_{0.9}S$	$Fe_{0.9}S$	$Fe_{0.8}S$	$Fe_{0.9}S$	$Fe_{0.9}S$	$Fe_{0.8}S$	$Fe_{0.8}S$
Description	inc. in sph	inc. in sph	inc. in sph	crack fill in pyrite	crack fill in pyrite	inc. in hm	inc. in hm	inc. in hm

Table 23:Composition of chlorite. aggr.=aggregate, chl=chlorite.

Sample/Spot	STO-18/1-1	STO-18/1-2	STO-18/1-3	STO-18/1-4	STO-18/3-1	STO-18/3-2	STO-18/3-3	STO-18/4-1	STO-18/4-2	STO-19b/1-1	STO-19b/1-2	STO-19b/1-3	STO-19b/2-1b	STO-19b/2-2	STO-19b/2-3
Ox%(Si)	28.2	29.1	27.9	27.6	27.9	28.0	29.2	28.9	28.7	30.2	31.5	30.7	31.1	30.5	30.8
Ox%(Ti)	0.0	0.0	0.1	0.1	0.0	0.0	0.0	0.0	0.0	0.0	0.0	0.0	0.0	0.0	0.0
Ox%(Al)	21.2	20.8	21.5	21.7	21.6	21.6	20.3	21.2	20.4	16.7	14.5	15.4	15.8	16.7	15.9
Ox%(Cr)	0.0	0.0	0.0	0.0	0.0	0.0	0.0	0.0	0.0	0.0	0.0	0.0	0.0	0.0	0.0
Ox%(Fe)	15.8	16.5	17.2	16.7	16.4	16.3	15.2	16.6	16.5	24.7	22.7	24.1	21.9	22.0	23.8
Ox%(Mn)	0.1	0.2	0.1	0.1	0.1	0.2	0.2	0.2	0.2	0.5	0.4	0.4	0.3	0.4	0.3
Ox%(Mg)	20.9	20.8	20.2	20.4	21.1	21.3	22.3	21.4	20.8	15.6	18.3	15.9	17.7	17.3	16.6
Ox%(Ca)	0.0	0.0	0.0	0.1	0.2	0.0	0.1	0.1	0.1	0.1	0.1	0.1	0.3	0.2	0.2
Ox%(Na)	0.0	0.0	0.0	0.0	0.0	0.0	0.0	0.0	0.0	0.0	0.0	0.0	0.0	0.0	0.0
Ox%(K)	0.0	0.0	0.0	0.0	0.0	0.0	0.0	0.1	0.0	0.0	0.0	0.0	0.0	0.0	0.0
%H_2O^*	11.9	12.0	11.9	11.8	12.0	12.0	12.0	12.1	11.9	11.5	11.6	11.4	11.6	11.6	11.6
Total	98.3	99.6	98.7	98.5	99.4	99.4	99.3	100.6	98.6	99.2	99.1	98.1	98.7	98.6	99.1
Formula (O=14)	$Si_{2.9}Al^{IV}_{1.1}Al^{VI}_{1.4}Mg_{3.2}Fe_{1.3}(OH)_8$	$Si_{2.9}Al^{IV}_{1.1}Al^{VI}_{1.4}Mg_{3.1}Fe_{1.4}(OH)_8$	$Si_{2.9}Al^{IV}_{1.2}Al^{VI}_{1.4}Mg_3Fe_{1.5}(OH)_8$	$Si_{2.8}Al^{IV}_{1.2}Al^{VI}_{1.4}Mg_{3.1}Fe_{1.4}(OH)_8$	$Si_{2.8}Al^{IV}_{1.2}Al^{VI}_{1.4}Mg_{3.2}Fe_{1.4}(OH)_8$	$Si_{2.8}Al^{IV}_{1.2}Al^{VI}_{1.4}Mg_{3.2}Fe_{1.4}(OH)_8$	$Si_{2.8}Al^{IV}_{1.1}Al^{VI}_{1.3}Mg_{3.3}Fe_{1.3}(OH)_8$	$Si_{2.8}Al^{IV}_{1.1}Al^{VI}_{1.3}Mg_{3.2}Fe_{1.4}(OH)_8$	$Si_{2.8}Al^{IV}_{1.1}Al^{VI}_{1.5}Mg_{3.1}Fe_{1.4}(OH)_8$	$Si_{3.1}Al^{IV}_{0.9}Al^{VI}_{1.2}Mg_{2.4}Fe_{2.2}(OH)_8$	$Si_{3.2}Al^{IV}_{0.7}Al^{VI}Mg_{2.6}Fe_2(OH)_8$	$Si_{3.2}Al^{IV}_{0.8}Al^{VI}_{1.1}Mg_{2.6}Fe_{2.1}(OH)_8$	$Si_{3.2}Al^{IV}_{0.8}Al^{VI}_{1.1}Mg_{2.7}Fe_{1.9}(OH)_8$	$Si_{3.2}Al^{IV}_{0.8}Al^{VI}_{1.2}Mg_{2.7}Fe_{1.9}(OH)_8$	$Si_{3.2}Al^{IV}_{0.8}Al^{VI}_{1.1}Mg_{2.6}Fe_{2.1}(OH)_8$
Description	vein, aggr. of needle-like chl	vein, aggr. of needle-like chl	vein, aggr. of needle-like chl	vein, aggr. of needle-like chl	vein, aggr. of needle-like chl	vein, aggr. of needle-like chl	vein, aggr. of needle-like chl	vein, aggr. of needle-like chl	vein, aggr. of needle-like chl	massive green chlorite	massive green chlorite	massive green chlorite	inside of a crack or veinlet	massive green chlorite	inside of a crack or veinlet
Sample/Spot	STO-19b/2-4	STO-19b/3-1	STO-19b/3-3	STO-19b/4-1	STO-19b/4-2	STO-19b/4-3	STOB-98070-100.3/1-1a	STOB-98070-100.3/1-1b	STOB-98070-100.3/1-2	STOB-98070-100.3/1-3	STOB-98070-100.3/1-4	STOB-98070-100.3/2-2	STOB-98070-100.3/2-3	STOB-98070-100.3/3-1	STOB-98070-100.3/3-2
Ox%(Si)	31.5	35.2	30.5	33.3	33.4	31.6	27.8	27.9	27.5	27.6	27.5	28.3	27.9	27.2	27.5
Ox%(Ti)	0.0	0.0	0.1	0.0	0.0	0.0	0.0	0.0	0.1	0.1	0.1	0.1	0.1	0.1	0.1
Ox%(Al)	15.3	13.6	17.6	13.2	14.6	15.9	21.2	21.4	21.1	20.2	20.0	20.5	20.5	21.9	22.2
Ox%(Cr)	0.0	0.0	0.0	0.0	0.0	0.0	0.0	0.0	0.0	0.0	0.0	0.0	0.0	0.0	0.0
Ox%(Fe)	24.1	18.8	24.5	21.9	22.1	22.2	18.5	18.2	18.0	17.4	17.3	18.2	17.9	18.8	19.0
Ox%(Mn)	0.2	0.3	0.4	0.1	0.3	0.3	0.3	0.2	0.2	0.2	0.2	0.2	0.2	0.2	0.2
Ox%(Mg)	16.5	19.8	16.2	17.6	18.7	17.0	19.7	19.7	19.5	19.8	19.2	18.9	19.0	19.8	19.5
Ox%(Ca)	0.3	0.5	0.1	0.3	0.3	0.3	0.0	0.1	0.0	0.0	0.0	0.0	0.1	0.1	0.0
Ox%(Na)	0.0	0.0	0.0	0.0	0.0	0.0	0.0	0.1	0.0	0.0	0.0	0.0	0.0	0.0	0.0
Ox%(K)	0.0	0.0	0.1	0.0	0.0	0.0	0.1	0.1	0.1	0.1	0.2	0.1	0.2	0.0	0.0
%H_2O^*	11.6	12.0	11.8	11.6	12.0	11.7	11.8	11.9	11.7	11.6	11.5	11.7	11.6	11.9	12.0
Total	99.4	100.2	101.3	98.0	101.4	99.1	99.4	99.4	98.3	97.0	96.0	98.1	97.6	100.0	100.4
Formula (O=14)	$Si_{3.3}Al^{IV}_{0.7}Al^{VI}_{1.1}Mg_{2.5}Fe_{2.1}(OH)_8$	$Si_{3.8}Al^{IV}_{0.8}Al^{VI}_{1.1}Mg_{2.9}Fe_{1.6}Ca_{0.1}(OH)_8$	$Si_{3.1}Al^{IV}_{0.9}Al^{VI}_{1.2}Mg_{2.5}Fe_{2.1}(OH)_8$	$Si_{3.8}Al^{IV}_{0.8}Al^{VI}_{1.1}Mg_{2.7}Fe_{1.9}(OH)_8$	$Si_{3.3}Al^{IV}_{0.7}Al^{VI}_{1.1}Mg_{2.9}Fe_{1.9}(OH)_8$	$Si_{3.3}Al^{IV}_{0.7}Al^{VI}_{1.2}Mg_{2.6}Fe_{1.9}(OH)_8$	$Si_{2.9}Al^{IV}_{1.2}Al^{VI}_{1.3}Mg_3Fe_{1.6}(OH)_8$	$Si_{2.9}Al^{IV}_{1.2}Al^{VI}_{1.4}Mg_3Fe_{1.5}(OH)_8$	$Si_{2.9}Al^{IV}_{1.2}Al^{VI}_{1.4}Mg_3Fe_{1.5}(OH)_8$	$Si_{2.9}Al^{IV}_{1.1}Al^{VI}_{1.3}Mg_{2.1}Fe_{1.5}(OH)_8$	$Si_{2.9}Al^{IV}_{1.1}Al^{VI}_{1.3}Mg_3Fe_{1.5}(OH)_8$	$Si_{2.9}Al^{IV}_{1.1}Al^{VI}_{1.4}Mg_{2.9}Fe_{1.6}(OH)_8$	$Si_{2.9}Al^{IV}_{1.1}Al^{VI}_{1.4}Mg_{2.9}Fe_{1.6}(OH)_8$	$Si_{2.7}Al^{IV}_{1.3}Al^{VI}_{1.3}Mg_3Fe_{1.6}(OH)_8$	$Si_{2.9}Al^{IV}_{1.2}Al^{VI}_{1.4}Mg_{2.9}Fe_{1.6}(OH)_8$
Description	host rock close to crack edge	inside of a crack or veinlet	host rock further from crack	green chlorite w/ weak lineation	massive green chlorite	massive green chlorite	aggr. of green needle-like chl	aggr. of green needle-like chl	aggr. of green needle-like chl	aggr. of green needle-like chl	aggr. of green needle-like chl	aggr. of pale needle-like chl	aggr. of pale needle-like chl	aggr. of pale needle-like chl	aggr. of pale needle-like chl
Sample/Spot	STOB-98070-100.3/3-3	STOB-98070-100.3/3-4	STOB-98070-105.6/1-2	STOB-98070-105.6/1-3	STOB-98070-105.6/1-4	STOB-98070-105.6/2-1	STOB-98070-105.6/2-2	STOB-98070-105.6/2-3	STOB-98070-105.6/3-1	STOB-98070-105.6/3-2	STOB-98070-105.6/3-3	STOB-98070-107.6/1-1	STOB-98070-107.6/1-2	STOB-98070-107.6/1-3	STOB-98070-107.6/2-1
Ox%(Si)	26.4	26.7	26.5	26.9	26.4	26.1	26.0	25.9	26.3	26.2	26.6	26.1	25.7	25.8	26.7
Ox%(Ti)	0.0	0.0	0.1	0.0	0.2	0.0	0.0	0.0	0.1	0.1	0.0	0.0	0.0	0.1	0.0
Ox%(Al)	21.8	21.9	22.2	22.2	21.8	22.2	21.6	21.8	21.3	21.9	21.4	21.7	20.9	21.0	20.6
Ox%(Cr)	0.0	0.0	0.0	0.0	0.0	0.0	0.0	0.0	0.0	0.0	0.0	0.0	0.0	0.0	0.0
Ox%(Fe)	17.3	18.2	23.1	23.2	22.5	23.7	23.1	23.0	22.5	22.3	22.5	25.7	25.9	25.0	26.6
Ox%(Mn)	0.2	0.2	0.3	0.2	0.2	0.3	0.2	0.3	0.3	0.3	0.2	0.5	0.4	0.4	0.4
Ox%(Mg)	19.1	19.3	16.5	16.8	16.8	16.3	16.5	15.9	16.5	16.3	17.0	14.9	14.4	14.5	15.0
Ox%(Ca)	0.0	0.0	0.0	0.0	0.0	0.0	0.0	0.0	0.0	0.0	0.0	0.0	0.0	0.0	0.1
Ox%(Na)	0.0	0.0	0.0	0.0	0.0	0.0	0.0	0.0	0.0	0.0	0.0	0.0	0.0	0.0	0.0
Ox%(K)	0.0	0.0	0.0	0.0	0.1	0.0	0.0	0.0	0.0	0.0	0.0	0.0	0.0	0.0	0.0
%H_2O^*	11.5	11.7	11.7	11.8	11.6	11.6	11.5	11.4	11.5	11.5	11.6	11.5	11.3	11.3	11.6
Total	96.4	97.9	100.3	101.2	99.5	100.2	99.0	98.3	98.6	98.5	99.4	100.4	98.7	98.3	100.9
Formula (O=14)	$Si_{2.8}Al^{IV}_{1.2}Al^{VI}_{1.4}Mg_3Fe_{1.5}(OH)_8$	$Si_{2.7}Al^{IV}_{1.3}Al^{VI}_{1.4}Mg_3Fe_{1.5}(OH)_8$	$Si_{2.7}Al^{IV}_{1.3}Al^{VI}_{1.4}Mg_{2.6}Fe_2(OH)_8$	$Si_{2.7}Al^{IV}_{1.3}Al^{VI}_{1.4}Mg_{2.6}Fe_2(OH)_8$	$Si_{2.7}Al^{IV}_{1.3}Al^{VI}_{1.4}Mg_{2.6}Fe_{1.9}(OH)_8$	$Si_{2.7}Al^{IV}_{1.3}Al^{VI}_{1.4}Mg_{2.6}Fe_2(OH)_8$	$Si_{2.7}Al^{IV}_{1.3}Al^{VI}_{1.4}Mg_{2.6}Fe_2(OH)_8$	$Si_{2.7}Al^{IV}_{1.3}Al^{VI}_{1.4}Mg_{2.8}Fe_2(OH)_8$	$Si_{2.7}Al^{IV}_{1.3}Al^{VI}_{1.4}Mg_{2.6}Fe_2(OH)_8$	$Si_{2.7}Al^{IV}_{1.2}Al^{VI}_{1.4}Mg_{2.5}Fe_{1.9}(OH)_8$	$Si_{2.8}Al^{IV}_{1.2}Al^{VI}_{1.4}Mg_{2.6}Fe_{1.9}(OH)_8$	$Si_{2.7}Al^{IV}_{1.3}Al^{VI}_{1.4}Mg_{2.3}Fe_{2.2}(OH)_8$	$Si_{2.7}Al^{IV}_{1.3}Al^{VI}_{1.3}Mg_{2.3}Fe_{2.3}(OH)_8$	$Si_{2.7}Al^{IV}_{1.3}Al^{VI}_{1.4}Mg_{2.3}Fe_{2.2}(OH)_8$	$Si_{2.8}Al^{IV}_{1.2}Al^{VI}_{1.3}Mg_{2.3}Fe_{2.3}(OH)_8$
Description	aggr. of pale needle-like chl	aggr. of pale needle-like chl	aggr. of green needle-like chl	aggr. of needle-like chl	aggr. of pale needle-like chl	green chlorite	green chl w/ weak foliation	pale chlorite	green chlorite	green chlorite	green chlorite	massive green chlorite	massive green chlorite	massive green chlorite	green chlorite

Table 24: Composition of chlorite (continued). inc.=inclusions, chl=chlorite.

Sample/Spot	STOB-98070-107.6/2-2	STOB-98070-107.6/2-3	STOB-98070-107.6/3-1	STOB-98070-107.6/3-2	STOB-98070-107.6/3-3	STOB-98070-107.6/3-5	STOB-98070-107.6/4-1	STOB-98070-107.6/4-2	STOB-98070-107.6/4-3	STO-04b/1-1a	STO-04b/1-1b	STO-04b/1-1c	STO-04b/1-2a	STO-04b/1-2b	STO-04b/1-2c
Ox%(Si)	29.6	26.1	26.1	27.1	26.4	26.7	25.7	25.6	26.6	31.1	31.0	31.1	31.3	31.5	31.5
Ox%(Ti)	0.1	0.1	0.1	0.1	0.3	0.0	0.1	0.1	0.1	0.0	0.0	0.0	0.1	0.0	0.1
Ox%(Al)	17.0	21.0	21.1	21.8	20.7	20.4	21.1	20.7	19.8	16.1	16.3	16.2	16.1	16.4	16.5
Ox%(Cr)	0.0	0.0	0.0	0.0	0.0	0.0	0.0	0.0	0.0	0.0	0.0	0.0	0.0	0.0	0.0
Ox%(Fe)	25.7	25.7	25.8	24.6	24.5	24.3	25.2	24.5	23.4	23.0	22.9	22.9	23.2	22.8	22.6
Ox%(Mn)	0.3	0.4	0.4	0.4	0.4	0.4	0.3	0.4	0.4	0.5	0.4	0.4	0.5	0.5	0.5
Ox%(Mg)	14.3	14.8	14.6	14.3	14.6	15.0	14.9	14.6	15.4	16.5	16.7	16.8	16.6	16.9	16.8
Ox%(Ca)	0.1	0.0	0.0	0.7	0.3	0.1	0.0	0.0	0.0	0.5	0.5	0.5	0.5	0.5	0.5
Ox%(Na)	0.0	0.0	0.0	0.1	0.0	0.0	0.0	0.0	0.0	0.0	0.0	0.0	0.0	0.0	0.0
Ox%(K)	0.0	0.0	0.1	0.0	0.0	0.0	0.0	0.0	0.0	0.1	0.1	0.1	0.1	0.1	0.1
%H_2O*	11.4	11.4	11.4	11.6	11.4	11.4	11.3	11.2	11.3	11.6	11.6	11.7	11.7	11.8	11.8
Total	98.4	99.6	99.7	100.6	98.6	98.3	98.6	97.1	97.0	99.6	99.7	99.7	100.0	100.4	100.3
Formula (O=14)	$Si_{3.1}Al^{IV}_{0.9}Al^{VI}_{1.2}Mg_{2.2}Fe_{2.3}(OH)_8$	$Si_{2.7}Al^{IV}_{1.3}Al^{VI}_{1.3}Mg_{2.3}Fe_{2.3}(OH)_8$	$Si_{2.7}Al^{IV}_{1.3}Al^{VI}_{1.3}Mg_{2.3}Fe_{2.3}(OH)_8$	$Si_{2.9}Al^{IV}_{1.2}Al^{VI}_{1.4}Mg_{2.2}Fe_{2.1}Ca_{0.1}(OH)_8$	$Si_{2.9}Al^{IV}_{1.2}Al^{VI}_{1.4}Mg_{2.3}Fe_{2.2}(OH)_8$	$Si_{2.9}Al^{IV}_{1.2}Al^{VI}_{1.4}Mg_{2.4}Fe_{2.1}(OH)_8$	$Si_{2.7}Al^{IV}_{1.3}Al^{VI}_{1.3}Mg_{2.3}Fe_{2.2}(OH)_8$	$Si_{2.7}Al^{IV}_{1.3}Al^{VI}_{1.4}Mg_{2.3}Fe_{2.2}(OH)_8$	$Si_{2.9}Al^{IV}_{1.2}Al^{VI}_{1.3}Mg_{2.3}Fe_{2.1}(OH)_8$	$Si_{3.2}Al^{IV}_{0.8}Al^{VI}_{1.2}Mg_{2.5}Fe_2Ca_{0.1}(OH)_8$	$Si_{3.2}Al^{IV}_{0.8}Al^{VI}_{1.2}Mg_{2.6}Fe_2Ca_{0.1}(OH)_8$	$Si_{3.2}Al^{IV}_{0.8}Al^{VI}_{1.2}Mg_{2.6}Fe_2Ca_{0.1}(OH)_8$	$Si_{3.2}Al^{IV}_{0.8}Al^{VI}_{1.2}Mg_{2.5}Fe_{1.9}Ca_{0.1}(OH)_8$	$Si_{3.2}Al^{IV}_{0.8}Al^{VI}_{1.2}Mg_{2.6}Fe_{1.9}Ca_{0.1}(OH)_8$	$Si_{3.2}Al^{IV}_{0.8}Al^{VI}_{1.2}Mg_{2.6}Fe_{1.9}Ca_{0.1}(OH)_8$
Description	green chlorite	green chlorite	pale spot in massive green chl	massive green chlorite	border of green chlr inclusion.	brown chlorite	massive green chlorite	massive green chlorite	green chlorite	massive green-brown chlorite	massive green-brown chlorite	massive green-brown chlorite	massive green-brown chlorite	massive green-brown chlorite	massive greenish-brown chlorite
Sample/Spot	STO-04b/1-3a	STO-04b/1-3b	STO-04b/1-3c	STO-04b/1-4a	STO-04b/1-4b	STO-04b/1-4c	STO-04b/1-5a	STO-04b/1-5b	STO-04b/1-5c	STO-04b/2-1a	STO-04b/2-1b	STO-04b/2-1c	STO-04b/2-2a	STO-04b/2-2b	STO-04b/2-2c
Ox%(Si)	30.5	30.4	30.2	30.1	30.2	30.2	30.3	30.5	30.3	30.7	30.8	30.9	28.9	27.6	27.8
Ox%(Ti)	0.0	0.0	0.0	0.0	0.1	0.0	0.0	0.1	0.0	0.0	0.0	0.0	0.0	0.0	0.0
Ox%(Al)	15.7	15.6	15.9	15.9	16.1	15.9	15.9	16.1	15.9	16.1	16.0	16.0	21.2	21.8	21.0
Ox%(Cr)	0.0	0.0	0.0	0.0	0.0	0.0	0.0	0.0	0.0	0.0	0.0	0.0	0.0	0.0	0.0
Ox%(Fe)	20.0	20.3	19.7	20.5	20.3	20.8	20.6	20.1	20.7	22.9	22.8	23.0	17.5	19.0	19.0
Ox%(Mn)	0.4	0.3	0.4	0.3	0.3	0.3	0.4	0.4	0.4	0.4	0.4	0.4	0.2	0.2	0.2
Ox%(Mg)	20.4	20.3	20.3	20.0	20.0	20.2	20.0	20.1	20.2	17.6	17.4	17.8	19.9	19.6	19.3
Ox%(Ca)	0.1	0.1	0.1	0.1	0.1	0.1	0.1	0.1	0.1	0.3	0.4	0.4	0.0	0.0	0.0
Ox%(Na)	0.0	0.0	0.0	0.0	0.0	0.0	0.0	0.0	0.0	0.0	0.0	0.0	0.0	0.0	0.0
Ox%(K)	0.0	0.0	0.0	0.0	0.0	0.0	0.0	0.0	0.0	0.1	0.1	0.1	0.0	0.0	0.0
%H_2O*	11.7	11.7	11.6	11.6	11.7	11.7	11.7	11.7	11.7	11.7	11.7	11.7	12.0	11.9	11.8
Total	98.7	98.8	98.1	98.6	98.8	99.4	99.1	99.1	99.2	99.8	99.7	100.3	99.8	100.1	99.1
Formula (O=14)	$Si_{3.1}Al^{IV}_{0.9}Al^{VI}Mg_{3.1}Fe_{1.7}(OH)_8$	$Si_{3.1}Al^{IV}_{0.9}Al^{VI}Mg_{3.1}Fe_{1.7}(OH)_8$	$Si_{3.1}Al^{IV}_{0.9}Al^{VI}_{1.1}Mg_{3.1}Fe_{1.7}(OH)_8$	$Si_{3.1}Al^{IV}_{0.9}Al^{VI}Mg_{3.1}Fe_{1.8}(OH)_8$	$Si_{3.1}Al^{IV}_{0.9}Al^{VI}_{1.1}Mg_{3.1}Fe_{1.7}(OH)_8$	$Si_{3.1}Al^{IV}_{0.9}Al^{VI}Mg_{3.1}Fe_{1.8}(OH)_8$	$Si_{3.1}Al^{IV}_{0.9}Al^{VI}Mg_{3.1}Fe_{1.8}(OH)_8$	$Si_{3.1}Al^{IV}_{0.9}Al^{VI}_{1.1}Mg_{3.1}Fe_{1.7}(OH)_8$	$Si_{3.1}Al^{IV}_{0.9}Al^{VI}Mg_{3.1}Fe_{1.8}(OH)_8$	$Si_{3.2}Al^{IV}_{0.8}Al^{VI}_{1.1}Mg_{2.7}Fe_2(OH)_8$	$Si_{3.2}Al^{IV}_{0.8}Al^{VI}_{1.1}Mg_{2.7}Fe_2(OH)_8$	$Si_{3.2}Al^{IV}_{0.8}Al^{VI}_{1.1}Mg_{2.7}Fe_2(OH)_8$	$Si_{2.8}Al^{IV}_{1.1}Al^{VI}_{1.4}Mg_3Fe_{1.8}(OH)_8$	$Si_{2.8}Al^{IV}_{1.1}Al^{VI}_{1.4}Mg_3Fe_{1.8}(OH)_8$	$Si_{2.8}Al^{IV}_{1.2}Al^{VI}_{1.3}Mg_{2.8}Fe_{1.6}(OH)_8$
Description	massive grey-brown chlorite	massive grey-brown chlorite	massive grey-brown chlorite	massive pale chlorite	massive pale chlorite	massive pale chlorite	massive grey-brown chlorite	massive grey-brown chlorite	massive grey-brown chlorite	greenish-brown chlorite	greenish-brown chlorite	greenish-brown chlorite	greenish-brown chlorite	greenish-brown chlorite	greenish-brown chl
Sample/Spot	STO-04b/2-4a	STO-04b/2-4b	STO-04b/3-1a	STO-04b/3-1b	STO-04b/3-1c	STO-04b/3-2a	STO-04b/3-2b	STO-04b/3-2c	STO-04b/3-3a	STO-04b/4-1a	STO-04b/4-1b	STO-04b/4-1c	STO-04b/4-4a	STO-04b/4-4b	STO-13/2-1a
Ox%(Si)	29.4	28.1	30.4	30.7	31.0	29.9	30.4	30.5	30.0	28.4	28.3	28.1	27.7	28.1	36.4
Ox%(Ti)	0.0	0.0	0.0	0.1	0.0	0.0	0.1	0.0	0.0	0.1	0.0	0.1	0.1	0.1	0.0
Ox%(Al)	20.0	20.9	16.2	15.6	15.6	16.1	16.0	16.2	15.9	21.5	21.0	20.9	21.9	21.3	11.7
Ox%(Cr)	0.0	0.0	0.0	0.0	0.0	0.0	0.0	0.0	0.0	0.0	0.0	0.0	0.0	0.0	0.0
Ox%(Fe)	18.7	17.4	21.1	20.1	20.1	19.8	21.0	20.8	21.1	15.5	15.2	15.2	16.4	15.7	7.8
Ox%(Mn)	0.3	0.2	0.4	0.4	0.4	0.4	0.3	0.3	0.4	0.2	0.2	0.2	0.2	0.2	1.2
Ox%(Mg)	19.4	19.5	19.9	20.5	20.2	19.8	19.6	19.4	18.7	21.1	22.4	22.6	22.0	22.4	30.0
Ox%(Ca)	0.0	0.0	0.1	0.1	0.1	0.1	0.2	0.2	0.2	0.2	0.0	0.0	0.0	0.0	0.3
Ox%(Na)	0.0	0.0	0.0	0.0	0.1	0.0	0.0	0.0	0.0	0.0	0.0	0.0	0.0	0.0	0.0
Ox%(K)	0.0	0.0	0.0	0.0	0.0	0.0	0.0	0.0	0.0	0.3	0.1	0.1	0.1	0.1	0.0
%H_2O*	11.9	11.7	11.8	11.7	11.7	11.5	11.7	11.7	11.5	12.0	12.0	12.0	12.1	12.1	12.5
Total	99.6	97.9	100.0	99.2	99.1	97.6	99.3	99.2	97.8	99.3	99.1	99.1	100.5	100.0	99.9
Formula (O=14)	$Si_3Al^{IV}Al^{VI}_{1.3}Mg_{2.9}Fe_{1.8}(OH)_8$	$Si_{2.9}Al^{IV}_{1.1}Al^{VI}_{1.4}Mg_3Fe_{1.5}(OH)_8$	$Si_{3.1}Al^{IV}_{0.9}Al^{VI}Mg_3Fe_{1.8}(OH)_8$	$Si_{3.1}Al^{IV}_{0.9}Al^{VI}Mg_{3.1}Fe_{1.7}(OH)_8$	$Si_{3.2}Al^{IV}_{0.8}Al^{VI}_{1.1}Mg_{3.1}Fe_{1.7}(OH)_8$	$Si_{3.1}Al^{IV}_{0.9}Al^{VI}_{1.1}Mg_{3.1}Fe_{1.7}(OH)_8$	$Si_{3.1}Al^{IV}_{0.9}Al^{VI}_{1.1}Mg_3Fe_{1.8}(OH)_8$	$Si_{3.1}Al^{IV}_{0.9}Al^{VI}_{1.1}Mg_3Fe_{1.8}(OH)_8$	$Si_{3.1}Al^{IV}_{0.9}Al^{VI}_{1.1}Mg_{2.8}Fe_{1.8}(OH)_8$	$Si_{2.9}Al^{IV}_{1.2}Al^{VI}_{1.4}Mg_{3.1}Fe_{1.3}(OH)_8$	$Si_{2.9}Al^{IV}_{1.2}Al^{VI}_{1.3}Mg_{3.3}Fe_{1.3}(OH)_8$	$Si_{2.9}Al^{IV}_{1.2}Al^{VI}_{1.3}Mg_{3.4}Fe_{1.3}(OH)_8$	$Si_{2.9}Al^{IV}_{1.2}Al^{VI}_{1.3}Mg_{3.2}Fe_{1.4}(OH)_8$	$Si_{2.9}Al^{IV}_{1.2}Al^{VI}_{1.3}Mg_{3.3}Fe_{1.3}(OH)_8$	$Si_{3.9}Al^{IV}_{0.9}Al^{VI}_{0.8}Mg_{4.3}Fe_{0.6}Ca_{0.1}(OH)_8$
Description	chlorite inc. in chl+quartz	chlorite inc. in chl+quartz	massive grey-brown chlorite	massive grey-brown chlorite	massive grey-brown chlorite	massive pale greyish chl	massive pale greyish chl	massive pale chlorite	massive pale chlorite	fine-grained pale chlorite	fine-grained pale chlorite	fine-grained pale chlorite	fine-grained pale chlorite	fine-grained pale chlorite	fine-grained brown chlorite

Table 25: Composition of chlorite (continued). chl=chlorite.

Sample/Spot	STO-13/2-1b	STO-13/2-1c	STO-13/2-3a	STO-13/2-3b	STO-13/2-3c	STO-13/3-2a	STO-13/3-2b	STO-13/3-2c	STO-13/3-4a	STO-13/3-4b	STO-13/3-5b	STO-13/3-5c	STO-22b/1-2a	STO-22b/1-2b	STO-22b/1-2c
Ox%(Si)	35.4	35.5	36.6	36.1	36.6	39.1	39.5	39.9	39.3	38.9	37.2	37.4	27.2	27.4	27.2
Ox%(Ti)	0.1	0.0	0.0	0.0	0.0	0.0	0.0	0.0	0.0	0.0	0.0	0.0	0.0	0.0	0.0
Ox%(Al)	11.8	11.6	10.8	11.0	11.0	8.9	8.8	9.0	9.3	9.7	11.0	11.1	20.6	20.8	20.7
Ox%(Cr)	0.0	0.0	0.0	0.0	0.0	0.0	0.0	0.0	0.0	0.0	0.0	0.1	0.0	0.0	0.0
Ox%(Fe)	8.7	8.2	6.2	6.7	6.7	3.7	4.7	3.4	2.6	3.6	5.5	5.2	18.6	18.9	18.8
Ox%(Mn)	1.1	1.1	1.0	1.0	1.1	1.2	0.8	1.1	0.8	0.9	1.0	1.0	0.3	0.4	0.3
Ox%(Mg)	29.1	30.0	31.3	31.2	31.3	32.0	33.8	32.9	33.3	33.2	32.2	32.2	20.1	20.0	19.7
Ox%(Ca)	0.2	0.3	0.2	0.1	0.2	0.8	0.4	0.8	0.5	0.4	0.3	0.3	0.0	0.0	0.0
Ox%(Na)	0.0	0.0	0.0	0.0	0.0	0.0	0.1	0.0	0.0	0.0	0.0	0.0	0.0	0.0	0.0
Ox%(K)	0.0	0.0	0.0	0.0	0.0	0.0	0.0	0.0	0.0	0.0	0.0	0.0	0.0	0.0	0.0
%H_2O*	12.3	12.4	12.4	12.4	12.5	12.6	12.9	12.8	12.7	12.7	12.7	12.7	11.7	11.8	11.7
Total	98.6	98.9	98.6	98.7	99.4	98.3	101.0	99.9	98.6	99.5	100.0	100.1	98.6	99.2	98.5
Formula (O=14)	$Si_{3.6}Al^{IV}_{0.5}Al^{VI}_{0.8}Mg_{4.2}$ $Fe_{0.7}Mn_{0.1}(OH)_8$	$Si_{3.4}Al^{IV}_{0.6}Al^{VI}_{0.8}Mg_{4.3}$ $Fe_{0.7}Mn_{0.1}(OH)_8$	$Si_{3.5}Al^{IV}_{0.5}Al^{VI}_{0.8}Mg_{4.5}$ $Fe_{0.6}Mn_{0.1}(OH)_8$	$Si_{3.5}Al^{IV}_{0.5}Al^{VI}_{0.7}Mg_{4.6}$ $Fe_{0.6}Mn_{0.1}(OH)_8$	$Si_{3.5}Al^{IV}_{0.5}Al^{VI}_{0.8}Mg_{4.5}$ $Fe_{0.6}Mn_{0.1}(OH)_8$	$Si_{3.7}Al^{IV}_{0.3}Al^{VI}_{0.7}Mg_{4.6}$ $Fe_{0.3}Mn_{0.1}Ca_{0.1}(OH)_8$	$Si_{3.7}Al^{IV}_{0.3}Al^{VI}_{0.7}Mg_{4.7}$ $Fe_{0.4}Mn_{0.1}(OH)_8$	$Si_{3.7}Al^{IV}_{0.3}Al^{VI}_{0.7}Mg_{4.6}$ $Fe_{0.3}Mn_{0.1}Ca_{0.1}(OH)_8$	$Si_{3.7}Al^{IV}_{0.3}Al^{VI}_{0.7}Mg_{4.7}$ $Fe_{0.2}Mn_{0.1}Ca_{0.1}(OH)_8$	$Si_{3.7}Al^{IV}_{0.3}Al^{VI}_{0.7}Mg_{4.7}$ $Fe_{0.3}Mn_{0.1}(OH)_8$	$Si_{3.5}Al^{IV}_{0.5}Al^{VI}_{0.8}Mg_{4.5}$ $Fe_{0.4}Mn_{0.1}(OH)_8$	$Si_{3.6}Al^{IV}_{0.5}Al^{VI}_{0.9}Mg_{4.5}$ $Fe_{0.4}Mn_{0.1}(OH)_8$	Si2.8AlIV1.2AlVI1.3 $Mg_{3.1}Fe_{1.6}(OH)_8$	Si2.8AlIV1.2AlVI1.3 $Mg_3Fe_{1.6}(OH)_8$	Si2.8AlIV1.2AlVI1.3 $Mg_3Fe_{1.6}(OH)_8$
Description	fine-grained brown chlorite	fine-grained brown chlorite	massive pale chlorite	massive pale chlorite	massive pale chlorite	Small cracks w/ chlorite	Small cracks w/ chlorite	Small cracks w/ chlorite	Small cracks w/ chlorite	Small cracks w/ chlorite	brown chlorite	brown chlorite	pale green fine-grained chl	pale green fine-grained chl	pale green fine-grained chl
Sample/Spot	STO-22b/2-1c	STO-22b/1-3a	STO-22b/1-3b	STO-22b/1-3c	STO-22b/1-1b	STO-22b/1-1c	STO-22b/2-2a	STO-22b/2-2b	STO-22b/2-2c	STO-22b/3-1a	STO-22b/3-1b	STO-22b/3-1c	STO-22b/3-2b	STO-22b/3-2c	STO-22b/4-1a
Ox%(Si)	27.0	28.0	27.8	27.5	27.5	27.2	28.2	28.1	28.1	27.2	27.3	27.1	27.0	26.9	27.5
Ox%(Ti)	0.0	0.0	0.0	0.0	0.0	0.0	0.0	0.1	0.0	0.0	0.0	0.0	0.0	0.0	0.0
Ox%(Al)	21.0	19.8	20.2	20.6	20.4	20.5	20.2	20.2	20.3	20.8	20.5	20.4	20.4	21.0	20.2
Ox%(Cr)	0.0	0.0	0.0	0.0	0.0	0.0	0.0	0.0	0.0	0.0	0.0	0.0	0.0	0.0	0.0
Ox%(Fe)	19.8	20.1	19.8	19.4	18.9	18.9	19.4	19.4	19.2	19.3	18.8	20.1	19.9	19.5	19.4
Ox%(Mn)	0.4	0.4	0.3	0.4	0.3	0.3	0.3	0.4	0.3	0.3	0.4	0.4	0.3	0.4	0.4
Ox%(Mg)	19.2	18.8	19.5	19.7	19.9	20.2	20.4	20.5	20.5	19.9	19.9	19.1	19.2	19.4	20.1
Ox%(Ca)	0.0	0.0	0.0	0.0	0.0	0.0	0.0	0.0	0.0	0.0	0.0	0.0	0.0	0.0	0.0
Ox%(Na)	0.0	0.0	0.0	0.0	0.0	0.0	0.0	0.0	0.0	0.0	0.0	0.0	0.0	0.0	0.0
Ox%(K)	0.0	0.0	0.0	0.0	0.3	0.1	0.0	0.0	0.0	0.0	0.0	0.0	0.0	0.0	0.0
%H_2O*	11.7	11.7	11.8	11.8	11.7	11.7	11.9	11.9	11.9	11.7	11.7	11.7	11.6	11.7	11.8
Total	99.2	98.8	99.5	99.4	99.2	98.8	100.6	100.7	100.5	99.2	98.6	98.8	98.4	98.9	99.4
Formula (O=14)	Si2.8AlIV1.2AlVI1.3 $Mg_{2.9}Fe_{1.7}(OH)_8$	Si2.9AlIV1.1AlVI1.3 $Mg_{2.9}Fe_{1.7}(OH)_8$	Si2.8AlIV1.2AlVI1.3 $Mg_3Fe_{1.7}(OH)_8$	Si2.8AlIV1.2AlVI1.3 $Mg_3Fe_{1.7}(OH)_8$	Si2.8AlIV1.2AlVI1.3 $Mg_3Fe_{1.6}(OH)_8$	Si2.8AlIV1.2AlVI1.3 $Mg_{3.1}Fe_{1.6}(OH)_8$	$Si_{2.8}Al^{IV}_{1.2}Al^{VI}_{1.2}$ $Mg_{3.1}Fe_{1.6}(OH)_8$	$Si_{2.8}Al^{IV}_{1.2}Al^{VI}_{1.2}$ $Mg_{3.1}Fe_{1.6}(OH)_8$	$Si_{2.8}Al^{IV}_{1.2}Al^{VI}_{1.2}$ $Mg_{3.1}Fe_{1.6}(OH)_8$	$Si_{2.8}Al^{IV}_{1.2}Al^{VI}_{1.3}$ $Mg_3Fe_{1.6}(OH)_8$	$Si_{2.8}Al^{IV}_{1.2}Al^{VI}_{1.3}$ $Mg_3Fe_{1.6}(OH)_8$	$Si_{2.8}Al^{IV}_{1.2}Al^{VI}_{1.3}$ $Mg_{2.9}Fe_{1.7}(OH)_8$	$Si_{2.8}Al^{IV}_{1.2}Al^{VI}_{1.3}$ $Mg_3Fe_{1.7}(OH)_8$	$Si_{2.8}Al^{IV}_{1.2}Al^{VI}_{1.3}$ $Mg_3Fe_{1.7}(OH)_8$	$Si_{2.8}Al^{IV}_{1.2}Al^{VI}_{1.2}$ $Mg_{3.1}Fe_{1.7}(OH)_8$
Description	green needle-like chlorite	pale green fine-grained chl	pale green fine-grained chl	pale green fine-grained chl	pale green fine-grained chl	pale green fine-grained chl	green chlorite	green chlorite	green chlorite	green chlorite	green chlorite	green chlorite	Small amounts of green chlorite	Small amounts of green chlorite	green chlorite
Sample/Spot	STO-22b/4-1b	STO-22b/4-1c	STO-22b/4-2a	STO-22b/4-2b	STO-22b/4-2c	STO-22b/4-3a	STO-22b/4-3b	STO-22b/4-3c	STO-22b/4-4a	STO-22b/4-4b	STO-22b/4-4c	STO-28c/1-3b	STO-28c/1-6a	STO-28c/2-6a	STO-36b/1-2a
Ox%(Si)	27.4	27.3	27.3	27.6	27.6	27.3	26.9	27.0	27.0	27.1	27.0	38.5	36.9	39.7	27.7
Ox%(Ti)	0.0	0.0	0.0	0.0	0.1	0.0	0.0	0.0	0.0	0.0	0.0	0.1	0.0	0.0	0.1
Ox%(Al)	20.3	20.6	20.2	20.0	20.3	20.3	20.2	20.7	20.6	20.6	20.4	11.4	12.4	10.1	20.7
Ox%(Cr)	0.0	0.0	0.0	0.0	0.0	0.1	0.1	0.0	0.0	0.0	0.0	0.0	0.0	0.0	0.0
Ox%(Fe)	18.9	19.6	19.8	19.5	20.4	18.9	18.6	19.0	19.3	19.5	18.4	9.0	8.4	11.1	14.5
Ox%(Mn)	0.4	0.4	0.3	0.3	0.3	0.3	0.3	0.3	0.3	0.3	0.3	0.1	0.2	0.2	0.3
Ox%(Mg)	19.9	19.5	19.5	19.8	18.7	19.9	19.9	19.7	19.7	19.6	19.8	25.4	24.6	24.2	22.2
Ox%(Ca)	0.0	0.0	0.0	0.0	0.0	0.0	0.0	0.0	0.0	0.0	0.0	0.6	0.5	2.2	0.0
Ox%(Na)	0.0	0.1	0.0	0.0	0.0	0.0	0.0	0.0	0.0	0.0	0.0	0.0	0.0	0.1	0.0
Ox%(K)	0.0	0.0	0.0	0.0	0.0	0.0	0.0	0.0	0.0	0.0	0.0	0.0	0.0	0.0	0.1
%H_2O*	11.7	11.7	11.7	11.7	11.7	11.7	11.6	11.6	11.7	11.7	11.6	12.3	12.0	12.4	11.8
Total	98.7	99.1	98.9	99.0	99.2	98.5	97.5	98.3	98.6	98.9	97.4	97.3	95.0	100.0	97.4
Formula (O=14)	$Si_{2.8}Al^{IV}_{1.2}Al^{VI}_{1.3}$ $Mg_3Fe_{1.6}(OH)_8$	$Si_{2.8}Al^{IV}_{1.2}Al^{VI}_{1.3}$ $Mg_3Fe_{1.7}(OH)_8$	$Si_{2.8}Al^{IV}_{1.2}Al^{VI}_{1.2}$ $Mg_3Fe_{1.7}(OH)_8$	$Si_{2.8}Al^{IV}_{1.2}Al^{VI}_{1.2}$ $Mg_3Fe_{1.7}(OH)_8$	$Si_{2.8}Al^{IV}_{1.2}Al^{VI}_{1.3}$ $Mg_{2.8}Fe_{1.6}(OH)_8$	$Si_{2.8}Al^{IV}_{1.2}Al^{VI}_{1.3}$ $Mg_3Fe_{1.6}(OH)_8$	$Si_{2.8}Al^{IV}_{1.2}Al^{VI}_{1.3}$ $Mg_{3.1}Fe_{1.6}(OH)_8$	$Si_{2.8}Al^{IV}_{1.2}Al^{VI}_{1.3}$ $Mg_3Fe_{1.6}(OH)_8$	$Si_{2.8}Al^{IV}_{1.2}Al^{VI}_{1.3}$ $Mg_3Fe_{1.7}(OH)_8$	$Si_{2.8}Al^{IV}_{1.2}Al^{VI}_{1.3}$ $Mg_3Fe_{1.7}(OH)_8$	$Si_{2.8}Al^{IV}_{1.2}Al^{VI}_{1.3}$ $Mg_{3.1}Fe_{1.6}(OH)_8$	$Si_{3.0}Al^{IV}_{0.2}Al^{VI}_{1.1}Mg_{3.7}$ $Fe_{0.7}Ca_{0.1}(OH)_8$	$Si_{3.7}Al^{IV}_{0.3}Al^{VI}_{1.1}Mg_{3.7}$ $Fe_{0.7}Ca_{0.1}(OH)_8$	$Si_{3.9}Al^{IV}_{0.2}Al^{VI}Mg_{3.5}$ $Fe_{0.9}Ca_{0.2}(OH)_8$	$Si_{2.8}Al^{IV}_{1.2}Al^{VI}_{1.3}$ $Mg_{3.1}Fe_{1.2}(OH)_8$
Description	green chlorite	green chlorite	greenish-gray chlorite	greenish-gray chlorite	greenish-gray chlorite	green chlorite	green chlorite	green chlorite	pale chlorite	pale chlorite	pale chlorite	vein, chlorite crack-fill	vein, chlorite crack-fill	vein, fine-grained chlorite	pale needle-like chlorite

Table 26: Composition of chlorite (continued).

Sample/Spot	STO-36b/1-2b	STO-36b/1-3a	STO-36b/1-3b	STO-36b/2-1a	STO-36b/2-1b	STO-36b/2-4a	STO-36b/2-4b	STO-36b/2-4c	STO-36b/2-5a	STO-36b/2-5b	STO-36b/2-5c	STO-36b/2-6a	STO-36b/2-6b
Ox%(Si)	28.3	27.6	28.1	28.3	32.8	29.2	28.2	28.1	27.6	27.9	27.8	28.1	28.1
Ox%(Ti)	0.0	0.1	0.0	0.0	0.0	0.0	0.1	0.0	0.0	0.0	0.0	0.1	0.1
Ox%(Al)	20.6	20.8	20.7	20.5	18.1	20.4	20.8	21.2	21.8	21.3	21.4	20.6	21.1
Ox%(Cr)	0.0	0.0	0.0	0.0	0.0	0.0	0.0	0.0	0.0	0.0	0.0	0.0	0.0
Ox%(Fe)	13.8	14.2	14.1	14.3	13.6	14.1	14.5	14.1	15.1	14.3	14.9	14.3	14.5
Ox%(Mn)	0.4	0.4	0.4	0.4	0.3	0.3	0.4	0.4	0.4	0.4	0.4	0.4	0.4
Ox%(Mg)	23.1	23.0	23.2	23.3	21.7	22.6	23.0	23.0	22.1	22.8	22.1	22.9	23.0
Ox%(Ca)	0.0	0.0	0.0	0.0	0.0	0.0	0.0	0.0	0.0	0.0	0.0	0.0	0.0
Ox%(Na)	0.0	0.0	0.0	0.0	0.0	0.0	0.0	0.0	0.0	0.0	0.0	0.0	0.0
Ox%(K)	0.1	0.0	0.0	0.0	0.0	0.6	0.2	0.0	0.0	0.0	0.1	0.1	0.1
%H_2O*	11.9	11.9	12.0	12.0	12.1	12.1	12.0	12.0	12.0	12.0	11.9	11.9	12.0
Total	98.2	97.9	98.4	98.8	98.7	99.4	99.0	99.0	99.1	98.7	98.6	98.3	99.1
Formula (O=14)	$Si_{2.8}Al^{IV}_{1.2}Al^{VI}_{1.3}Mg_{3.5}Fe_{1.2}(OH)_8$	$Si_{2.8}Al^{IV}_{1.2}Al^{VI}_{1.3}Mg_{3.5}Fe_{1.2}(OH)_8$	$Si_{2.8}Al^{IV}_{1.2}Al^{VI}_{1.3}Mg_{3.5}Fe_{1.2}(OH)_8$	$Si_{2.8}Al^{IV}_{1.2}Al^{VI}_{1.3}Mg_{3.5}Fe_{1.2}(OH)_8$	$Si_{3.2}Al^{IV}_{0.8}Al^{VI}_{1.4}Mg_{3.2}Fe_{1.1}(OH)_8$	$Si_{2.9}Al^{IV}_{1.1}Al^{VI}_{1.3}Mg_{3.4}Fe_{1.2}K_{0.1}(OH)_8$	$Si_{2.8}Al^{IV}_{1.2}Al^{VI}_{1.3}Mg_{3.4}Fe_{1.2}(OH)_8$	$Si_{2.8}Al^{IV}_{1.2}Al^{VI}_{1.3}Mg_{3.4}Fe_{1.2}(OH)_8$	$Si_{2.8}Al^{IV}_{1.2}Al^{VI}_{1.3}Mg_{3.3}Fe_{1.3}(OH)_8$	$Si_{2.8}Al^{IV}_{1.2}Al^{VI}_{1.3}Mg_{3.4}Fe_{1.2}(OH)_8$	$Si_{2.8}Al^{IV}_{1.2}Al^{VI}_{1.3}Mg_{3.3}Fe_{1.3}(OH)_8$	$Si_{2.8}Al^{IV}_{1.2}Al^{VI}_{1.3}Mg_{3.4}Fe_{1.2}(OH)_8$	$Si_{2.8}Al^{IV}_{1.2}Al^{VI}_{1.3}Mg_{3.4}Fe_{1.2}(OH)_8$
Description	pale needle-like chlorite	pale needle-like chlorite	pale needle-like chlorite	pale needle-like chlorite	pale needle-like chlorite	massive pale chlorite	massive pale chlorite	massive pale chlorite	massive pale chlorite	massive pale chlorite	massive pale chlorite	massive pale chlorite	massive pale chlorite
Sample/Spot	STO-36b/2-6c	STO-36b/3-1a	STO-36b/3-2a	STO-36b/3-2b	STO-36b/3-2c	STO-36b/4-1a	STO-36b/4-1c	STO-36b/4-2a	STO-36b/4-2b	STO-36b/4-2c	STO-36b/4-3a	STO-36b/4-3b	STO-36b/4-3c
Ox%(Si)	28.4	28.3	28.2	28.1	28.0	27.9	27.6	28.8	27.4	28.2	28.2	28.6	28.3
Ox%(Ti)	0.2	0.1	0.0	0.0	0.0	0.0	0.0	0.1	0.1	0.0	0.0	0.0	0.0
Ox%(Al)	20.8	21.4	21.0	20.7	20.8	21.9	22.3	20.3	21.8	21.3	21.0	20.6	21.0
Ox%(Cr)	0.0	0.0	0.0	0.0	0.0	0.0	0.0	0.0	0.0	0.0	0.0	0.0	0.0
Ox%(Fe)	14.2	14.6	14.1	13.8	13.7	14.1	14.6	13.7	14.5	13.8	14.4	14.4	14.2
Ox%(Mn)	0.4	0.4	0.4	0.4	0.4	0.4	0.5	0.4	0.5	0.4	0.4	0.4	0.4
Ox%(Mg)	22.3	22.9	23.1	23.0	21.8	22.4	22.4	23.7	22.2	23.0	22.9	22.6	22.8
Ox%(Ca)	0.0	0.0	0.0	0.0	0.0	0.0	0.0	0.0	0.0	0.0	0.0	0.0	0.0
Ox%(Na)	0.0	0.0	0.0	0.0	0.0	0.0	0.0	0.0	0.0	0.0	0.0	0.0	0.0
Ox%(K)	0.2	0.1	0.0	0.0	0.0	0.0	0.0	0.0	0.0	0.0	0.0	0.2	0.0
%H_2O*	11.9	12.1	12.0	11.9	11.8	12.0	12.0	12.1	11.9	12.0	12.0	12.0	12.0
Total	98.3	100.0	99.0	98.0	96.6	98.7	99.4	99.1	98.4	98.7	99.0	98.9	98.9
Formula (O=14)	$Si_{2.9}Al^{IV}_{1.1}Al^{VI}_{1.3}Mg_{3.3}Fe_{1.2}(OH)_8$	$Si_{2.8}Al^{IV}_{1.2}Al^{VI}_{1.3}Mg_{3.4}Fe_{1.2}(OH)_8$	$Si_{2.8}Al^{IV}_{1.2}Al^{VI}_{1.3}Mg_{3.4}Fe_{1.2}(OH)_8$	$Si_{2.8}Al^{IV}_{1.2}Al^{VI}_{1.3}Mg_{3.5}Fe_{1.2}(OH)_8$	$Si_{2.9}Al^{IV}_{1.1}Al^{VI}_{1.4}Mg_{3.3}Fe_{1.2}(OH)_8$	$Si_{2.9}Al^{IV}_{1.2}Al^{VI}_{1.4}Mg_{3.3}Fe_{1.2}(OH)_8$	$Si_{2.7}Al^{IV}_{1.3}Al^{VI}_{1.4}Mg_{3.3}Fe_{1.2}(OH)_8$	$Si_{2.9}Al^{IV}_{1.1}Al^{VI}_{1.2}Mg_{3.5}Fe_{1.1}(OH)_8$	$Si_{2.8}Al^{IV}_{1.2}Al^{VI}_{1.3}Mg_{3.3}Fe_{1.2}(OH)_8$	$Si_{2.8}Al^{IV}_{1.2}Al^{VI}_{1.3}Mg_{3.4}Fe_{1.2}(OH)_8$	$Si_{2.8}Al^{IV}_{1.2}Al^{VI}_{1.3}Mg_{3.4}Fe_{1.2}(OH)_8$	$Si_{2.9}Al^{IV}_{1.1}Al^{VI}_{1.3}Mg_{3.4}Fe_{1.2}(OH)_8$	$Si_{2.8}Al^{IV}_{1.2}Al^{VI}_{1.3}Mg_{3.4}Fe_{1.2}(OH)_8$
Description	massive pale chlorite	fine-grained pale chlorite	pale needle-like chlorite	pale needle-like chlorite	pale needle-like chlorite	fine-grained pale chlorite	fine-grained pale chlorite	fine-grained pale chlorite	fine-grained pale chlorite	fine-grained pale chlorite	pale needle-like chlorite	pale needle-like chlorite	pale needle-like chlorite

Table 27: Temperatures calculated from chlorite in the host rock.

Sample/Spot	STO-19b/1-1	STO-19b/1-2	STO-19b/1-3	STO-19b/2-2	STO-19b/2-4	STO-19b/3-3	STO-19b/4-1	STO-19b/4-2	STO-19b/4-3	STOB-98070-100.3/1-1a	STOB-98070-100.3/1-1b	STOB-98070-100.3/1-2	STOB-98070-100.3/1-3	STOB-98070-100.3/1-4	STOB-98070-100.3/2-2	STOB-98070-100.3/2-3	STOB-98070-100.3/3-1	STOB-98070-100.3/3-2	STOB-98070-100.3/3-3	STOB-98070-100.3/3-4	STOB-98070-105.6/1-2	STOB-98070-105.6/1-3
T (°C) (B13)	165	169	149	160	142	175	103	127	136	296	273	285	273	249	218	236	390	323	298	326	357	354
T (°C) (L14) (P=2.5 kbar)	99	97	98	99	97	98	87	93	97	196	204	202	171	163	144	168	268	239	257	270	317	302
T (°C) (L14) (P=5 kbar)	121	118	119	121	118	120	108	114	119	223	232	229	197	188	169	194	299	269	288	301	351	335
T (°C) (L14) (P=7.5 kbar)	142	140	141	142	140	141	129	135	140	251	260	257	222	214	193	220	330	299	318	333	385	368
T (°C) (L14) (P=10 kbar)	164	161	162	164	161	163	149	156	161	278	287	284	248	239	217	245	362	328	349	364	419	402
T (°C) (CN85)	199	176	181	196	175	205	133	156	177	268	268	268	260	255	250	255	283	279	282	284	288	287
T (°C) (C88)	213	178	186	209	176	223	114	147	180	318	318	318	305	299	291	299	341	334	339	342	349	347
T (°C) (J91)	219	182	191	212	181	228	118	151	184	318	318	318	305	299	292	299	341	335	339	342	352	350
Sample/Spot	STOB-98070-105.6/1-4	STOB-98070-105.6/2-1	STOB-98070-105.6/2-2	STOB-98070-105.6/2-3	STOB-98070-105.6/3-1	STOB-98070-105.6/3-2	STOB-98070-105.6/3-3	STOB-98070-107.6/1-1	STOB-98070-107.6/1-2	STOB-98070-107.6/1-3	STOB-98070-107.6/2-1	STOB-98070-107.6/2-2	STOB-98070-107.6/2-3	STOB-98070-107.6/3-1	STOB-98070-107.6/3-2	STOB-98070-107.6/3-3	STOB-98070-107.6/3-5	STOB-98070-107.6/4-1	STOB-98070-107.6/4-2	STOB-98070-107.6/4-3	STO-04b/1-1a	STO-04b/1-1b
T (°C) (B13)	397	455	447	344	356	325	363	420	474	366	458	159	454	414	250	317	276	497	372	280	148	152
T (°C) (L14) (P=2.5 kbar)	300	430	352	326	257	294	262	324	310	270	236	99	278	293	209	203	191	324	264	176	177	178
T (°C) (L14) (P=5 kbar)	333	471	389	361	288	327	293	359	344	301	266	121	310	326	237	231	218	359	295	202	203	204
T (°C) (L14) (P=7.5 kbar)	366	511	425	395	318	360	324	393	377	333	295	142	342	359	265	258	245	393	326	228	230	230
T (°C) (L14) (P=10 kbar)	400	552	461	430	349	393	355	428	411	364	325	164	374	392	293	286	272	428	358	255	256	256
T (°C) (CN85)	286	295	290	289	282	286	283	289	287	283	279	201	284	285	271	270	268	289	283	263	185	188
T (°C) (C88)	345	358	352	350	339	345	341	350	347	341	334	217	342	344	323	321	318	350	341	310	192	197
T (°C) (J91)	348	362	355	354	342	348	343	355	352	345	339	223	347	349	328	326	323	355	345	314	196	201
Sample/Spot	STO-04b/1-1c	STO-04b/1-2a	STO-04b/1-2b	STO-04b/1-2c	STO-04b/1-3a	STO-04b/1-3b	STO-04b/1-3c	STO-04b/1-4a	STO-04b/1-4b	STO-04b/1-4c	STO-04b/1-5a	STO-04b/1-5b	STO-04b/1-5c	STO-04b/2-1a	STO-04b/2-1b	STO-04b/2-1c	STO-04b/2-2a	STO-04b/2-2b	STO-04b/2-2c	STO-04b/2-4a	STO-04b/2-4b	STO-04b/3-1a
T (°C) (B13)	153	149	146	144	231	252	233	251	234	275	245	223	256	179	172	184	213	320	279	201	223	261
T (°C) (L14) (P=2.5 kbar)	179	177	175	172	230	246	226	238	222	256	236	217	242	196	193	201	202	325	272	163	217	240
T (°C) (L14) (P=5 kbar)	206	203	201	198	260	276	255	267	251	286	266	245	272	224	220	228	230	359	304	189	245	270
T (°C) (L14) (P=7.5 kbar)	232	229	227	224	289	306	284	297	280	317	295	274	302	251	247	256	257	394	336	214	274	300
T (°C) (L14) (P=10 kbar)	258	255	253	249	318	336	313	327	308	348	325	302	332	278	275	283	285	429	367	239	302	330
T (°C) (CN85)	187	183	185	183	202	203	205	207	206	209	205	203	207	195	193	195	253	278	267	238	257	209
T (°C) (C88)	195	190	191	189	217	219	223	226	223	228	222	220	225	208	204	207	295	333	316	272	301	228
T (°C) (J91)	200	194	196	194	219	221	225	228	225	230	224	221	227	212	208	211	295	333	316	273	301	231
Sample/Spot	STO-04b/3-1b	STO-04b/3-1c	STO-04b/3-2a	STO-04b/3-2b	STO-04b/3-2c	STO-04b/3-3a	STO-04b/4-1a	STO-04b/4-1b	STO-04b/4-1c	STO-04b/4-4a	STO-04b/4-4b	STO-13/2-1a	STO-13/2-1b	STO-13/2-1c	STO-13/2-3a	STO-13/2-3b	STO-13/2-3c	STO-13/3-5b	STO-13/3-5c	STO-22b/1-1b	STO-22b/1-1c	STO-22b/1-2a
T (°C) (B13)	233	203	232	226	208	205	249	323	386	442	389	135	149	162	133	155	140	133	125	419	560	451
T (°C) (L14) (P=2.5 kbar)	232	220	220	221	208	209	269	324	352	405	365	199	209	226	203	222	209	202	197	556	545	430
T (°C) (L14) (P=5 kbar)	262	248	248	250	236	237	300	359	388	444	402	226	237	254	231	250	237	229	225	604	593	471
T (°C) (L14) (P=7.5 kbar)	291	277	277	279	264	265	331	393	424	484	439	254	265	283	258	279	265	257	252	652	640	512
T (°C) (L14) (P=10 kbar)	320	305	305	307	292	293	363	428	461	523	476	281	293	312	286	308	293	284	279	700	688	553
T (°C) (CN85)	198	194	208	203	202	202	262	266	268	281	272	127	133	135	118	126	121	118	116	270	275	275
T (°C) (C88)	212	206	226	219	218	218	309	315	318	337	323	104	113	116	90	103	95	90	87	321	329	328
T (°C) (J91)	214	208	228	221	220	221	308	313	316	336	322	99	109	111	84	97	90	85	82	321	329	328

B13=Bourdelle et al (2013), L14=Lanari et al (2014a), CN85=Cathelineau and Nieva (1985), C88=Cathelineau (1988), J91=Jowett (1991).

Table 28: Temperatures calculated from chlorite in the host rock (continued).

Sample/Spot	STO-22b/1-2b	STO-22b/1-2c	STO-22b/1-3a	STO-22b/1-3b	STO-22b/1-3c	STO-22b/2-1c	STO-22b/2-2a	STO-22b/2-2b	STO-22b/2-2c	STO-22b/3-1a	STO-22b/3-1b	STO-22b/3-1c	STO-22b/3-2b	STO-22b/3-2c	STO-22b/4-1a	STO-22b/4-1b	STO-22b/4-1c	STO-22b/4-2a	STO-22b/4-2b	STO-22b/4-2c	STO-22b/4-3a	STO-22b/4-3b
T (°C) (B13)	412	407	289	361	387	441	420	517	450	510	449	466	465	505	593	433	465	504	441	339	477	550
T (°C) (L14) (P=2.5 kbar)	389	391	268	327	369	440	374	419	398	475	429	429	422	479	573	420	466	433	411	312	451	493
T (°C) (L14) (P=5 kbar)	427	430	299	361	406	482	412	459	437	519	470	470	462	523	622	460	509	474	451	345	493	537
T (°C) (L14) (P=7.5 kbar)	465	468	331	396	443	523	449	499	476	562	511	510	503	567	671	501	552	515	491	379	535	582
T (°C) (L14) (P=10 kbar)	504	507	362	431	480	565	487	539	515	606	551	551	543	610	720	541	595	556	530	413	577	626
T (°C) (CN85)	274	274	256	264	271	280	264	266	266	277	273	273	274	281	271	270	274	272	267	265	272	275
T (°C) (C88)	327	328	300	313	323	335	311	314	315	332	326	326	327	338	323	321	327	323	316	313	324	328
T (°C) (J91)	328	328	302	314	324	336	312	315	316	333	326	327	328	339	323	322	328	324	316	314	325	328
Sample/Spot	STO-22b/4-3c	STO-22b/4-4a	STO-22b/4-4b	STO-22b/4-4c	STO-36b/1-1a	STO-36b/1-2a	STO-36b/1-2b	STO-36b/1-3a	STO-36b/1-3b	STO-36b/2-1a	STO-36b/2-1b	STO-36b/2-4a	STO-36b/2-4b	STO-36b/2-4c	STO-36b/2-5a	STO-36b/2-5b	STO-36b/2-5c	STO-36b/2-6a	STO-36b/2-6b	STO-36b/2-6c	STO-36b/3-1a	STO-36b/3-2a
T (°C) (B13)	465	537	509	408	300	341	326	480	397	395	116	249	398	350	366	357	330	367	382	283	367	354
T (°C) (L14) (P=2.5 kbar)	430	498	485	382	371	318	325	393	357	354	150	304	412	343	368	346	332	325	359	278	354	338
T (°C) (L14) (P=5 kbar)	471	543	529	420	409	352	359	432	393	391	174	337	451	378	405	382	367	360	396	310	390	373
T (°C) (L14) (P=7.5 kbar)	512	588	573	458	446	387	394	470	430	427	199	370	491	414	442	418	402	394	432	342	427	409
T (°C) (L14) (P=10 kbar)	552	632	617	496	483	421	429	509	466	463	223	404	531	450	480	454	437	429	469	374	463	444
T (°C) (CN85)	277	277	277	273	269	267	264	272	268	265	179	251	268	270	280	273	274	264	270	259	270	268
T (°C) (C88)	332	332	332	326	319	317	311	324	318	314	182	291	318	321	336	325	326	312	321	304	321	319
T (°C) (J91)	332	333	332	326	317	315	309	322	316	311	181	289	315	319	334	323	325	310	319	302	319	316
Sample/Spot	STO-36b/3-2b	STO-36b/3-2c	STO-36b/4-1a	STO-36b/4-1c	STO-36b/4-2a	STO-36b/4-2b	STO-36b/4-2c	STO-36b/4-3a	STO-36b/4-3b	STO-36b/4-3c												
T (°C) (B13)	330	246	297	364	343	378	318	342	290	314												
T (°C) (L14) (P=2.5 kbar)	326	245	294	368	302	355	302	323	306	311												
T (°C) (L14) (P=5 kbar)	361	275	327	405	335	391	335	358	340	345												
T (°C) (L14) (P=7.5 kbar)	396	305	360	442	368	428	369	393	374	379												
T (°C) (L14) (P=10 kbar)	430	335	393	479	402	464	402	427	407	413												
T (°C) (CN85)	265	260	274	284	258	280	269	268	259	266												
T (°C) (C88)	314	305	328	342	302	336	319	318	305	315												
T (°C) (J91)	311	303	325	340	300	334	317	315	303	312												

B13=Bourdelle et al (2013), L14=Lanari et al (2014a), CN85=Cathelineau and Nieva (1985), C88=Cathelineau (1988), J91=Jowett (1991).

Table 29: Temperatures calculated from chlorite in the veins.

Sample/Spot	STO-18/1-1	STO-18/1-2	STO-18/1-3	STO-18/1-4	STO-18/3-1	STO-18/3-2	STO-18/3-3	STO-18/4-1	STO-18/4-2	STO-19b/2-1b	STO-19b/2-3	STO-19b/3-1	STO-13/3-2a	STO-13/3-2b	STO-13/3-2c	STO-13/3-4a	STO-13/3-4b	STO-28c/1-3b	STO-28c/1-6a	STO-28c/2-6a
T (°C) (B13)	243	215	261	278	300	299	251	253	234	154	159	88	75	100	75	78	93	45	54	36
T (°C) (L14) (P=2.5 kbar)	173	135	188	208	206	202	138	167	141	98	99	84	157	185	156	159	172	120	125	118
T (°C) (L14) (P=5 kbar)	198	159	215	236	234	229	162	193	165	120	120	105	182	211	181	184	197	143	148	141
T (°C) (L14) (P=7.5 kbar)	224	182	242	264	262	257	185	218	189	141	142	125	207	238	206	209	223	166	171	164
T (°C) (L14) (P=10 kbar)	250	206	268	292	289	285	209	244	213	163	164	146	232	264	231	234	249	188	195	186
T (°C) (CN85)	262	249	267	272	271	270	250	259	251	184	188	123	74	85	74	78	90	68	84	54
T (°C) (C88)	308	289	316	324	323	321	291	304	292	191	197	97	24	40	23	30	48	15	39	-7
T (°C) (J91)	307	289	316	324	322	320	289	303	292	194	202	100	18	34	17	23	41	12	36	-8

B13=Bourdelle et al (2013), L14=Lanari et al (2014a), CN85=Cathelineau and Nieva (1985), C88=Cathelineau (1988), J91=Jowett (1991).